OPTIMAL BIDDING AND REAL-TIME OPERATION STRATEGIES FOR WIND AND PUMPED HYDRO STORAGE SYSTEMS USING STOCHASTIC PROGRAMMING AND MODEL PREDICTIVE CONTROL

by

İsmail Kayahan

Submitted to Graduate School of Natural and Applied Sciences
in Partial Fulfillment of the Requirements
for the Degree of Doctor of Philosophy in
Systems Engineering

Yeditepe University
2019

OPTIMAL BIDDING AND REAL-TIME OPERATION STRATEGIES FOR WIND AND PUMPED HYDRO STORAGE SYSTEMS USING STOCHASTIC PROGRAMMING AND MODEL PREDICTIVE CONTROL
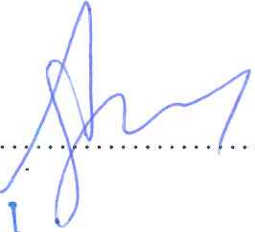
APPROVED BY:

Assist. Prof. Dr. Uğur Yıldıran
(Thesis Supervisor)
(Yeditepe University)

Prof. Dr. Duygun Erol Barkana
(Yeditepe University)
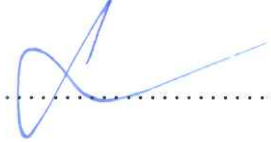
Assist. Prof. Dr. Ali Fuat Ergenç
(İstanbul Technical University)

Assist. Prof. Dr. Mustafa Alper Özpınar
(İstanbul University of Commerce)

Assist. Prof. Dr. Semih Yalçındağ
(Yeditepe University)

DATE OF APPROVAL: ..../..../2019

ACKNOWLEDGEMENTS

ABSTRACT

OPTIMAL BIDDING AND REAL-TIME OPERATION STRATEGIES FOR WIND AND PUMPED HYDRO STORAGE SYSTEMS USING STOCHASTIC PROGRAMMING AND MODEL PREDICTIVE CONTROL

Trading wind energy in deregulated markets is a challenging task due to uncertainties involved. To be more specific, a company participating into day-ahead market has to submit its bids for the next day without knowing actual generation that will occur. Consequently, there will be discrepancies between bids promised and energy generated. This leads to imbalances which causes penalties to be paid in the balancing market. Incorporating a pumped hydro storage system may be a remedy to this problem. In the literature, a significant body of work is devoted for the joint wind-PHS systems that participates in day-ahead bidding. However, the problem of real-time operation is not studied well. Motivated by this fact, in this thesis, a new strategy in which the day-ahead bids are computed by solving a risk-averse stochastic program, and real-time operation is performed by a stochastic model predictive control-based algorithm with a risk control capability is proposed. This is a rolling horizon approach in which a MILP problem constructed from a stochastic scenario tree is solved repeatedly at every time instant within the day. By this way, optimal actions for the storage device can be computed exploiting the latest available information. The proposed algorithm is applied to a realistic system located in Turkey, and its performance is compared with the algorithms in the literature by using daily schedule, Pareto optimality and long-term analysis. Simulation studies shows that the proposed approach outperforms the available methods owing to its ability to exploit the most recent information available within the day and ability to take into account contingencies of wind energy production.

ÖZET

RÜZGAR VE POMPAJLI HİDRO ELEKTRİK SANTRALLERİNDE EN İYİ TEKLİF VE GERÇEK ZAMANLI OPERASYON İÇİN STOKASTİK MODEL ÖNGÖRÜLÜ KONTROLÜN KULLANILMASI

Serbest enerji piyasasında rüzgar enerjisi ticareti yapmak rüzgarın sahip olduğu belirsizlik nedeniyle zorlu bir iştir. Daha açık olmak gerekirse, gün öncesi piyasasına katılan bir şirketin, gerçekleşecek olan asıl üretimi bilmeden ertesi gün için tekliflerini sunması gerekir. Sonuç olarak, vaat edilen teklifler ile üretilen enerji arasında farklar olacaktır. Bu farklar, dengeleme pazarında belirli cezaların ödenmesine yol açar. Pompaj depolamalı bir hidro elektrik sisteminin eklenmesi bu soruna çare olabilir. Literatürde, gün öncesi ihalesine katılan ortak rüzgar-PHS sistemlerine önemli bir çalışma alanı ayrılmıştır. Ancak, gerçek zamanlı operasyon sorunu iyi çalışılmamıştır. Bu gerçeğe dayanarak, bu tezde, gün öncesi tekliflerinin riskten kontrollü stokastik bir program çözülerek hesaplandığı ve gerçek zamanlı operasyonun risk kontrolüne sahip stokastik model öngörülü kontrol yaklaşımına dayalı bir algoritma ile gerçekleştirildiği yeni bir strateji önerildi. Bu, stokastik bir senaryo ağacından inşa edilen bir lineer karışık tamsayı probleminin, günün her anında, tekrar tekrar çözüldüğü bir yaklaşımıdır. Bu şekilde, depolama cihazı için en uygun eylemler, mevcut olan en son bilgilerden yararlanılarak hesaplanabilir. Önerilen algoritma, Türkiye'de bulunan gerçekçi bir sisteme uygulanmakta ve performansı günlük program, Pareto optimallik ve uzun vadeli analizler kullanılarak literatürdeki algoritmalarla karşılaştırılmaktadır. Simülasyon çalışmaları, önerilen yaklaşımın, gün içinde mevcut olan en yeni bilgileri kullanabilme kabiliyeti ve rüzgar enerjisi üretimindeki beklenmedik durumları dikkate alma kabiliyeti sayesinde mevcut yöntemleri geride bıraktığını göstermektedir.

TABLE OF CONTENTS

LIST OF FIGURES

LIST OF TABLES

LIST OF SYMBOLS/ABBREVIATIONS

B	Day-ahead market bid in period t and scenario k
C	Number of reversible turbines
k	Scenario index
K	Total number of scenarios
l	Logic variable for preventing simultaneous pumping and generation
M	Order of the wind speed SARIMA model
n	Node index
P_d^c	Power generated by turbine c in period t and scenario k
$\overline{P}_d^c$	Maximum power generation of turbine c
$\underline{P}_d^c$	Minimum power generation of turbine c
P_{grid}	Energy drawn from the grid in period t and scenario k
P_p^c	Power consumed by turbine c in period t and scenario k
$\tilde{P}_p^c$	The power consumption of turbine c in pumping mode
P_T	Total energy exchange with the grid in period t and scenario k
q_d^c	Water discharged by turbine c in period t and scenario k
q_δ^c	Deviation of water discharge from technical minimum for turbine c
$\overline{q}_d^c$	Maximum water discharge of the turbine c
$\underline{q}_d^c$	Minimum water discharge of turbine c
$\tilde{q}_p^c$	Water pumped by turbine c in pumping mode
q_p^c	Water pumped by turbine c in period t and scenario k
r^+	Penalty ratio for positive imbalance
r^-	Penalty ratio for negative imbalance
t	Time index
T	Optimization horizon
u_d^c	Discharge status (on-off) of turbine c in period t and scenario k
u_p^c	Pumping status (on-off) of turbine c in period t and scenario k
V	The water level in the upper reservoir in period t and scenario k
$V_{initial}$	Initial water volume in the reservoir at the start of the day

$\overline{V}$	Maximum water volume of the upper reservoir
$\underline{V}$	Minimum water volume of the upper reservoir
W	Total wind power in period t and scenario k
W_{grid}	Wind energy supplied to the grid in period t and scenario k
W_{pump}	Wind energy consumed by turbines in pumping mode
y_d^c	Startup status for the discharge of turbine c in period t and scenario k
y_p^c	Startup status for pumping of turbine c in period t and scenario k
z_d^c	Shutdown status for the discharge of turbine c
z_p^c	Shutdown status for pumping of turbine c in period t and scenario k
α_d^{up}	The startup cost for discharging (TL)
α_d^{down}	Shutdown cost for discharging (TL)
α_p^{up}	The startup cost for pumping (TL)
α_p^{down}	Shutdown cost for pumping (TL)
β	Risk-control weight
Δ^+	Positive deviation of the generation from the contract (MWh)
Δ^-	Negative deviation of the generation from the contract (MWh)
ζ	Value at risk
δ^c	Energy coefficient (MWh/m^3)
$\underline{\eta}_d^c$	The efficiency of turbine c at minimum flow in discharge mode
$\overline{\eta}_d^c$	The efficiency of turbine c at maximum flow in discharge mode
η_p^c	The efficiency of turbine c in pumping mode
η_T	Transmission efficiency
λ	Day-ahead market price
μ	The confidence level for CVaR
π	The probability of scenario k
τ	Auxiliary variable for computing CVaR in scenario k
Ω	Set of indices of scenarios passing through scenario tree node (n, t)
ACF	Autocorrelation Function
ANN	Artificial Neural Networks

AR	AutoRegressive
ARIMA	Autoregressive Integrated Moving Average
ARMA	AutoRegressive Moving Average
BES	Battery Energy Storage
BOO	Build-Operate-Own
BOT	Build - Operate – Transfer
CAES	Compressed Air Energy Storage
CHP	Combined Heat and Power
CSPP	Concentrated Solar Power Plant
CVaR	Conditional Value at Risk
DFIG	Double-Fed Induction Generator
DMPC	Deterministic Model Predictive Control
EESG	Electrically Excited Synchronous Generator
EİE	Electric Power Resources Survey and Development Administration
EMRA	Energy Market Regulatory Authority
EPİAŞ	Energy Markets Operating Corporation
ESS	Energy Storage System
EÜAŞ	Electricity Generation Company
FBES	Flow Batteries Energy Storage
FC	Fuel Cell
FCM	Fuzzy C-Means
FES	Flywheel Energy Storage
GARCH	Generalized AutoRegressive Conditional Heteroscedastic
GenCo	Generation Company
GWEC	Global Wind Energy Council
HAWT	Horizontal Axis Wind Turbine
IC	Imbalance Cost
IRENA	International Renewable Energy Agency
LDR	Linear Decision Rules
Li-ion	Lithium-Ion
MA	Moving Average
MCP	Market Clearing Price
MILP	Mixed-Integer Linear Programming

NiCd	Nickel Cadmium
NiMH	Nickel Metal Hybrid
NWP	Numeric Weather Prediction
PACF	Partial Autocorrelation Function
PHS	Pumped Hydro Storage
PMSG	Permanent Magnet Synchronous Generator
PV	PhotoVoltaic
RO	Robust optimization
SARIMA	Seasonal Autoregressive Integrated Moving Average
SBP	System Buy Price
SCIG	Squirrel Cage Induction Generator
SMES	Superconduction Magnetic Energy Storage
SMPC	Stochastic Model Predictive Control
SP	Stochastic Programming
SSP	System Sell Price
SUSD	Startup Shutdown Cost
TEAŞ	Turkish Electricity Generation and Transmission Company
TEDAŞ	Turkish Electricity Distribution Corporation
TEİAŞ	Turkish Electricity Transmission Company
TEK	Turkish Electricity Authority
TETAŞ	Turkish Electricity Trading and Contracting Company
VaR	Value-at-Risk
VAWT	Vertical Axis Wind Turbine
VSS	Value of Stochastic Solution
WPP	Wind Power Plant
WRIG	Wound Rotor Induction Generator
WT	Wind Turbines
YEKDEM	Renewable energy support mechanism

1. INTRODUCTION

In the last decades, the energy infrastructure in many countries went through a transition from a regulated structure to a deregulated structure. A regulated electricity market consists of a monopolist that manages all of the generation, transmission and distribution utilities. However, investing in all services need a massive amount of capital, which is paid by the customers. Another significant problem was the low power generation efficiency because of the lack of competition. Thus, in order to struggle with these problems, the countries started to privatize their generation, transmission and distribution utilities, and all utilities are separated in order to create a competitive and transparent market structure. As a result, the change in the energy infrastructure in the world began in the late 1980s with the UK and continued in the USA and European Union.

With the deregulation, the main change occurred in the generation side of the energy. With the liberation of the energy generation, new generation companies (GENCO) has acted in the energy generation. In addition to private-sector owned conventional power plants, the penetration of renewable energy has increased rapidly all over the world. Environmental concerns, along with decreasing capital costs, low operation costs and improvements in technology, constitute the driving forces behind this growth. However, higher utilization of renewable energy leads to significant challenges due to its intermittent nature, which diminishes its reliability.

Due to the variability of demand and renewable energy generation, there are uncertainties that can be dealt with two different solution. One of the solutions is introduced by the system operator. With this solution, multiple market structures are established in different time scales, which are day-ahead, intraday, real-time balancing, and ancillary markets. Within these markets, most of the energy is traded in the day-ahead market. However, due to the uncertainties arising from the renewable energy sources, the imbalance between the generation and demand can occur in the power system. In order to reduce these imbalances, the intra-day market is established. Although the system is tried to be balanced with these market structures, some unpredictable short-term imbalances may still exist in the system. To cope with this problem, real-time imbalances are compensated in the balancing market.

Also, ancillary markets are mostly used to provide energy for frequency regulation and safety issues.

The second solution is proposed by energy producers because of their profit decrease due to imbalances in the production plans. While these imbalances can be eliminated with conventional power plants, storage devices are an effective solution to alleviate problems of intermittency by energy shifting and imbalance reduction. Various storage technologies can be used for this purpose, such as Pumped Hydro Storage (PHS) plants, batteries, compressed air storage devices, flywheels [1]. Among these, PHS plants are one of the most promising solutions for large-scale storage due to their high capacity, rapid response time and long lifetime [2].

In this thesis, a wind energy producer supported by a PHS system was investigated. Two different, but closely located wind farms are sited in Manisa, and the PHS plant is planned to be built near the wind farms in the feasibility study carried out by the government. The producer is participating in the day-ahead market for trading energy and compensating its deviations in the balancing market. Thus, the joint wind-PHS energy producer implements a two-step decision-making process. In the first stage, which can be called as bidding, the day-ahead market bids are decided without knowing the actual energy prices and wind energy production so that the maximum income can be obtained. In the second stage, the producer determines the energy supplied to the grid for each hour in the real-time operation with the available data which are accepted bid, actual energy price, and system state.

Thus, for this energy producer, an integrated strategy for day-ahead market bidding and real-time operation was developed. The proposed real-time operation algorithm is based on a Stochastic Model Predictive Control (SMPC) algorithm while the bidding is formulated as a Mixed-Integer Linear Programming (MILP)-based stochastic program. In both phases, random information is modeled as scenario trees, imbalance costs are considered realistically, and risk aversion based on Conditional Value at Risk (CVaR) measure is a part of the objective.

Different real-time operation methods from the literature were implemented along with the proposed SMPC algorithm, and their performances were compared. To be more specific, first, daily operation schedules of the algorithms were analyzed. Second, because the problem studied has two conflicting objectives of expectation maximization and risk

aversion, Pareto optimality of the methods relative to each other was investigated. Finally, long-term simulations were performed to compare the economic benefits of the strategies considered in a more general setting under changing imbalance market conditions.

The overall structure of the thesis takes the form of ten chapters, including this introductory chapter. The wind energy and energy storage systems are introduced in Section 2 and Section 3, respectively. In Section 4, the pumped energy storage device is investigated in detail with its historical background, capacity in the world and Turkey, main-use case applications and technical aspects. In Section 5, the general electricity market structure is explained with the detailed information about Turkey electricity market. In Section 6, a general background on stochastic programming and solution methods is provided. The scenario generation and reduction methods used in this thesis are also given in detail in this section. Section 7 begins by laying out the problem formulation of the joint wind-PHS system and market model, then presents a review about the related literature of the bidding and real-time operation. In Section 8, the proposed method for the bidding and real-time operation is given with the optimization model. In Section 9, the case study is described, and the simulation results are presented and analyzed. Finally, the main outcomes of this work are summarized in Section 10.

2. WIND ENERGY

Wind energy is an important renewable energy source which is used considerably today, and its share in total energy production has increased recently. Its popularity is due to the facts that it is a fuel-free, clean and environmentally friendly source. Although it is a popular energy source today, actually it has been used for a long time in history.

The first applications of wind energy date back to 2800 BC as a power source for the sailing ships. In the next centuries, it was utilized for irrigation and grain milling purposes. Until the beginning of the 19th century, the use of wind energy had expanded, and its use in water pumps had become widespread. In the 19th century, with the invention of the steam engine in the Industrial Revolution, stable energy could be produced with fossil fuels. Thus, wind energy began to lose importance. However, after the oil crisis in the 1970s, countries made significant efforts to diversify energy sources by looking for alternatives. This triggered the use of wind as the electrical energy source. After that, small turbines were designed to provide electricity to houses and wind farms with capacity ranging between 10-15 MW were started to generate energy before the 1990s.

Since the 1990s, wind energy technology has made significant progress, and high capacity wind power plants have been developed. The wind power in the world was only 2160 MW at the beginning of the 1990s, and the installed wind power over the world increased by six times to 13455 MW at the end of 1999. This trend continued in the 2000s, as shown in Figure 2.1, and the total capacity increased to 539123 MW at the end of 2017 [3]. According to the market forecasts accomplished by Global Wind Energy Council (GWEC), the installed wind power capacity is expected to 840 GW by the end of 2022.
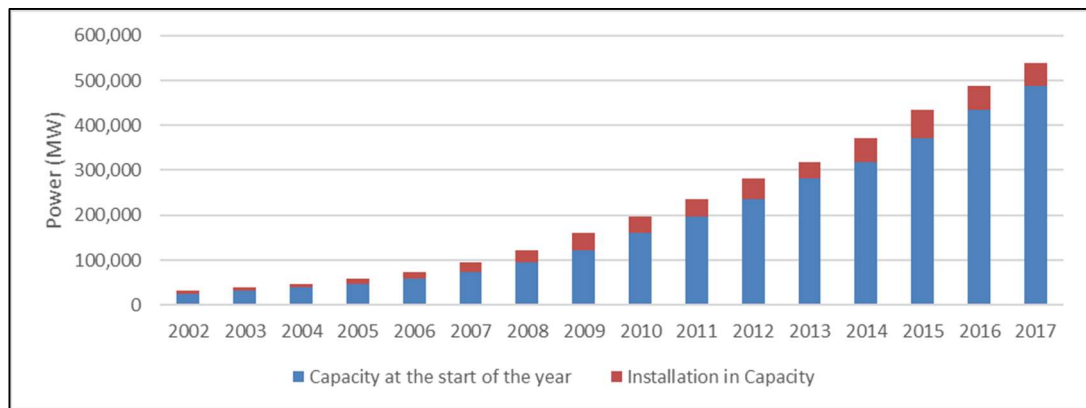
Figure 2.1. Installed wind power capacity - worldwide 2002-2017

According to a report published by GWEC, 42.3 percent of the installed capacity was located in Asia at the end of 2017. Europe follows the Asia region with 33 percent, North America with 19.5 percent. The most crucial factor that makes the Asia leader in the world is China's recent investments in wind energy. At the end of 2017, China had the largest share across the globe, as can be seen from Figure 2.2.
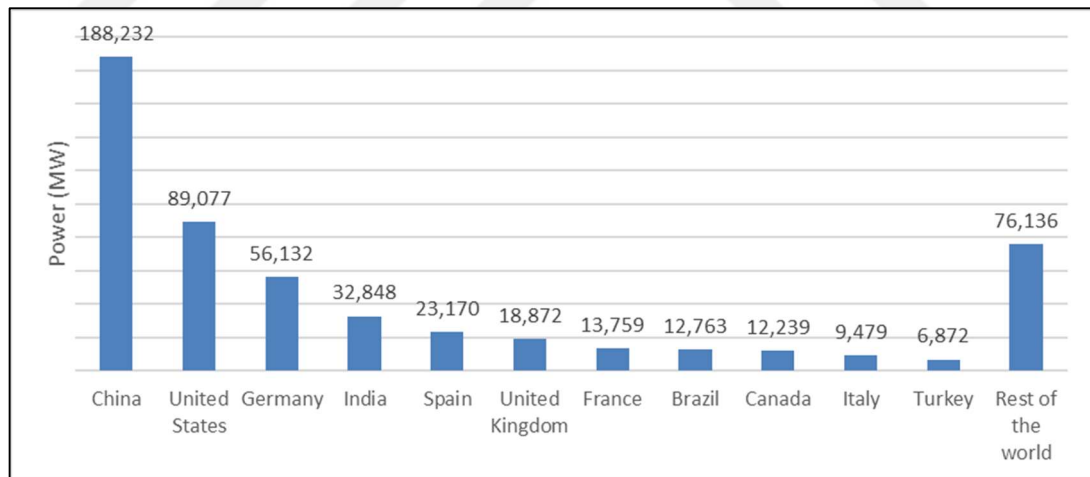
Figure 2.2. Cumulative installed capacity in 2017

From Figure 2.2, it can be observed that Turkey became the sixth-largest wind energy producer in Europe and eleventh in the world. According to the same report in 2017, Turkey had increased its wind capacity by 766 MW and ranked 4th in Europe in this category and ranked 8th in the world. Turkey has an advantageous position compared to other countries because it has considerable potential for wind energy, which is estimated at approximately

48000 MW [4]. Two wind farms were built in 1998 with an 8.7 MW installed capacity, and there was no significant increase in capacity until the government's new investment policies in renewable energy sources in 2005. After that investment policies, the capacity increased each year gradually and reached to 6872 MW at the end of 2017. The evolution of the installed wind power in Turkey is given in Figure 2.3.
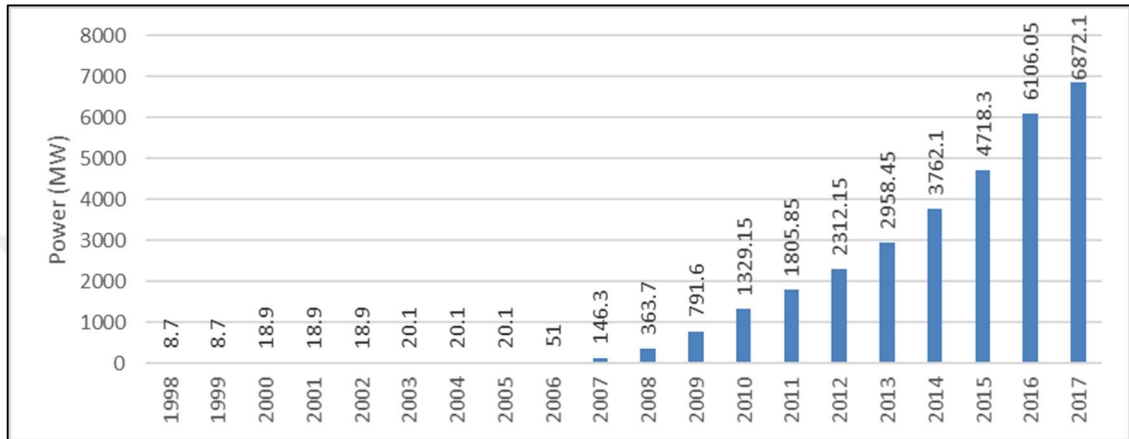
Figure 2.3. Installed wind capacity over the years

In 2007, Turkey Wind Energy Potential Atlas was formed to determine the characteristics and distribution of wind energy resources in Turkey. The detailed wind source maps given in this atlas provide a guide for deciding suitable regions for wind energy production. The territories with the highest wind potential are Marmara and Aegean regions according to this atlas, and these were the places having 164 plants operational in Turkey by the end of 2017 [5] and the distribution of these wind power plants by regions is depicted in Figure 2.4.
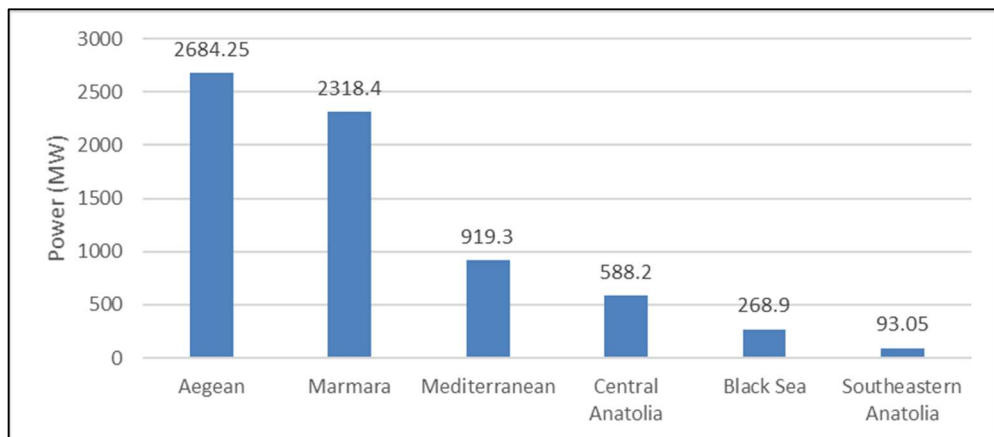
Figure 2.4. Operational WPP's according to regions

2.1. WIND TURBINES

Wind Turbines (WT) convert the kinetic energy from the movement of air into electrical energy as in Figure 2.5. Firstly, the rotor of the wind turbine gathers the wind energy through aerodynamically designed blades and converts it into mechanical energy. Because the generator rotates at high speed, the low mechanical rotation speed must be increased with the gearbox. If the generator has a high number of poles, then it can operate at low speed. Thus, the mechanical energy can be transmitted to the generator without the need for a gearbox. After the generator converts mechanical energy to electrical energy, the electrical energy is transferred to the grid with the transformers and transmission lines. However, depending on the type of wind turbine, it may be necessary to use a power converter before the electrical energy is transmitted to the power transformers.
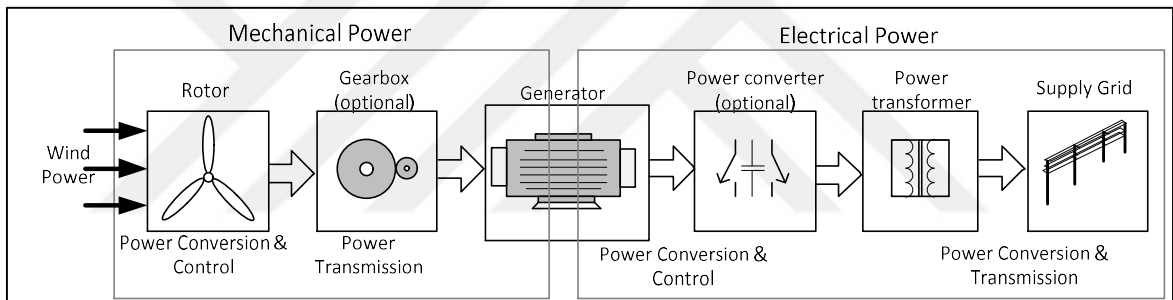
Figure 2.5. Energy conversion of wind to electricity
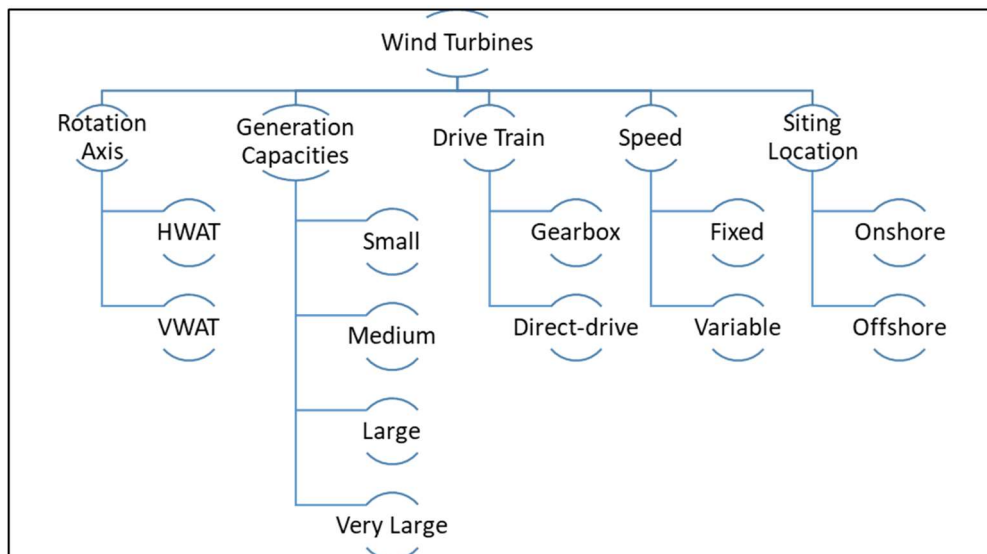
Figure 2.6. Classification of wind turbines

As depicted in Figure 2.6, WTs can be classified with respect to different aspects. One criterion is the rotation axis. There are Horizontal Axis Wind Turbines (HAWT) and Vertical Axis Wind Turbines (VAWT). Due to their higher efficiency and energy output characteristics, HWATs are preferred for large scale energy generation [6]. Details of the horizontal and vertical axis wind turbines will be presented in Section 2.1.1 and 2.1.2

WTs can also be classified based on the generation capacities as follows.

- Small (<25 kW)
- Medium (25-100 kW)
- Large (100 kW-1000 kW)
- Very large (>1000 kW)

WTs also differ in the mechanism used to transform mechanical power into electrical power. Some WTs transmit power with a gearbox, whereas new WT types make use of direct-drive technology. Gearbox turbines may have a Squirrel Cage Induction Generator (SCIG), Wound Rotor Induction Generator (WRIG) and Double-Fed Induction Generator (DFIG) with a small number of poles. While SCIG and WRIG are connected to the grid directly with a transformer, DFIG uses a partial scale converter before connecting to the network. Turbines with direct-drive technology may have an Electrically Excited Synchronous Generator (EESG) and Permanent Magnet Synchronous Generator (PMSG). Such generators have a large number of poles and need a full-scale converter before connecting to the grid. Grid connections for the generators mentioned above are depicted in Figure 2.7 and   Figure 2.8.
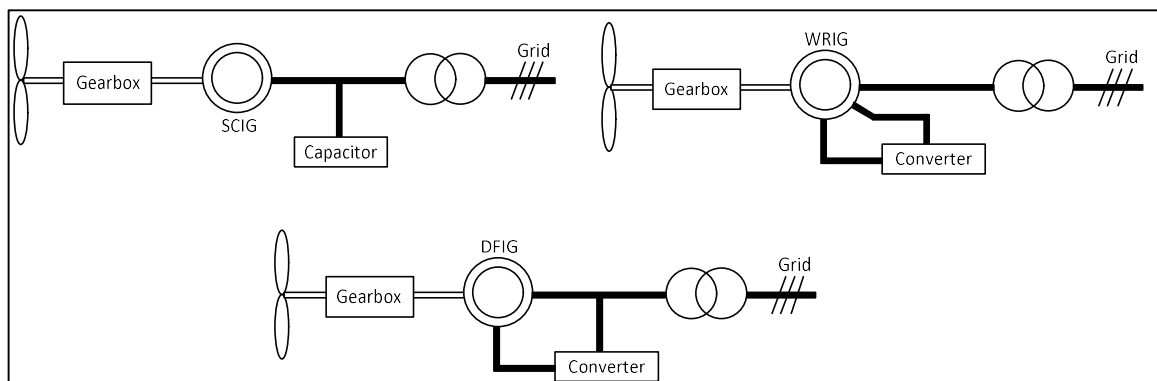
Figure 2.7. Grid connection of gearbox coupled generators
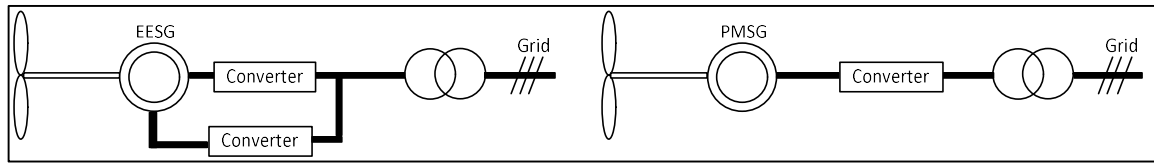
Figure 2.8. Grid connection of direct-drive generators

Another way for classifying wind turbines is their operating speed. They may be fixed or variable speed depending on the drive technology and generator type as shown in Table 2.1

Table 2.1. Technical comparison of geared and direct drive generators

	Geared			Direct-drive	
	SCIG	**WRIG**	**DFIG**	**EESG**	**PMSG**
Grid Connection	Direct via transformer	Direct via transformer	Partial scale converter	Full scale converter	Full scale converter
Speed	Fixed	Limited variable	Variable	Variable	Variable

When the turbine sittings are investigated, it can be seen that most of the wind turbines are built on the land since installation costs are lower when compared with offshore areas. However, offshore wind turbines are becoming widespread since wind speed are higher over the sea, and available onshore areas are limited over Europe [6]. First offshore wind turbines were installed in shallow regions close to shores. The first offshore establishment had a 5 MW turbine build near the island of Lolland in Denmark (Vindeby Windfarm). In the projections for the future, it is foreseen that the offshore wind power plants will generate 549 TWh energy by the 2030s.

The designs of the offshore and onshore WTs are very similar except the structure of the foundation. The types of offshore WT foundations are given in Figure 2.9 [6]. The first offshore WTs were building with an underwater tower but the later ones used floating foundations in order to locate the WTs on deeper waters. A company developed a floating WT which was designed to be used at places having depth up to 400 m, however, with the

recent technological improvements, it will be possible to place WTs to deeper regions in the near future.
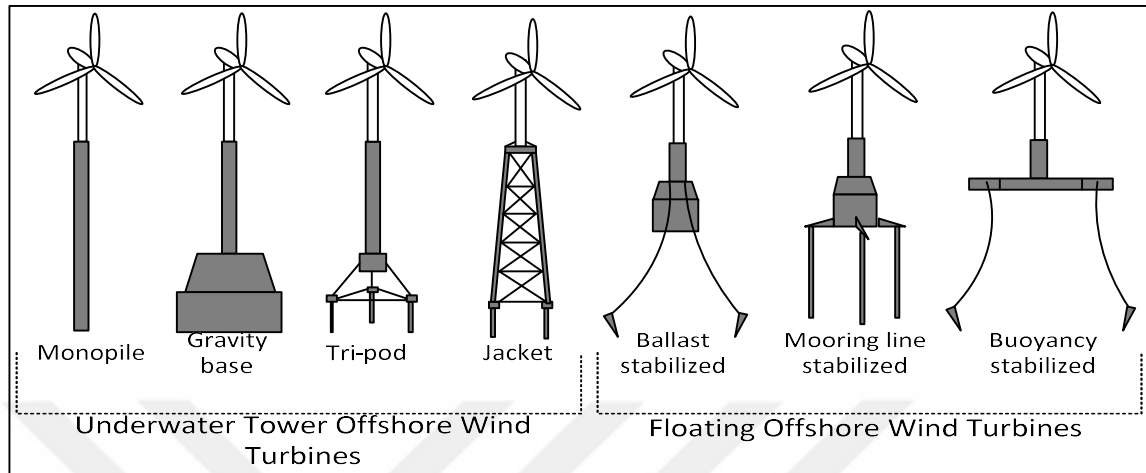
Figure 2.9. Offshore wind turbines and types of foundations

2.1.1. Horizontal Axis Wind Turbines

HAWTs have their axis of rotation parallel to the ground and perpendicular to wind direction, as shown in Figure 2.10. Because these type of wind turbines work most efficiently when blades are perpendicular to the wind direction, a yaw control mechanism should be employed. Also, this wind turbine should have a tower to place the rotor at high altitudes because the wind speed increases with height. A nacelle which contains the primary parts such as shaft and generator is located at the top of the tower and connected to the rotor.

HAWTs are classified depending on the number of blades as follows.

a. Single-bladed: The reason for the construction of single-bladed wind turbines is to increase the rotational speed on the blade by decreasing the inertia of the rotor. This reduces the machine mass and rotational torque of the rotor. However, the aerodynamic noise level of the rotor caused by the blade tip speed is very high. Also, a counterweight has to be placed on the other side of the hub to balance the rotor.

b. Two-bladed: The balance of the two-blade rotor is more uniform than a single-bladed rotor, and it seems more economical compared to the three-bladed wind turbine. However, two-bladed wind turbines need additional equipment because of the

gyroscopic precession, which results in wobbling. The need for this additional equipment naturally raises costs and, as a result, its cost is close to that of three-bladed wind turbines.

c. Three-bladed: It is the most widely preferred blade type. This is because the blades have a constant moment of inertia at different speeds. Due to this feature, the three-bladed structure does not need additional equipment, which reduces the installation cost.

d. Multi-bladed: Multi-bladed turbines can operate at low wind speeds and produce high moment. Due to this property, it has been used for water pumping for many years. On the other hand, this blade configuration reduces the electricity generation efficiency because turbines face higher wind resistance, which reduces the energy generation.
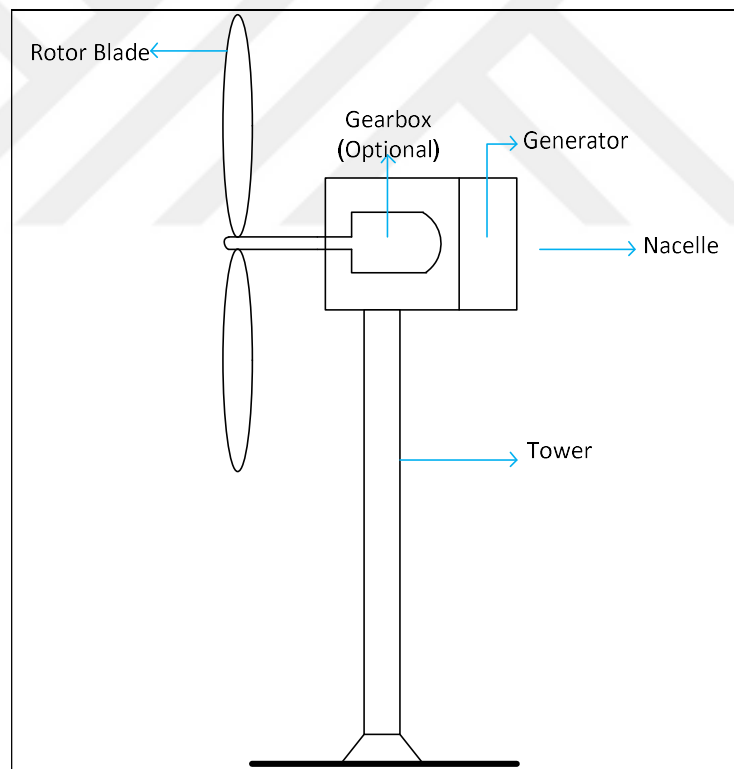
Figure 2.10. Horizontal axis wind turbine with components

The two and three-bladed HAWTs can also be classified based on the direction of the wind coming to the blades, as shown in Figure 2.11. In an upwind turbine, the rotor faces the wind. Their most important feature is the minimization of the wake effect of the tower. However,

a yaw mechanism is required for these turbine types because it is necessary to align the rotor with the wind direction. In the downwind turbines, the rotor is placed behind the tower. Hence, a yaw mechanism is not necessary to turn the turbine to the wind because nacelle and rotor follow the wind direction passively. A more important advantage is that the blades can bend at high wind speed to reduce the stress at the tower. Also, this makes the machine lighter and leads to better power dynamics. However, the power fluctuation that occurs when the wind passes through the tower leads to significant energy losses. The comparison of the characteristics of upwind and downwind turbines can be summarized as in Table 2.2

Table 2.2. Comparison of turbines according to the wind direction

	Yaw mechanism	Blade material structure	Load on the tower	Damage to the turbine
Upwind Turbines	Yes	Hard	Heavy	Low
Downwind Turbines	No	Soft	Light	High
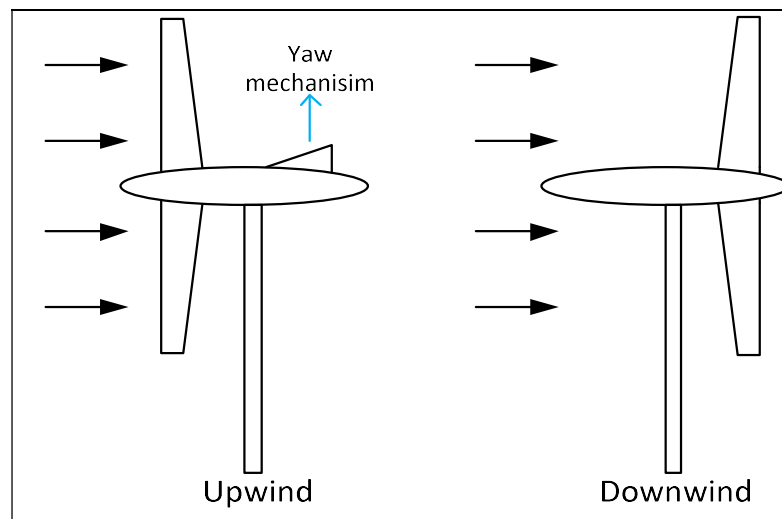
Figure 2.11. Upwind and downwind turbines

2.1.2.   Vertical Axis Wind Turbines

In this type of turbine, the rotor is vertical and perpendicular to the wind direction. Since the generator and gearbox can be housed on the ground, it is not necessary to place the turbine on the tower, which reduces the installation cost and the weight. Also, it is easier to transmit the generated power as the generator is at ground level. Furthermore, there is no need to turn the turbine to the direction of the wind, and therefore, the yaw mechanism system is not required. However, due to the turbine blades design, their efficiency is lower than the horizontal axis turbines. Also, since the blades are placed close to the ground, their rotation speed is lower than HWATs. These turbine types, which have a minimal share in commercial use, have different varieties such as Savonius and Darrieus, as shown in Figure 2.12.

Savonius wind turbine: It was discovered in 1925 by Finnish engineer Sigurd J. Savonius. It consists of two half-cylinders placed between two flat discs, whose centers are symmetrically shifted relative to each other, as shown in Figure 2.12.a. The wind creates a positive moment on one of the half-cylinder while creates a negative moment on the other. Since the positive moment is larger than the negative moment, the rotation occurs in the positive moment direction. Compared to the other VAWTs, Savonius WTs have excellent starting characteristics at low wind speeds, and they can generate energy with self-starting. Moreover, their installation is easy and cheap. However, these turbines require adequate speed control to maintain efficiency at acceptable values and require mechanical braking to stop the turbine operation.

Darrieus wind turbine: It was invented in 1931 by the French engineer George J.M. Darrieus. The blades rotate about its axis due to the difference between the push and pull forces formed on concave and convex surfaces. The power generated by the Darrieus wind turbine produces a sine curve that oscillates between the highest value and the lowest value twice per revolution. Darrieus WTs provide higher efficiency because they reduce friction losses compared to Savonius turbines. However, because this turbine cannot generate energy with self-starting, they require an additional device such as a Savonius turbine or a drive motor. In addition to the ellipse-shaped Darrieus wind turbines (Figure 2.12.b), H-shaped designs are also available (Figure 2.12.c).
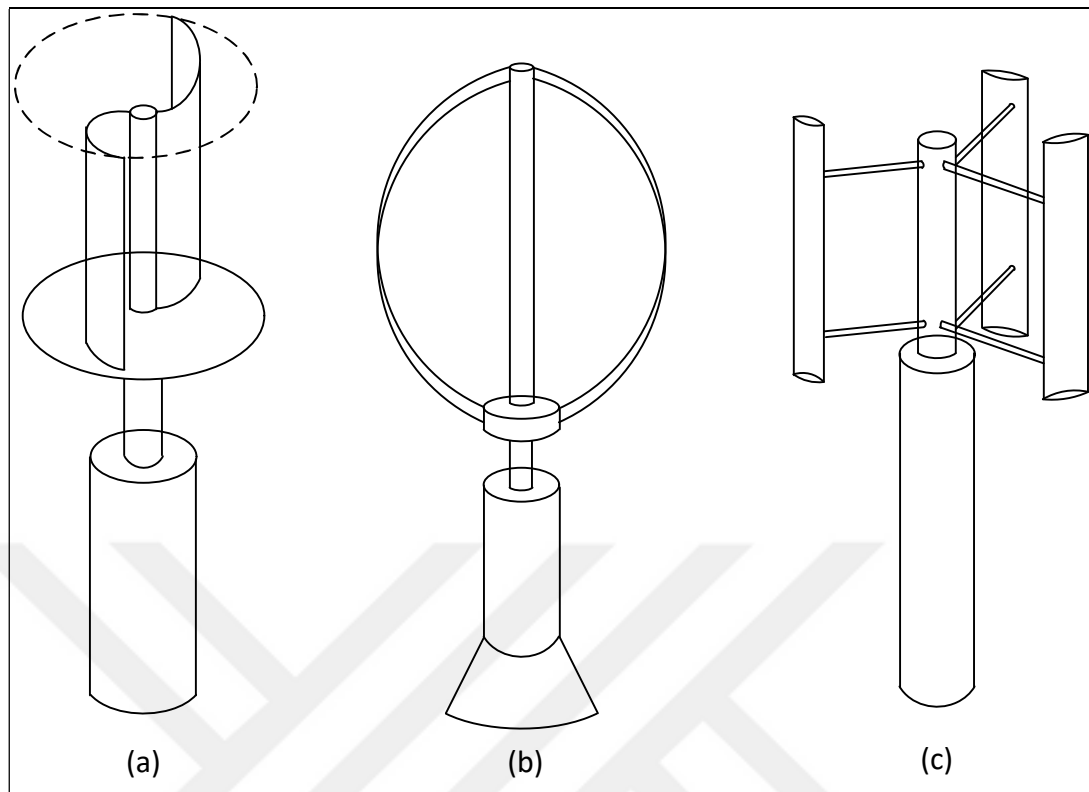
Figure 2.12. Vertical axis wind turbines (a) Savonius, (b) Darrieus, (c) Darrieus –H

2.1.3. Comparison of Wind Turbines Based on Axis

During the installation of wind farms, the characteristics of the wind farms should be known to make the right choice. These characteristics are shown in Table 2.3 for the wind turbine types described above. The table shows how a turbine selection should be made based on the usage purpose, the amount of wind in the region and the financial aspects [7].

Table 2.3. Comparison of wind turbine characteristics

	HAWT				VAWT	
	Single-bladed	Two-bladed	Three-bladed	Multi-bladed	Savonius	Darrieus
Cost	Low	Low	High	High	Low	Low

Aesthetic appearance	Bad	Bad	Good	Good	Good	Good
Noise	High	High	Low	Low	Low	Low
Operating Speed	Very High	High	Medium	Very Low	Very Low	Low
Existence of Tower	Yes	Yes	Yes	Yes	No	No
Commercial Usage	Electricity	Electricity	Electricity	Rarely Electricity & Usually Water pumping	Rarely Electricity & Usually Water pumping	Rarely Electricity & Usually Water pumping
Efficiency	Medium	Medium	Very High	Low	Very Low	Medium

2.2. ENERGY CONVERSION IN WIND TURBINES

In a WT, blades of a wind turbine convert the kinetic energy of the airflow into mechanical energy. This conversion can be formulated as

$$P = \frac{1}{2}\rho A_{WT} U^3 \qquad (2.1)$$

where ρ is the air density, A_{WT} is the swept area of the turbine and U represents the wind speed. However, all of the wind reaching the blades cannot be transformed into mechanical energy. Otherwise, wind passing through the rotor would stop. Therefore, the actual power captured by the rotor blades is given by the kinetic energy difference of inlet and outlet airflow of the wind channels, as illustrated in Figure 2.13. Thus, the power transferred to the rotor can be formulated as

$$P_k = \frac{1}{2}\dot{m}(U_i^2 - U_o^2) \qquad (2.2)$$

where P_k is the mechanical wind power obtained from the rotor, $\dot{m}$ is the mass flow rate of the air and U_i and U_o are the wind speed at the inlet and outlet, respectively.
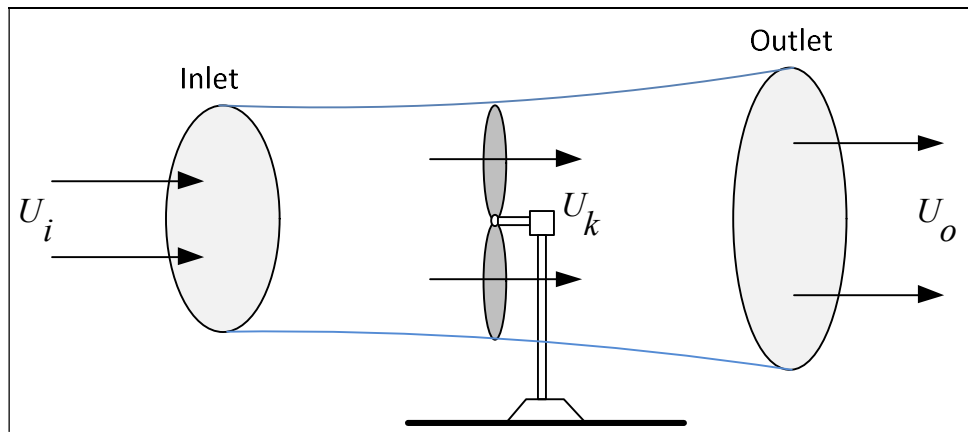
Figure 2.13. Wind speed across a wind turbine

In general, the wind speed is not uniform along the channel. Therefore, the mass flow of air moving through the rotating blades can be written as in Equation (2.3)

$$\dot{m} = \rho A U_k \tag{2.3}$$

where U_k is the average velocity difference of the air between inlet and outlet and it can be formulated as in Equation (2.4)

$$U_k = \frac{U_i + U_o}{2} \tag{2.4}$$

Thus, the mechanical power transferred to the rotor can be found by substituting the Equation (2.3) and (2.4) into Equation (2.2).

$$P_k = \frac{1}{2}\rho A \frac{U_i + U_o}{2}(U_i^2 - U_o^2) \tag{2.5}$$

Although inlet wind speed cannot be controlled, the outlet wind speed can be controlled by the design of the turbine blades. This design affects the power efficiency, C_p, which is the ratio of the mechanical power obtained by the rotor to the power of the inlet airflow.

$$C_p = \frac{P_k}{P_i} \tag{2.6}$$

where the inlet air flow power is

$$P_i = \frac{1}{2}\rho A U_i^3 \tag{2.7}$$

By substituting the Equation (2.5) and (2.7) into the Equation (2.6), the following formulation can be found.

$$C_p = \frac{P_k}{P_i} = \frac{1}{2}\left(1 + \frac{U_o}{U_i}\right)\left(1 - \frac{U_o^2}{U_i^2}\right) \tag{2.8}$$

In order to simplify the formulation, the ratio between outlet and inlet wind speed can be written as $\lambda = U_o/U_i$, then C_p can be calculated as

$$C_p = \frac{1}{2}(1 + \lambda)(1 - \lambda^2) \tag{2.9}$$

The power coefficient curve with respect to λ is given in Figure 2.14. This power efficiency has to be maximum in order to obtain the maximum power from the inlet wind. Therefore, the maximum of C_p can be obtained by differantiating the Equation (2.9) with respect to λ.

$$\frac{dC_p}{d\lambda} = \frac{1}{2}(-3\lambda^2 - 2\lambda + 1) = 0 \tag{2.10}$$

The root of the Equation (2.10) can be found as $\lambda_1 = -1$ and $\lambda_2 = 1/3$ and because the speed ratios have to be positive, the speed ratio is found $1/3$. According to this result, to obtain the highest power from the turbine, the inlet speed of the wind should be 3 times the speed of the outlet. If this ratio is substituted into Equation (2.9), the maximum power factor is found as $C_{pmax} = 0.5926$. In this case, the maximum theoretical efficiency is 59.26 percent and is referred to as Betz Limit or Betz Law [8]. The power coefficient curve with respect to $\lambda = U_o/U_i$ the ratio is given in Figure 2.14. Finally, the actual power formula of a wind turbine is obtained in Equation (2.11) by subsituting the power coefficient formula in Equation (2.9) into Equation (2.5).

$$P_W = \frac{1}{2}\rho A C_p U^3 \tag{2.11}$$
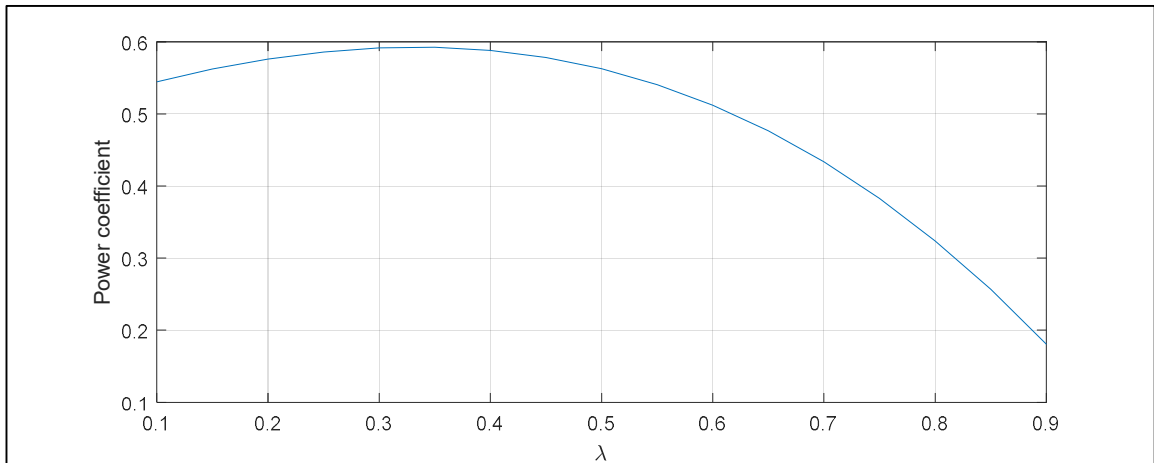
Figure 2.14. Power coefficient curve

Wind speeds are usually measured with anemometers at heights between 10 to 50 meters. However, the wind turbines can be placed more than 80 meters from the ground nowadays. Therefore, to estimate power generation accurately, it is necessary to calculate the wind speed at the turbine height. The relationship between wind speed and height can be expressed by the power-law given below, which is the commonly used formula in the literature. It is given as

$$U = U_0 * \left(\frac{h_t}{h_0}\right)^{\alpha} \tag{2.12}$$

where h_t is the turbine height and h_0 is the height at which the wind speed is measured. The measured wind speed (U_0) is scaled with the ratio in (2.12) to calculated the wind speed (U) of interest. Power law coefficient, α, depends on the surface roughness which is given in Table 2.4 for different terrain types [9].

Table 2.4. Power-law coefficient of various terrain

Terrain Type	α
Lake, ocean and smooth hard ground	0.10
Foot high grass on the level ground	0.15
Tall crops, hedges, and shrubs	0.20

A wooded country with many trees	0.25
A small town with some trees and shrubs	0.30
City area with tall buildings	0.40

2.3. WIND POWER PLANT USED IN THE THESIS

In this thesis, two closely located wind farms are investigated. The first wind farm is Soma Wind Power Plant (WPP), and it is located in Soma district of Manisa. In 2009, the first 20 wind turbines were commissioned, and electricity production was started with 18 MW capacity. Today, it is operated by Polat Energy and has installed capacity of 240.10 MW, which is the largest capacity among WPPs in Turkey. There are 169 WTs which generate energy with a yearly average of 486 GWh and can meet all the electrical energy needs of the daily life of 146987 people (housing, industry, metro transportation, official flat, environmental lighting). The installed capacity of the plant is planned to be increased to 672.7 MW by adding 103 wind turbines with 4.2 MW capacity. After this addition, Soma WPP is expected to be the eighth largest wind farm all over the world.

Sayalar WPP, which is the other farm used in this study, is located in Kırkağaç district of Manisa. It is established by a joint venture of the Polat Energy and Demirer Energy, and it has an installed capacity of 57.2 MW provided by 48 Enercon wind turbines. Sayalar WPP can meet all electrical energy needs of 33188 people in daily life with a yearly average of 110 GWh of electricity. The general specifications of both WPPs are given in Table 2.5.

Table 2.5. Specifications of WPPs used in this thesis

Farm Name	Total Installed Capacity (MW)	Turbine Manufacturer	Turbine Model	Turbine Power	Number of Turbines
Soma WPP	264.1	Enercon	E-70/ E-44	2 MW/ 0.9 MW	80/ 89
Sayalar WPP	57.2	Enercon	E-70/ E-44	2 MW/ 0.9 MW	10/ 38
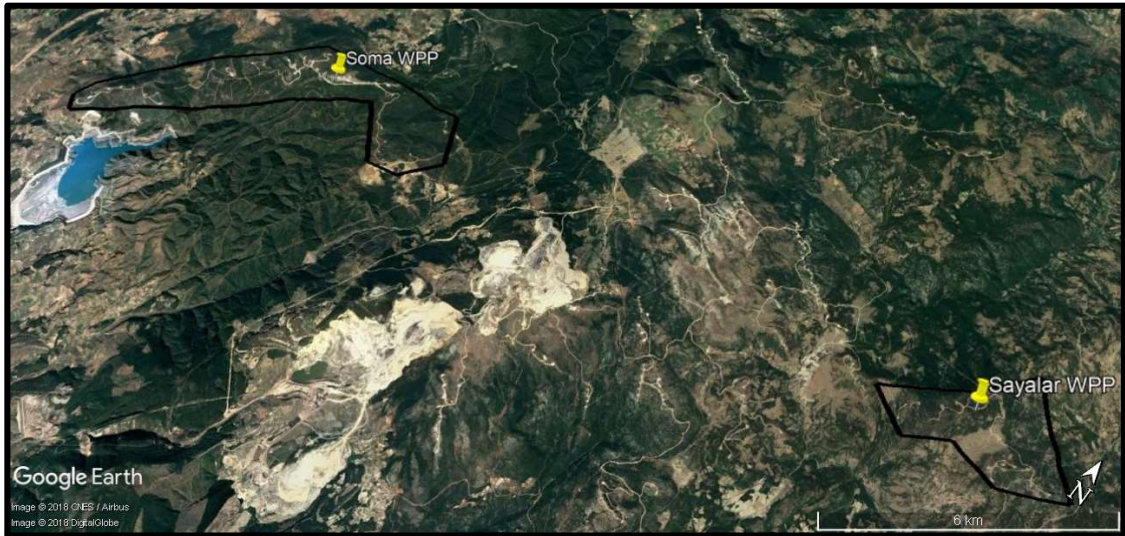
Figure 2.15. Location of wind farms

As mentioned above both wind farms consists of Enercon turbines. From Table 2.6, where different wind turbine manufacturers having sales in Turkey are shown together with data related to market shares, it can be seen that Enercon is the third-largest supplier in Turkey [10].

Table 2.6. List of manufacturers of wind turbines in Turkey

Manufacturer	Country	Number of Turbines	Installed Power (MW)	Market Share (%)
Nordex	Germany	651	1642.55	24.89
Vestas	Denmark	578	1528.25	23.16
Enercon	Germany	766	1264.50	19.16
GE	USA	436	1019.95	15.46
Siemens	Germany	241	640.85	9.71
Gamesa	Spain	81	154.3	2.34
Sinovel	China	96	108	1.64
Suzlon	India	52	106.25	1.61
Acciona	Spain	20	58	0.88
Alstom	France	29	60	0.91
Senvion	Germany	1	3	0.05
Unison	South Korea	2	1.25	0.02
Northel	Türkiye	7	0.82	0.01
Ayetek	Türkiye	1	0.5	0.01

Shriram	India	1	0.25	0.00
Other/Unknown		5	10.25	0.16

Because the wind farms are built in large areas, the topology of the terrain mostly varies. Thus, more than one kind of wind turbine can be installed in the same wind farm in order to increase efficiency. For this reason, two different wind turbines which are E44 and E70 were used in both wind farms. These are designed as upwind HWAT with three blades since they are more efficient, more aesthetic, less noisy and exposed to mechanical stresses less as explained in Section 2.1 and Table 2.3. Also, they operate at variable speed with a direct-drive generator. The characteristics and the power curves of these wind turbines are given in Table 2.7 and Figure 2.16, respectively [11].

Table 2.7. Technical specifications of wind turbines used in the thesis

Model	E44	E70
Rated power	900 kW	2000kW
Rotor diameter	44 m	70 m
Swept area	$1521\ m^2$	$3849\ m^2$
Power density	$1.69\ m^2/kW$	$1.93\ m^2/kW$
Cut-in wind speed	$3\ m/s$	$2.5\ m/s$
Rated wind speed	$17\ m/s$	$14\ m/s$
Cut-off wind speed	$25\ m/s$	$25\ m/s$
Generator Type	Direct-drive synchronous	Direct-drive synchronous
Hub Height	50 m	80 m
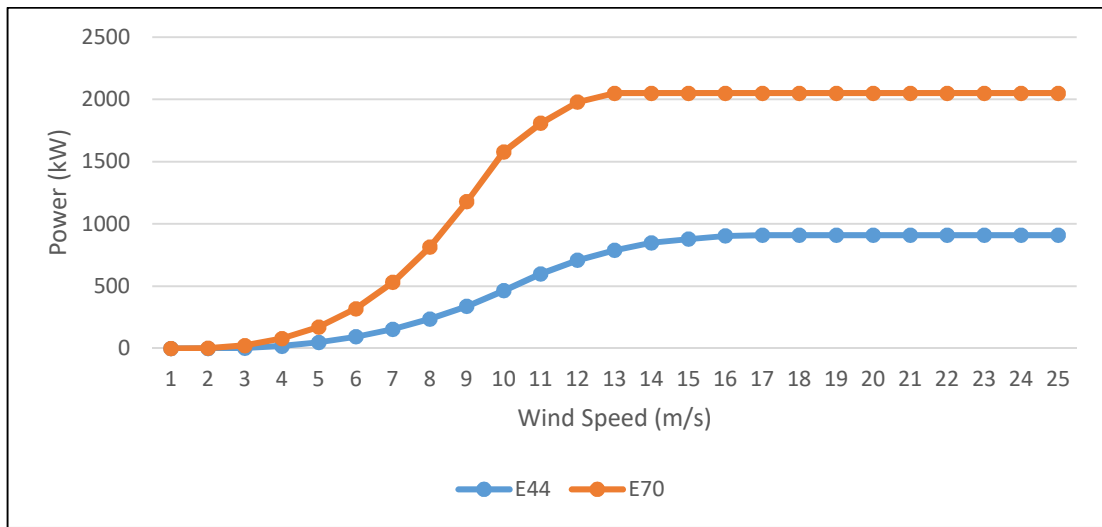
Figure 2.16. Power curves of wind turbines used in the thesis

The power efficiency coefficient C_p appearing in Equation (2.11) is a non-linear function of wind speed and depends on the turbine used. In general, it is difficult to derive an exact formula for C_p. Thus, the power curves can be approximated by a piecewise function as given in Equation (2.13). As can be seen from Equation (2.13) and Figure 2.16, WTs can not generate energy if the wind speed is less than the cut-in speed, U_{cutin}, and can generate electricity at maximum power, i.e., rated power, for speeds exceeds rated wind speed, U_{rated}, till the cut-off speed, U_{cutoff}. On the other hand, the power output is a nonlinear function, which is represented as $P_W^{nl}(U)$ between cut-in and rated speed. In order to approximate this function, different approaches are employed in practice [12].

$$P_W = \begin{cases} 0 & U < U_{cutin} \\ P_W^{nl}(U) & U_{cutin} \leq U \leq U_{rated} \\ P_W^{rated} & U_{rated} < U < U_{cutoff} \end{cases} \quad (2.13)$$

One approach is to use linear [13, 14], quadratic [15, 16] or cubic [15, 16] polynomials. Analytical expressions of the polynomial approximations up to third-degree can be obtained from turbine parameters rated power, cut-in speed and rated wind speed, as shown between Equations (2.14) - (2.16).

$$P_W^{nl}(U) = P_W^{rated} \left(\frac{U - U_{cutin}}{U_{rated} - U_{cutin}} \right) \quad (2.14)$$

$$P_W^{nl}(U) = P_W^{rated} \left(\frac{U - U_{cutin}}{U_{rated} - U_{cutin}} \right)^2 \qquad (2.15)$$

$$P_W^{nl}(U) = \frac{P_W^{rated} U^3}{U_{rated}^3 - U_{cutin}^3} - \frac{P_W^{rated} U_{rated}^3}{U_{rated}^3 - U_{cutin}^3} \qquad (2.16)$$

Although these approximations can be obtained from turbine parameters, they usually do not represent the actual curve well, as can be seen from Figure 2.17. Thus, in order to have an accurate approximation, one can use a higher-order polynomial as in Equation (2.17) and estimate its parameters by fitting the curve to a given wind power data [17, 18].

$$P_W^{nl}(U) = a_0 + a_1 U + a_2 U^2 + \cdots + a_{n-1} U^{n-1} + a_n U^n \qquad (2.17)$$

Alternatively, instead of using a single polynomial, one can use spline interpolation. In this method, a polynomial is fitted between each adjacent data points. These polynomials can be linear, quadratic or cubic. While the parameters of the quadratic and cubic spline polynomials should be fitted for the data points, linear spline polynomials can be formulated easily using the Equation (2.18) without any polynomial fitting. As can be seen from Figure 2.17, linear spline interpolation method adequately represents the function $P_W^{nl}(U)$ given in the Equation (2.13) within the mentioned methods. Thus, in this thesis, linear spline interpolation is used for wind power output calculations of the WTs used.

$$P_W^{nl}(U) = \begin{cases} P(U_0) + \dfrac{P(U_1) - P(U_0)}{U_1 - U_0}(U - U_0) & U_0 \leq U \leq U_1 \\[2mm] P(U_1) + \dfrac{P(U_2) - P(U_1)}{U_2 - U_1}(U - U_1) & U_1 \leq U \leq U_2 \\ \qquad\qquad\qquad \vdots \\ P(U_{n-1}) + \dfrac{P(U_n) - P(U_{n-1})}{U_n - U_{n-1}}(U - U_{n-1}) & U_{n-1} \leq U \leq U_n \end{cases} \qquad (2.18)$$
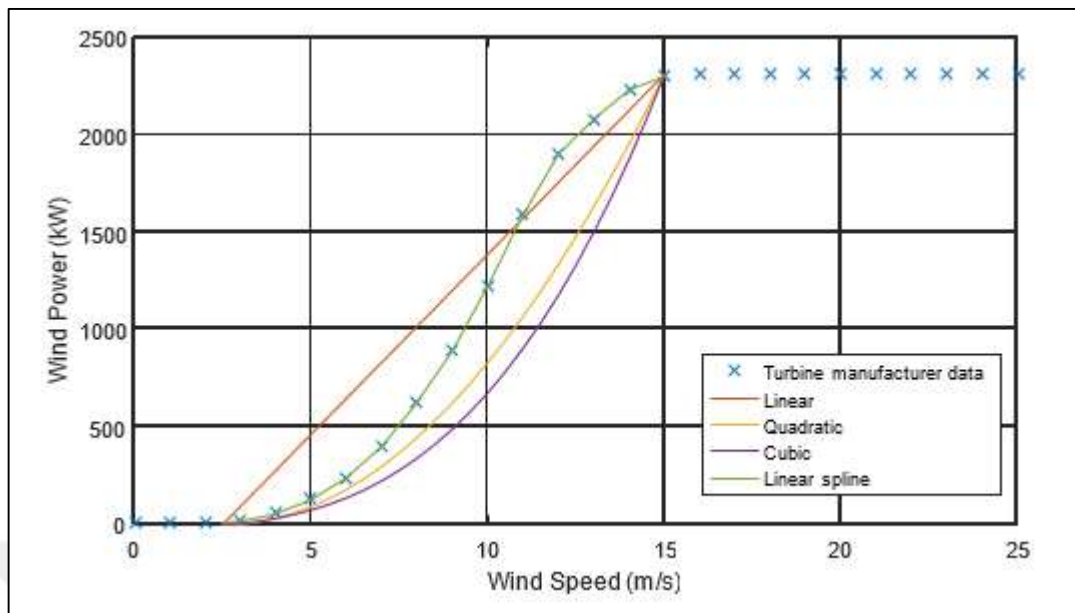
Figure 2.17 Comparison of approximation methods

3. AN OVERVIEW OF ENERGY STORAGE SYSTEMS

Today, most of the energy needs in the world are met by using conventional energy sources such as coal, natural gas, and oil. On the other hand, fossil fuel reserves are limited in the world and are gradually depleting due to increasing energy demand. Also, the use of conventional fuels causes a significant increase in greenhouse gas emissions and, consequently, results in global warming. Therefore, the importance of renewable energy systems, especially solar and wind-based systems, is increasing day by day. However, many of the renewable energy sources are extremely dependent on natural conditions. Therefore, the energy generated by these sources can vary in seasonally, daily or even instantly.

Energy Storage Systems (ESS) may bring essential benefits to conventional and renewable energy generation systems. In conventional energy systems, they can support system stability by responding to sudden changes in energy demand and renewable generation. In renewable systems, they can be utilized for reducing costs due to energy imbalances. On the other hand, in a market environment, both systems can benefit from energy arbitrage and earn higher profit. Moreover, it can help in meeting peak energy demand in the network.
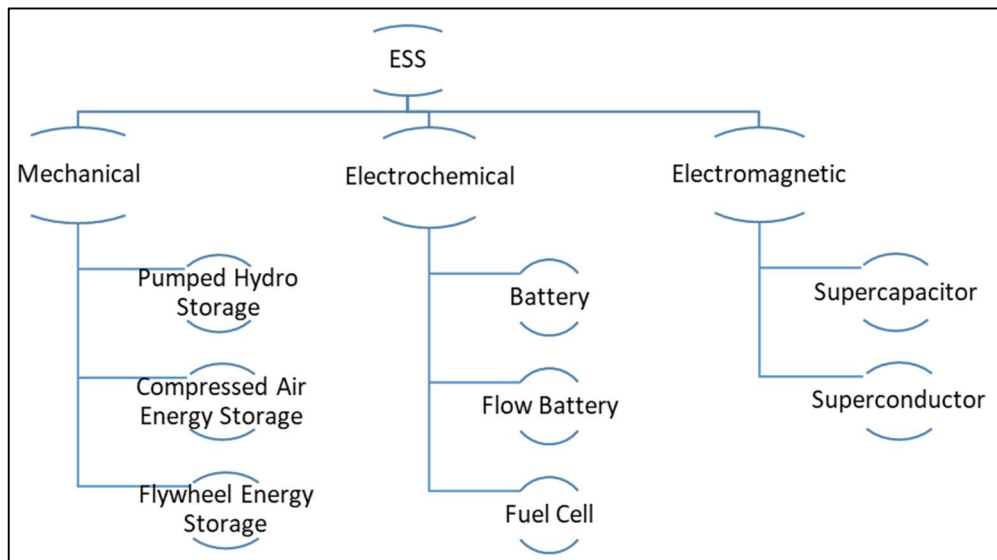
Figure 3.1. Energy storage systems

There are different types of energy storage technologies, which are mostly classified based on the form of the energy stored, as can be seen from Figure 3.1. Depending on the

application, one may choose a suitable technology by taking into account different factors such as response time, storage capacity, lifetime, etc. A detailed description of each category will be given in the following sections.

3.1. MECHANICAL ENERGY STORAGE

3.1.1. Pumped Hydro Storage System

Pumped Hydro Storage (PHS) system is the most mature, widely used and large scale ESS technology in the world. The components of a PHS are given in Figure 3.2. It is composed of two water reservoir located at different levels from the ground. The energy is stored by pumping water to the upper reservoir while it is discharged by releasing water from the upper reservoir. The amount of energy accumulated depends on the height difference as well as the volume of the water. There exist PHS systems at different capacities ranging from 1 MW to 3003 MW. Also, their cycle efficiency varies between 70-80 percent. Generally, a PHS system has a lifetime of more than 30 years [1]. In addition to these advantages, the self-discharge is very low with respect to the other ESS types. Due to their characteristics, they can be used for energy shifting, frequency control and reserve purposes. However, there are some drawbacks of PHS. The first is the necessity of finding closely located reservoirs with sufficient elevation between them. Also, the construction time is long. The detailed explanations about the PHS system will be given in Section 4.
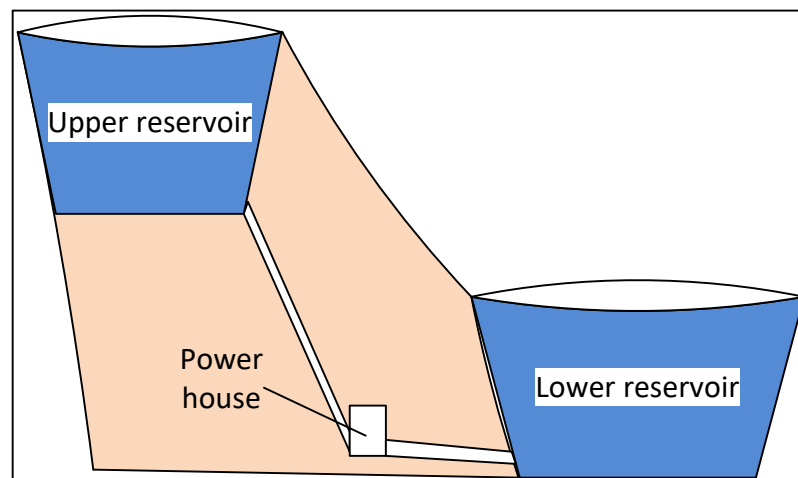
Figure 3.2. Schematic diagram of a PHS system

3.1.2. Compressed Air Energy Storage

A Compressed Air Energy Storage (CAES) system stores the energy in the form of high-pressure air. Schematic diagram of a CAES system is shown in Figure 3.3. The system is composed of a generator, motor, compressors, turbines, coolers, combustion chambers and underground cave or tanks. In order to store energy, the air can be compressed and filled into a storage unit, which can be an underground cave or vessel. The energy stored in this way can be retrieved later by heating the air and passing it through the turbines.
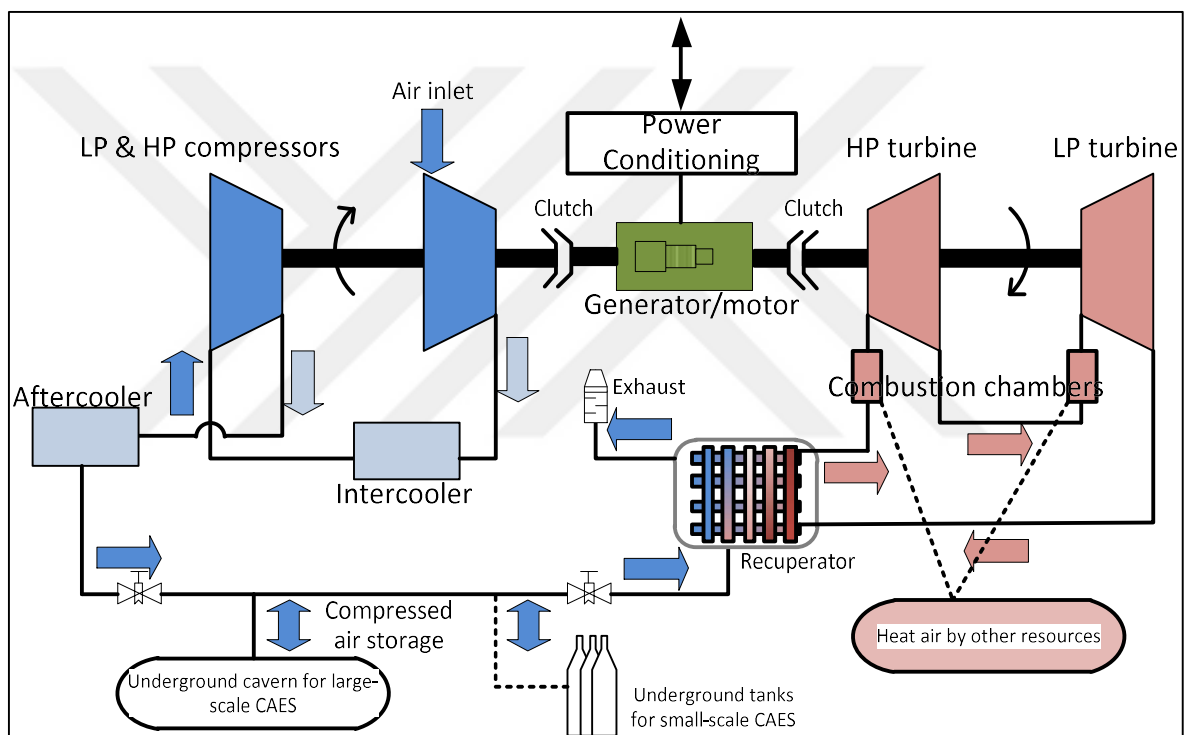
Figure 3.3. Schematic diagram of a CAES system

The CAES systems are not widely used in large scale, and there were only two operating CAES system in 2017 with a power capacity of 110 MW and 290 MW in Germany and USA, respectively [19]. However, a CAES power plant is being constructed in the USA with a 2700 MW installed power. The net efficiency of a typical CAES plant is between 40 percent and 75 percent with an expected lifetime of 40 years [1]. Due to the low self-discharge rate, it is suitable for long-term storage. Also, it can be used for black-start service for nuclear power plants, smoothing the power output of renewable power plants, cheap peak power and frequency and voltage control. However, this system has a short discharge time

at rated power because of its small storage capacity. A notable example of short discharge time is the CAES system in Germany with two hours. The other drawback of building a large-scale CAES system is finding a suitable geographical location because the main investment cost of the plant is dependent on the type of underground cave.

3.1.3. Flywheel Energy Storage

A Flywheel Energy Storage (FES) system stores electrical energy in the form of rotational kinetic energy. The flywheel is placed in a vacuum chamber with magnetic bearings and generator/motor unit. Figure 3.4 illustrates a cross-sectional diagram of the FES. During the periods of low energy demand, the surplus energy is used to accelerate the flywheel. Whenever necessary, the stored energy in the flywheel is transferred to the grid by reducing its rotational speed. The flywheels can be classified according to their rotational speeds. An FES with rotation speed less than 10,000 rpm is more suitable for a shorter period of storage with high power capacity, while the higher rotation speed FESs are suitable for the opposite case [20].
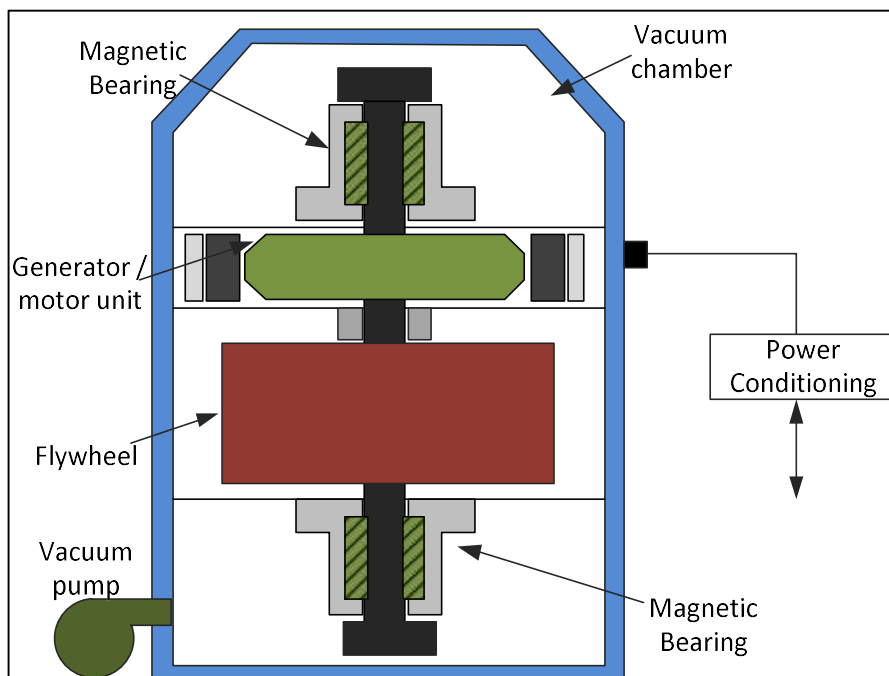
Figure 3.4. The schematic diagram of an FES system

A key aspect of FES is that it can react in short periods, such as milliseconds. Due to this fast response characteristics, it is suitable for frequency regulation and can be used as a UPS. Also, they have high energy efficiency (approximately 85 percent), long service life (about a hundred thousand discharges and 15 years) and low levels of environmental impact [1]. The most important disadvantages of flywheel systems are their high prices and the self-discharge rates. The idle period energy losses of flywheels can reach 10 percent per hour. Therefore, flywheel systems are not suitable for long-term energy storage.

3.2. ELECTROCHEMICAL ENERGY STORAGE

3.2.1. Battery Energy Storage (BES)

Batteries are one of the oldest devices for storing electrical energy. They store the energy in the form of electrochemical energy. Figure 3.5 shows the components and operational principle of the BES. A battery consists of one or more series or parallel connected electrochemical cells to provide the desired voltage and capacity. Each cell is composed of positive and negative electrodes, i.e., cathode and anode, respectively, with an electrolyte in solid or liquid form. Batteries are discharged by the chemical reactions that occurred in the electrolyte. By these chemical reactions, electrons are transferred from the anodes to cathodes. The reverse chemical reactions which are occurred by applying electrical energy charges the battery.

Different types of batteries are available for energy storage such a lead-acid, Nickel Cadmium (NiCd), Nickel Metal Hybrid (NiMH), Lithium-Ion (Li-ion), and Sodium Sulphur (NaS) batteries. They have different rated power ranging from 100W to several megawatts with efficiency between 60 percent to 90 percent [1]. Rapid response time of batteries makes them suitable for tracking instant load variations. Due to their cost and smaller sizes, batteries have a significant advantage over PHS and CAES. However, most of the batteries lead to environmental problems because of the toxic materials they contain. Also, limited lifetime usually makes them unsuitable for large-scale applications.
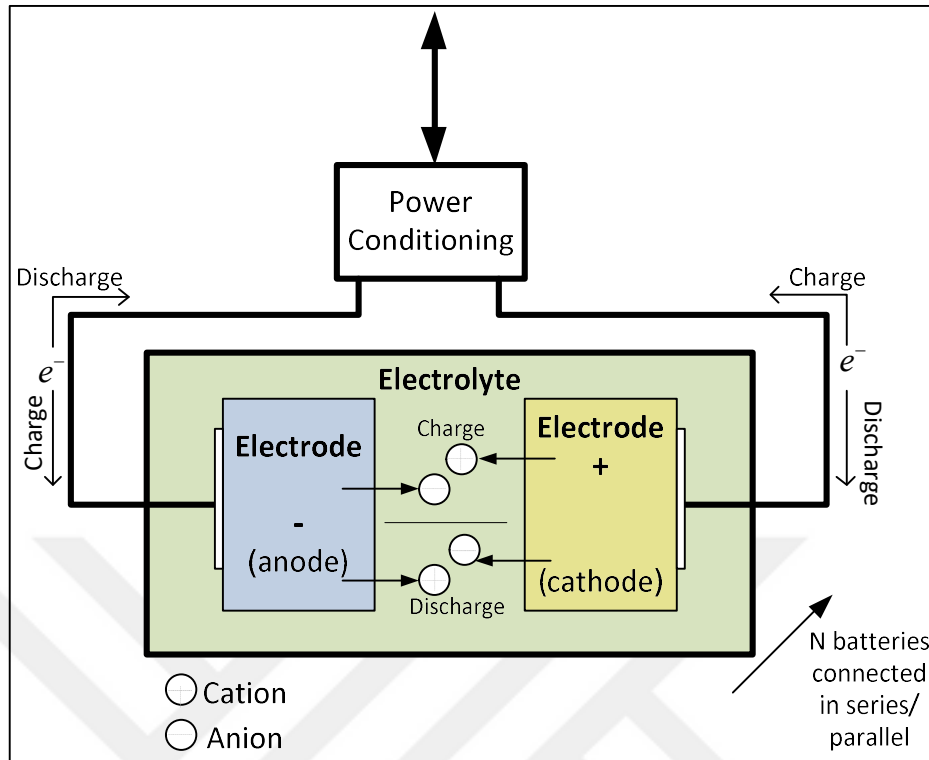
Figure 3.5. The schematic diagram of a BES system

3.2.2. Flow Batteries Energy Storage (FBES)

In flow batteries, unlike the conventional batteries, energy is stored in electrolyte solutions which are stored in different tanks. The user can set the energy capacity or power level by simply changing the amount of liquid in the containers. As can be seen from Figure 3.6, the electrolyte solutions are pumped into the cell stack where chemical reactions occur. During the discharge process, the cathode electrolyte is oxidized, and the positively charged ions pass through the ion-selective membrane. The process is reversed during the charging operation.

The FBES systems have not been fully commercialized since they have a low energy density, a narrow operating temperature range and high investment cost [21]. On the other hand, the energy capacity can easily be adjusted by increasing the volume in the reservoirs. Another essential advantage of the flow batteries is having a very small self-discharge because the electrolytes are stored in the separate tanks. Thus, FBES systems are suitable for long-term

energy storage. According to research and development studies, fluid batteries can be used in large-scale projects and economically better than other types of batteries in the future [22].
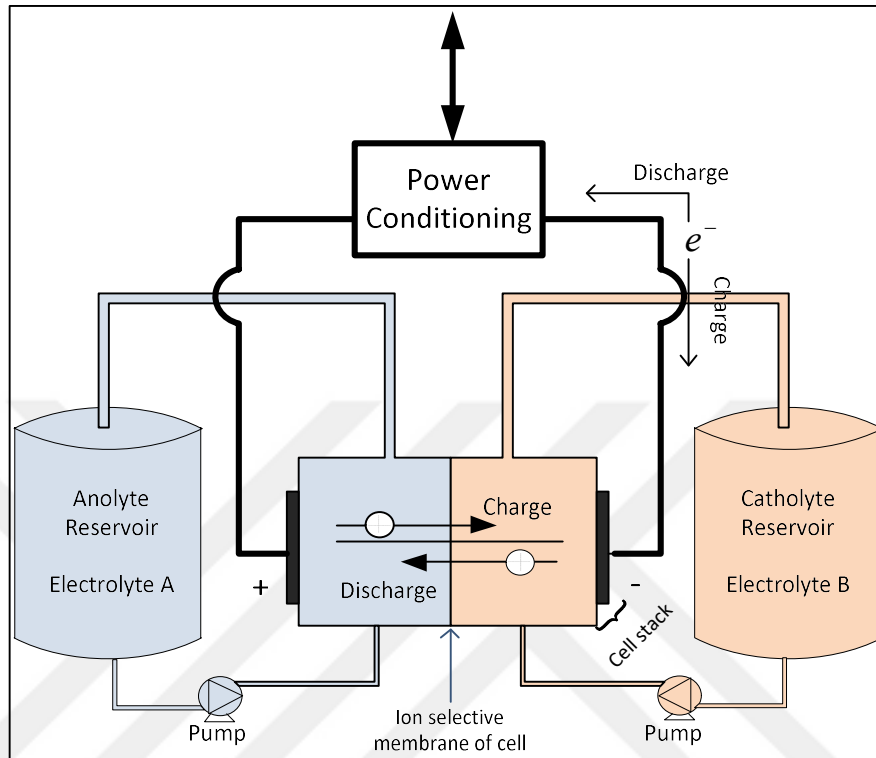
Figure 3.6. The schematic diagram of FBES system

3.2.3. Fuel Cells

Fuel Cells (FC) constitute another alternative to the batteries. FCs convert the chemical energy in the fuel with oxidants. Different types of fuel and oxidants can be used like methane, hydrocarbons, methanol. However, hydrogen is commonly preferred as fuel. For a hydrogen fuel cell, which is shown in Figure 3.7, the fuel is hydrogen, and the oxidizer is oxygen. The fact that they are very high in terms of energy density and that only water and heat emerge when they are burned is their significant advantages, whereas they have a relatively high cost, low power density, and low efficiency.
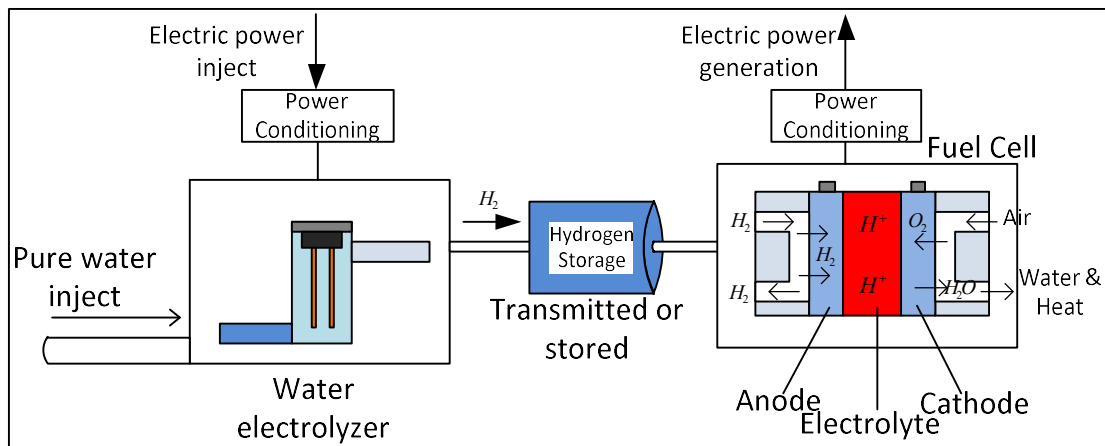
Figure 3.7. The schematic diagram of hydrogen storage and FC

3.3. ELECTROMAGNETIC ENERGY STORAGE

3.3.1. Supercapacitors

Supercapacitors, i.e., ultracapacitor, are based on the same principle with classical capacitors as can be seen from Figure 3.8. They store electrical energy directly without converting into any other form. However, they can store a large amount of energy when compared with ordinary capacitors. Moreover, their fast charge/discharge periods, long lifetimes and high efficiency (approx. 85-98 percent), makes them preferable alternative to other ESS [23]. One of the challenges facing supercapacitors is to increase its energy density. Also, their installation cost and daily self-discharge are high, which makes this system suitable for short-term storage applications.
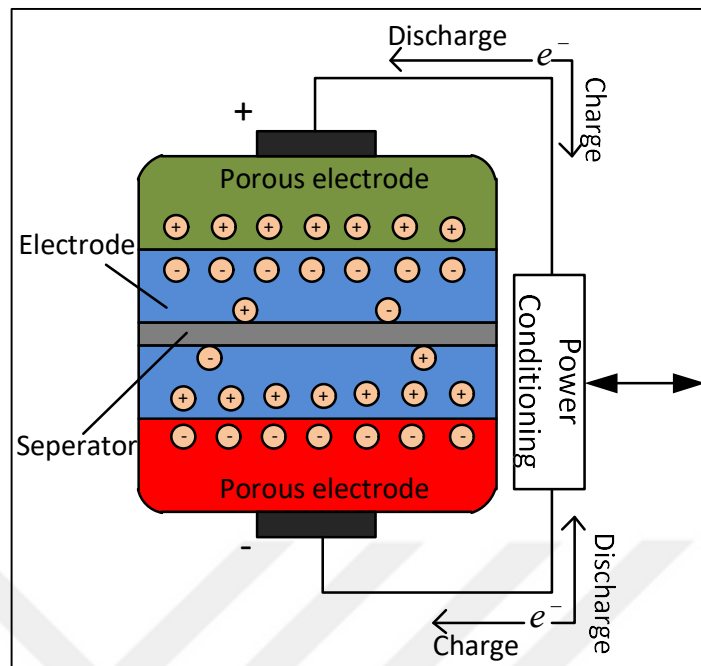
Figure 3.8. The schematic diagram of supercapacitors

3.3.2. Superconduction Magnetic Energy Storage

Superconduction Magnetic Energy Storage (SMES) system stores the energy in the magnetic field generated by direct current in a superconducting coil. A classic SMES system is composed of a superconducting coil unit, refrigeration, and vacuum system, as shown in Figure 3.9. In this system, a superconducting coil manufactured from mercury, vanadium or Niobium–Titanium is used to store energy. Energy stored in the magnetic field formed in the coil can be discharged at the desired time. Electrical energy can be stored with almost zero loss because it is not dissipated as heat when the temperature is reduced below the superconducting critical temperature by the refrigerator system. This makes the cycle efficiency approximately 95-98 percent [23]. Also, SMES systems have fast response times (milliseconds) and very long cycle life (100,000 cycles). Their significant drawbacks are high capital costs, high daily self-discharge (10-15 percent), and the environmental disturbance arising from the strong magnetic field. Also, the temperature of the superconducting material has to be controlled precisely in order to keep the energy efficiency stable.
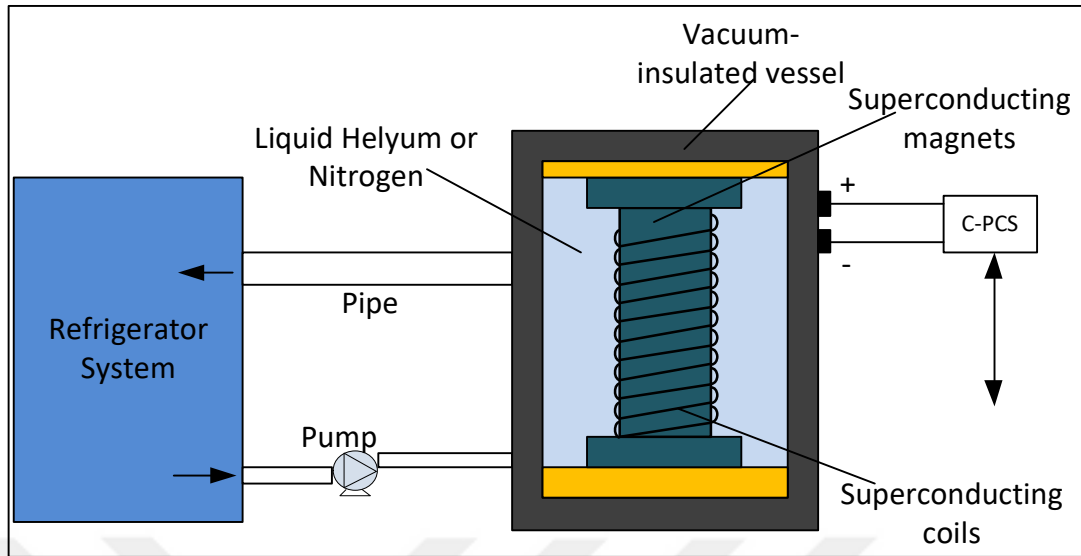
Figure 3.9. The schematic diagram of a SMES system

3.4.   COMPARISON OF ESS TECHNOLOGIES

For comparing ESSs, one needs to take into account their installation cost and operating cost, power capacity, generation rating, self-discharge rate, efficiency, response time, lifetime and cycle time [1]. The cost of an ESS is one of the most significant aspects of commercial usage. A comparison of ESSs described above is given in Table 3.1 based on their costs [20]. The total cost of an ESS should be analyzed based on both installation and operating costs. The primary source of the operating cost is energy generation. However, maintenance, disposal and replacement fees should be included as well.

With respect to energy capital cost ($/kWh), PHS and CAES systems are the most promising energy storage units. CAES has a lower energy capital cost while its power capital cost is higher with respect to PHS. Energy capital cost of FES and SMES are very high per kWh, but their operation and maintenance costs are very low relative to other storage systems which shows that these two systems are suitable for applications which require high power output for a short duration. FCs have both the highest installation and maintenance costs since they are still in the development stage for commercial use. As a result, when Table 3.1 is analyzed, it is clear that the PHS systems are the most suitable system among the ESSs.

Table 3.1. Capital costs of ESSs

Type	System	Installation Cost		Operating and Maintenance Cost ($/MW h and per cycle)
		Power capital cost ($ /kW)	**Energy capital cost ($/kW h)**	
Mechanical	*PHS*	600–2000	5–100	0.1–1.4
	CAES	400–8000	2–50	2–4
	FES	250–350	1000–5000	3–25
Battery	*LA*	300–600	200–400	20–100
	NiCd	500–1500	800–1500	20–100
	Li-on	1200–4000	600–2500	15–100
	NaS	1000–3000	300–500	8–20
Flow Battery	*VRB*	600–1500	150–1000	5–80
	ZnBr	700–2500	150–1000	5–80
Chemical	*FC*	10000+	-	6000–20000
Electromagnetic	*SC*	100–300	300–2000	2–20
	SMES	200–300	1000–10000	1-2

In addition to the costs of the ESS, one needs to take into account technical characteristics such as power rating, response time, efficiency, self-discharge rate and lifetime as well. These characteristics are given in Table 3.2 for the ESS investigated [1]. The power rating, which includes the power capacity and nominal discharge time at the rated power determines the general application area of the ESS. The ESS which has enormous power capacities like CAES and PHS are appropriate for large-scale storage. Moreover, the long discharge time indicates that the system can be used in arbitrage and energy shifting. In addition to power rating, self-discharge of the storage devices determine the storage duration, which is an important factor for selecting an appropriate system in applications. Because the ESSs like PHS, CAES, NaS, and flow battery systems have a low self-discharge rate, they are suitable to store energy for months. However, supercapacitors, SMES and FES can only be used for short time storage. Some applications like frequency regulation and oscillation damping require an almost immediate energy release from the ESS. FES, battery and electromagnetic storage systems are suitable for these applications because they have response times of orders of milliseconds. Another essential characteristic of an ESS is the efficiency (round trip efficiency) which is the ratio of the energy output to the input in a storage cycle. It is a measure of losses incurred with the charge and discharge of energy. While the systems

having high-efficiency are suitable for the applications in which charging and discharging takes place frequently, systems having low efficiency are mostly used for energy arbitrage applications which have long charge/discharge duration. Finally, the lifetime has also an essential role in ESS selection. The lifetime can be measured in different units, years or cycles.

Table 3.2. Technical characteristics of ESS

	Power Rating		Response time	Efficiency (%)	Self-discharge per day (%)	Lifetime	
	Power capacity (MW)	Discharge time at power rating				Years	Cycles
PHS	1-3000	1–24h+	min	70–80	Very small	30-50	20000-50000
CAES	5– 300	1–24h+	min	40–75	Small	30-40	10000-30000
FES	0–0.25	s–h	<s	80–90	100	15–20	>100000
LA	0–20	s–h	<s	75–90	0.1–0.3	3–15	250-3500
NiCd	0–40	s–h	<s	60–80	0.2–0.6	5–20	1500-3500
Li-on	0–0.1	min–h	<s	65–75	0.1–0.3	5–10	1500-3500
NaS	0.05–8	s–h	<s	70–85	Very small	10–15	2500-4500
VRB	0.03–3	s–10h	s	60–75	Small	5–20	1000-13000
ZnBr	0.05–2	s–10h	s	65–75	Small	5–10	1000–3650
FC	0– 50	s–24h+	s–min	34–44	0	10–30	>2000
SC	0–0.3	ms–1h	<s	85–98	5-20	4–12	>50000
SMES	0.1–10	ms–8s	<s	95–98	10–15	>20	>100000

3.5. ESS IN THE WORLD

In mid-2017, the total ESS capacity was 176 GW globally [24]. IRENA also reported that the PHS systems were by far the most widely used systems. Their installed capacity was approximately 169 MW. This was followed by the thermal storage with 3.3 GW constituting

1.4 percent of the total installed capacity. Among the thermal storage systems, molten salt technologies were dominating in this type with a share of 75 percent. Although electrochemical storage systems were one of the most promising storage devices, their installed capacity was only 1.9 GW. Among them, Li-on batteries were the most preferred units (59 percent). Mechanical storage systems other than PHS had a 1.6 GW (1 percent) installed capacity and the two technologies of this type have similar shares in the world storage capacity. The share of other storage units can be found in Figure 3.10.
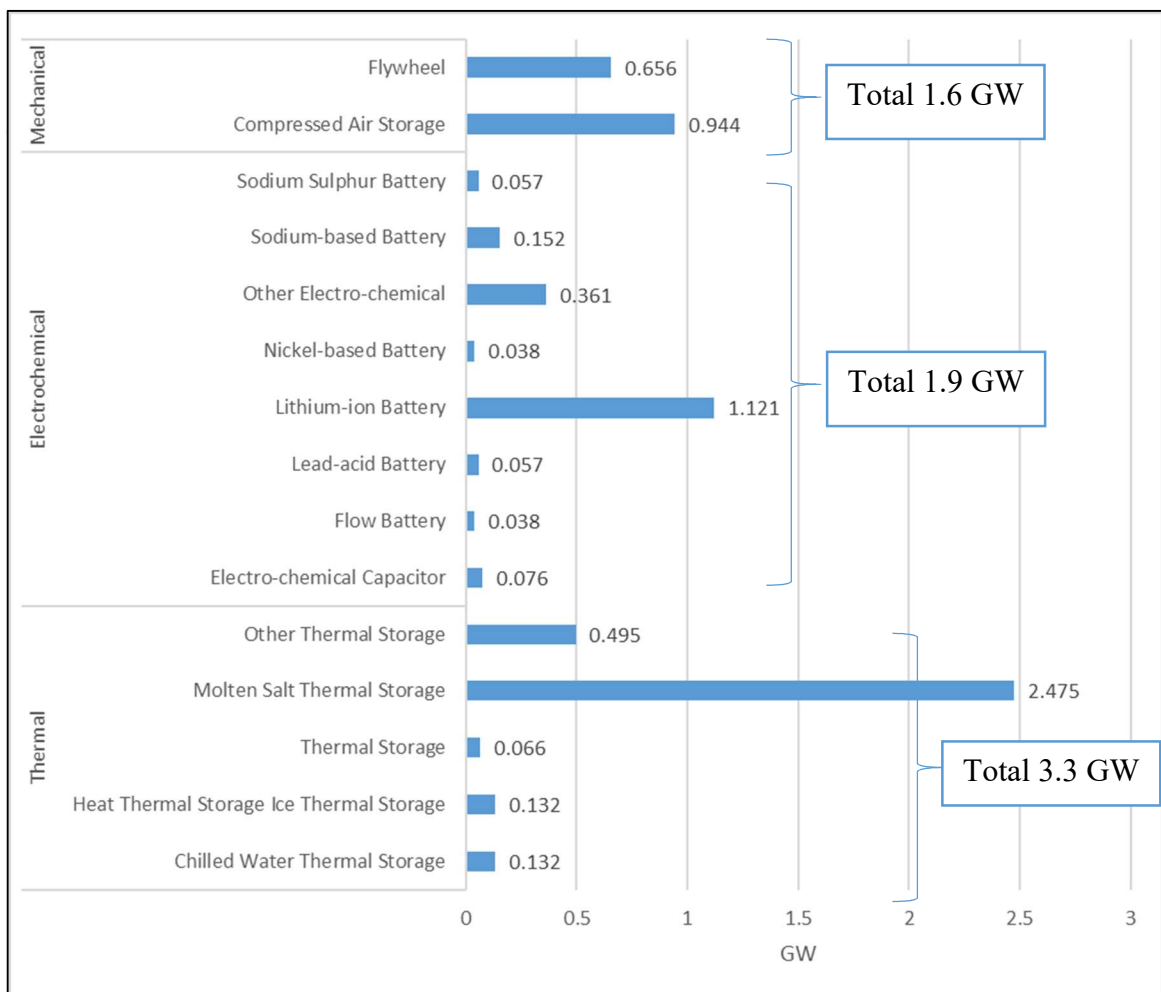
Figure 3.10. Installed capacity of ESS in the world (in 2017)

4. PUMPED HYDRO STORAGE SYSTEMS

In this chapter, PHS systems are investigated because they are the type of storage system used in this thesis. This chapter has been divided into three parts. The first part will explain the historical background briefly. The second part presents the PHS systems in the world and Turkey, focusing on the installed and potential capacity. The PHS system used in this thesis is also explained in detail by giving its general specification in this part. The third part gives brief information about the main-use case applications of PHS systems. The forth part reviews the technical properties of PHS, which were not given in Section 3.1.1. Finally, the mathematical modeling of the PHS power plant is presented.

4.1. HISTORICAL BACKGROUND

The first known conceptual design of pumped storage was proposed in 1882 in Zurich, Switzerland. The first facility was opened in 1909 in Schaffhausen, Switzerland with a capacity of 1500 kW. Subsequent installations followed throughout Europe for the next few decades. In the 1930s, reversible pump turbines were introduced, and the first installation took place in Baldeney, Germany. Reversible turbines had lead to cost savings as much as 30 percent, but early designs were difficult to set up and hence, installation times were long. However, these difficulties are alleviated over time, and later designs evolved to the currently used turbines in 1960-1970s. After the oil crises in the early 1970s, their installation has been dramatically accelerated. PHS systems had been used for energy time-shift applications until the 1970s. In the late 1980s, the variable speed reversible Pelton turbines were developed. Although they were more expensive than the prior turbines, their efficiency was considerably better. In the 1990s, the development of PHS systems had shown a severe decline. The cheap natural gas prices directed the countries towards the natural gas power plants which replaced PHS. However, after the high penetration of the renewables, PHS become popular in the world again to compensate for energy variations due to the intermittent nature of renewable generation.

PHS system has been used as a system tool to provide energy in high load demand and to allow units of baseload plants to operate in the primary load mode during the low load

demand period. However, in countries with abundant hydro-energy capacity, PHS system has been developed to increase the efficiency of large-scale hydroelectric power plants.

4.2. PHS SYSTEM IN THE WORLD AND TURKEY

PHS systems have the highest installed capacity among all ESS alternatives, as mentioned in Section 3.5. PHS power plants are operational in 42 countries with an installed capacity of approximately 169 GW. Among these countries, Japan ranks first with 27637 MW installed capacity, which corresponds to about 10 percent of Japan's total installed power. The US built the largest PHS power plant in the world with a 3003 MW rated power in 1985 and the overall installed capacity of PHS in the US was 22441 MW in 2017. Although the current PHS installed capacity of China is 23060 MW, the potential of PHS is increasing rapidly. China is currently constructing a PHS power plant with 3600 MW capacity, which is expected to be the largest PHS in the world when it is finished. PHS capacities of ten countries with the highest installed capacity in the world are given in Figure 4.1.
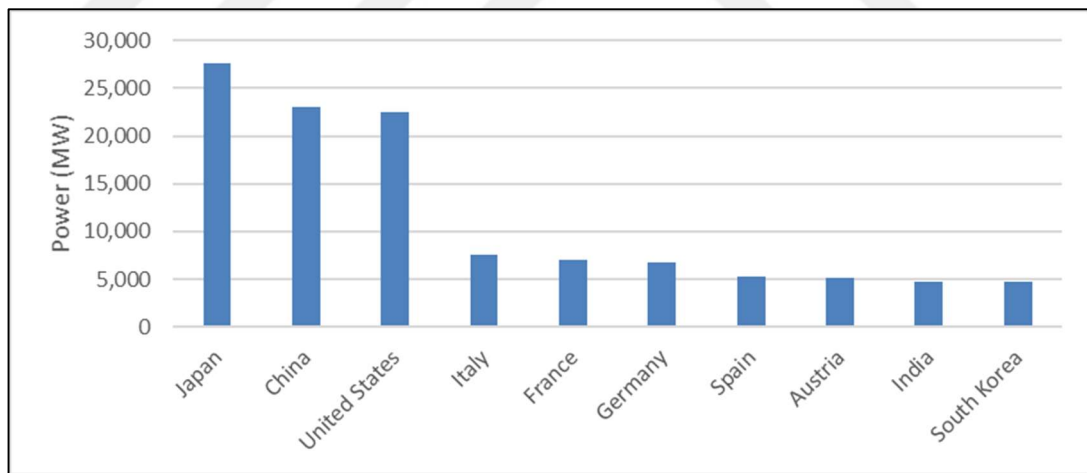
Figure 4.1. Installed PHS capacity of the top ten countries (in megawatts)

Considering the regions in the world, installed energy capacities were 3376 MW in Africa, 7541 MW in South and Central Asia, 66454 MW in East Asia and Pacific, 1004 MW in South America, 51769 MW in Europe, 22986 MW in North and Central America at the end of 2017 [25].

Among all regions, Europe has the second largest capacity, and PHS systems have been operational in Europe since the 1970s. More than 50 percent of these facilities are located in Germany, Italy, Spain, and France, and the PHS system in European countries can be ranked according to their installed power as shown in Figure 4.2. Italy has the largest capacity with 7.6 GW, which is followed by France, Germany, Spain and Austria.
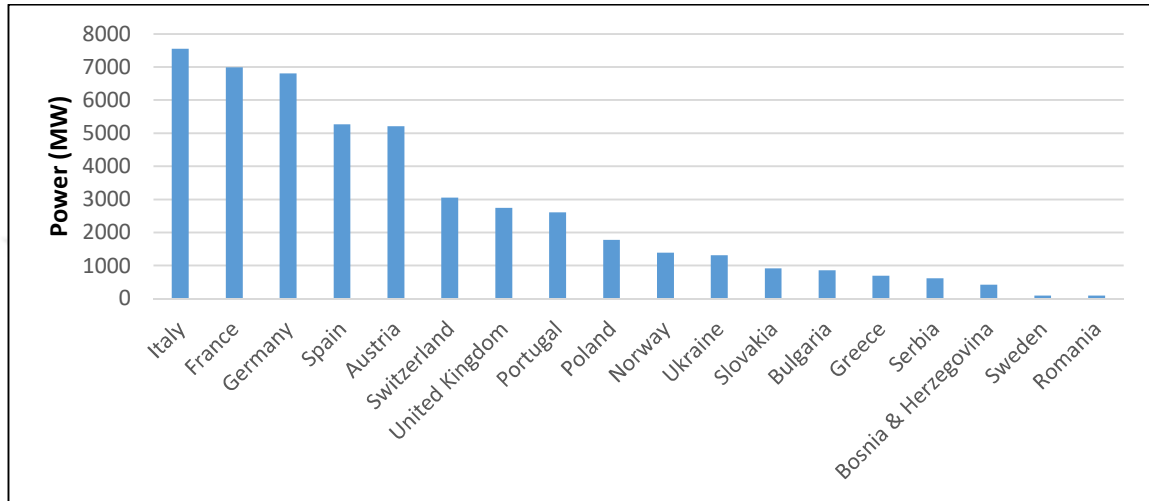
Figure 4.2. PHS capacity of selected European countries in 2017 (in megawatts)

Despite all this installed power, Gutiérrez and Arántegui reported that only 10 percent of the PHS potential had been used in most of the regions of Europe [26]. In this study, the PHS potential given in Table 4.1 was determined by theoretical and realizable capacities of two different scenarios. The scenarios were chosen based on the existing (T1) and existing and prospective (T2) reservoirs.

Table 4.1. PHS potential in Europe

Country	T1 theoretical (TWh)	T1 realizable (TWh)	T2 theoretical (TWh)	T2 realizable (TWh)
EU	12100	4111	67197	37059
Turkey	36829	19635	45351	32660
Other	6215	5082	26005	20433
TOTAL	55144	28828	138553	90152

In Table 4.1, Turkey is shown separately for comparison. Turkey has nearly two times more potent than the total potential of all other countries in Europe in T1 reasonable scenario. However, there is no PHS plant in Turkey despite that potential because the use of PHS in a country is directly related with the use of renewable energy sources such as solar and wind energy [27]. Since the installed capacity of solar and wind power in Turkey is planned to be 25 GW in 2023 [28], the importance of PHS systems in Turkey is expected to increase in the future.

In Turkey, the PHS studies were started by the Electric Power Resources Survey and Development Administration (EİE) in 2005. A feasibility analysis was carried out in several regions, and 16 candidate PHS projects given in Table 4.2 are proposed [29]. In 2011, the governments of Turkey and Japan carried out a joint project named "Study on Optimal Power Generation for Peak Demand in Turkey" [30]. This study aimed to review the development plan of reported PHS power plant projects in EİE feasibility analysis and to propose new potential sites based on technical, geological and environmental criteria. Gökçekaya PHS and Altınkaya PHS projects were selected as high-priority candidate sites. Based on this result, the conceptual design of Gökçekaya PHS and Altınkaya PHP were conducted. Final feasibility study of Gökçekaya PHS was carried out between 2014-2016 and ten years has been envisaged for the launch of Gökçekaya PHS.

Table 4.2. Proposed PHS power plants in Turkey by EİE

Name	Installed Power (MW)	Location	Discharge rate (m^3/s)	Head (m)
Kargı PHS	1000	Ankara	238	496
Sarıyar PHS	1000	Ankara	270	434
Gökçekaya PHS	1600	Eskişehir	193	962
Altınkaya PHS	1800	Samsun	350	611
İznik-I PHS	1500	Bursa	687	255
İznik-ll PHS	500	Bursa	221	263
Yalova PHS	500	Yalova	147	400
Demirköprü PHS	300	Manisa	166	213
Adıgüzel PHS	1000	Denizli	484	242
Burdur Gölü PHS	1000	Burdur	316	370
Eğridir Gölü PHS	1000	Isparta	175	672
Karacaören-ll PHS	1000	Burdur	190	615

Oymapınar PHS	500	Antalya		156	372
Aslantaş PHS	500	Osmaniye		379	154
Bayramhacılı PHS	1000	Kayseri		720	161
Yamula PHS	500	Kayseri		228	260
Hasan Uğurlu PHS	1000	Samsun		204	570

Demirköprü PHS power plant, which is chosen as the storage plant in this thesis due to its proximity to wind farms used, is expected to be built in Manisa province at the coordinates 38°39'01"N, 28°19'36"E. The upper reservoir will be a concrete covered pool with a height of 215 m. The project includes 473 m penstock, 157 m shaft and 832 m tail water tunnel. The investment cost of the project is estimated at $220,000,000 [31].

Technical data of the Demirköprü PHS power plant is provided in Table 4.3 [32]. The maximum volume of the upper reservoir is 3 hm^3. The higher gross head is taken as 215 m while the lower gross head as 205 m. The plant is assumed to have three identical reversible Francis turbines, whose characteristics are given in Table 4.3 for the generation and pumping modes.

Table 4.3. General specification of Demirköprü PHS power plant

Dam	Water storage capacity	3 hm^3
	Maximum head	215 m
	Minimum head	205 m
Turbine	Minimum energy generation of one turbine	37.3 MWh
	Maximum energy generation of one turbine	99.1 MWh
	Minimum discharge rate of one turbine	23.8 m^3/s
	Minimum discharge rate of one turbine	55.3 m^3/s
	Generation efficiency	0.87
	Energy consumption of one turbine in pumping mode	130.9 MWh
	Water pumped by one turbine in pumping mode	55.3 m^3/s
	Pumping efficiency	0.87

Figure 4.3. Demirköprü PHS power plant

4.3. MAIN-USE-CASE APPLICATIONS OF PHS SYSTEMS

According to the report published by the International Renewable Energy Agency (IRENA) [24], PHS systems can be used in many different applications, as illustrated in Figure 4.4. Among them, energy time-shifting (or arbitrage) in which energy is stored in low price periods and sold in high price periods, has the greatest share of 89 percent. This trend is expected to continue in the future with increasing penetration of renewable generation, which will increase the variation on energy prices. The generated renewable energy can be stored in off-peak periods to use at the peak power demand periods. Thus, 4 percent of the installed PHSs is utilized for peak shaving applications.

Many power plants need an initial power to start operation which can be obtained from the grid. However, when the entire electrical grid collapses, these power plants would be incapable of restarting. This leads to a need for a power plant that can restart without external power from the grid. This situation is called as black-start operation. Within different alternative power plants, the required energy for a black start can be obtained from the PHS system with its quick response ability. Approximately 3.5 percent of the generation capacity of PHS systems is used for black start operations.

In addition to the grid-based operations, 3.2 GW installed power of PHS is used for compensating the intermittent generation of renewable power plants. Also, PHS is preferred because of its low response time to stabilize the power output of wind and solar power plants. Furthermore, it can be used to eliminate the imbalance that may occur between production and load as it may damage the system in case of a sudden interruption of wind turbines.

PHS systems can provide more stable operation of the system by keeping a spinning reserve power to meet the regulation up or down requirements of the system. The spinning reserve must be synchronized to the system while it is running and able to be activated within 10 minutes if needed. There are also other applications like electric bill management, voltage support and on-site power which have a minimal share in the main-use-case applications.
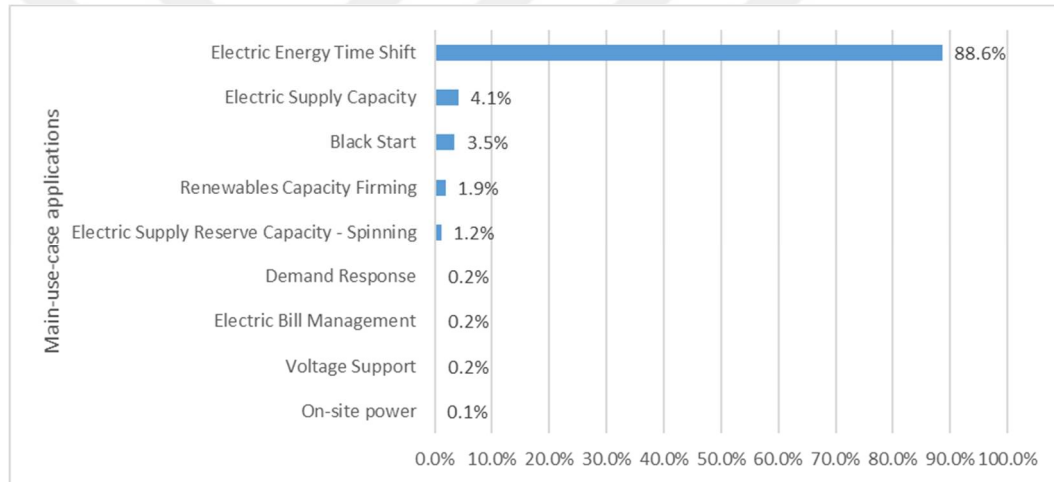
Figure 4.4. Main-use-case applications of PHS systems

4.4. TECHNICAL REVIEW OF PHS POWER PLANTS

As described in Section 3.1.1, PHS systems store energy in the form of potential energy. This storage is achieved by pumping water to an upper reservoir. The stored water can be released and converted to electricity by means of turbines. A detailed diagram of a PHS is shown in Figure 4.5. It can be seen from the figure that the PHS system is composed of the following parts.
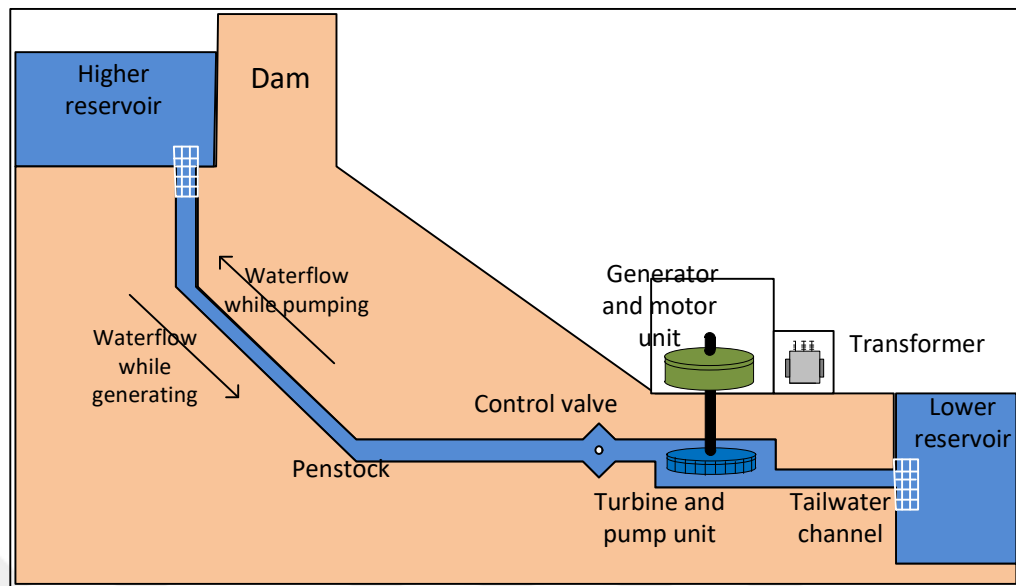
Figure 4.5. PHS system

Reservoirs: In general, a PHS system is composed of an upper and a lower reservoir. Usually, upper reservoirs can be built in three different ways. One is using a reservoir of an existing dam. Second, a reservoir can be formed by constructing a barrier around a pit on a mountain or hill. Third, an existing lake is turned into a reservoir by closing the outlet of the lake. As for the lower reservoir, they can be built much easier since an existing lake or sea can be used for this purpose.

Penstock: The long pipes that connect the pumps and turbines to the reservoirs.

Tailwater channel: It delivers turbine water to the lower reservoir and the water to be pumped is taken from the lower reservoir.

Control valve: This is an emergency valve for ensuring safety during pumping and generation.

Turbine / Pump: They can be separate or together. Turbines convert the potential energy to mechanical energy and transfer the mechanical energy to the generators through a shaft. Pumps store the water in the upper reservoir using electric energy.

Generator / Motor: They can be separate or together. The generator converts mechanical energy to electrical energy in generation mode. The motor converts the electrical energy to mechanical energy in pumping mode.

When the time scale of operation is considered, PHS systems can operate based on the daily, weekly or seasonal basis. While in the daily or weekly operation, water is pumped to the upper reservoir in the off-peak periods and used in peak periods, annual scheduling mostly depends on the flow rate of the river. The off-peak periods of daily schedule are usually between 5 h to 12 h of the day, and it is the weekend days in the weekly schedule.

When the water flow is considered, a PHS can be built in two different ways, as a closed-loop or open-loop system. The closed-loop PHS systems consist of a reservoir which does not have inflow from a river basin. The upper reservoir is filled using only water pumped from the lower reservoir. An open-loop storage hydropower plant, on the other hand, uses the natural flow from a river and water pumped from a lower reservoir. Because of this configuration, they are usually larger than the closed-loop PHS systems, and they are more suitable for weekly and seasonal operation [33]. This type of system is very similar to conventional cascaded hydroelectric power plants. The only difference is that they have pumping capabilities.

PHS systems can operate in three modes; pumping, generation or idle. In pumping mode, excess energy is stored as potential energy by pumping water from the lower reservoir to the upper reservoir. On the contrary, in generation mode, the water is released from the upper reservoir to generate energy. The idle mode means that the PHS units are not operating.

A PHS system can be classified as reversible turbines and ternary set according to the pump/turbine configuration. Reversible pump/turbine configuration is the most common and mature option [34]. With this configuration, PHS can operate only either in generation or pumping mode, which limits the flexibility of the operation. The ternary set is composed of separate turbines and pumps. This setup improves efficiency due to the separately optimized turbine and pump. Because the pumps are optimized better, the startup of the pumping is shorter in the ternary set [35]. This system can also operate in simultaneous operation with the implementation of hydraulic short-circuit setup. On the other hand, the investment cost is very high in contrast to the reversible pump/turbine configuration.

4.5. MATHEMATICAL MODELLING OF PHS SYSTEMS

There are different properties such as turbine/pump characteristics, head effects and efficiencies that one can think about when modeling a PHS system. These aspects have been investigated in the related literature [36–38] and the model introduced in [36] is employed for describing the turbine/pump characteristics in this thesis.

The storage capacity of the PHS system is determined by the water volume in the upper reservoir. PHS can operate within the lower (V_{min}) and upper (V_{max}) volume limits of the upper reservoir which can be expressed as

$$V_{min} \leq V(t) \leq V_{max} \tag{4.1}$$

where V is the water level in the upper reservoir at time t. The lower reservoir capacity can be limited or unlimited. The PHS systems which are built on islands, mostly use the sea as the lower reservoir which enables an unlimited capacity for the lower reservoir [39, 40]. On the other hand, studies consist of cascaded PHS systems [41] or PHS systems where a dam is used as a lower reservoir [42, 43] have limited lower reservoirs capacities. In that case, the lower reservoir limits can be written similar to Equation (4.1). However, since the upper reservoir capacity is very small when compared to the lower reservoir in this thesis, unlimited capacity is assumed at the lower reservoir like most of the studies.

The evolution of the water volume in the upper reservoir is given by Equation (4.2) as a first-order difference equation.

$$V(t+1) = V(t) + q_p(t) - q_d(t) + I_V(t) - S_V(t) \tag{4.2}$$

where q_d is discharged water from the upper reservoir, q_p is pumped water to the upper reservoir, $I_V(t)$ is the natural inflow into the reservoir and $S_V(t)$ is the spillage from the reservoir. If the upper reservoir is built on a river, i.e., open loop, as in the related studies [44, 45], the natural inflow and spilage can be used. However, because most of the upper reservoirs are closed loop systems, both variable $I_V(t)$ and $S_V(t)$ are neglected in most of the studies as in this thesis.

The power generation of a PHS system is similar to conventional power plants. It is a function of its discharge rate and net head. The latter is the difference between the upper and lower reservoir water levels. Therefore, the power generation can be written as

$$P_d = gq_d h_n \eta_d \qquad (4.3)$$

where g is the gravitational constant, h_n is the net head and η_d is the efficiency of the turbines in generation mode. When there is a huge head variation in comparison with respect to the total head between upper and lower reservoirs, the head effect can be modeled by equivalent energy curves as in the study [44]. On the other hand, as in this thesis, there are numerous studies in which the net head is assumed constant because of the small head variation.

In generation mode, turbines operate continuously within an allowable power and discharge rate ranges and which are given as

$$\underline{P_d} \le P_d \le \bar{P}_d \qquad (4.4)$$

$$\underline{q_d} \le q_d \le \bar{q}_d \qquad (4.5)$$

where $\underline{P_d}$ and $\bar{P}_d$ are minimum and maximum power generation and $\underline{q_d}$ and $\bar{q}_d$ are minimum and maximum discharge rates.

The dependence of turbine efficiency to the discharge rate can be considered in the model. In this case, the Equation (4.3) can be written as

$$P_d = gq_d h \eta_d(q_d) \qquad (4.6)$$

This equation can be linearized as follows

$$P_d = \delta^d q_\delta h + \underline{P_d} \qquad (4.7)$$

$$q_d = q_\delta + \underline{q_d} \qquad (4.8)$$

$$q_\delta \le \bar{q}_d - \underline{q_d} \qquad (4.9)$$

where δ^d is the energy coefficient and q_δ is the deviation of water discharge from its technical minimum.

The power consumption of turbines in pumping mode, P_p, can also be calculated in terms of net head and discharge rate, q_p. However, unlike generation mode, pumping power consumption is inverse proportional to its efficiency, η_p, and can be formulated as

$$P_p = \frac{g q_p h_n}{\eta_p} \tag{4.10}$$

Similar to the generation mode, the head effect can be ignored and taken constant in pumping mode. On the other hand, the turbines operate discontinuously (on-off). Thus, the power consumed can take two discrete values.

Power generation and consumption curves of the PHS system used in this thesis are given in Figure 4.6. In this figure, x and y axes represent the water flow and power generation/consumption, respectively. In the generation mode, the relation between the generated energy and discharged water is given by Equations (4.7)-(4.9). In pumping mode, the consumed power is calculated by the Equation (4.10).
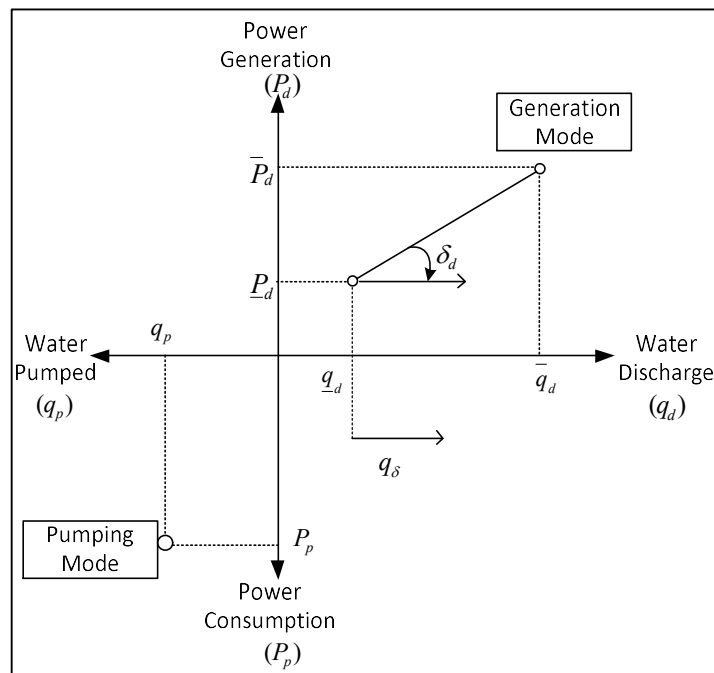
Figure 4.6. Characteristics of a conventional PHS unit

5. ELECTRICITY MARKET

The electric energy industry consists of four core components; generation, transmission, distribution, and supply or retail activities. These functions are implemented in many parts of the world under a monopoly by vertically integrated companies or government agencies (Figure 5.1.a). As a result of the liberalization of the world, the vertically integrated energy industry has transformed into separated properties, creating a deregulated energy market. Structure of deregulated systems varies according to the conditions of each country. In many energy systems where deregulated structure exists, transmission and distribution systems can still be operated by the monopolies. Figure 5.1 shows examples of regulated and deregulated energy systems.
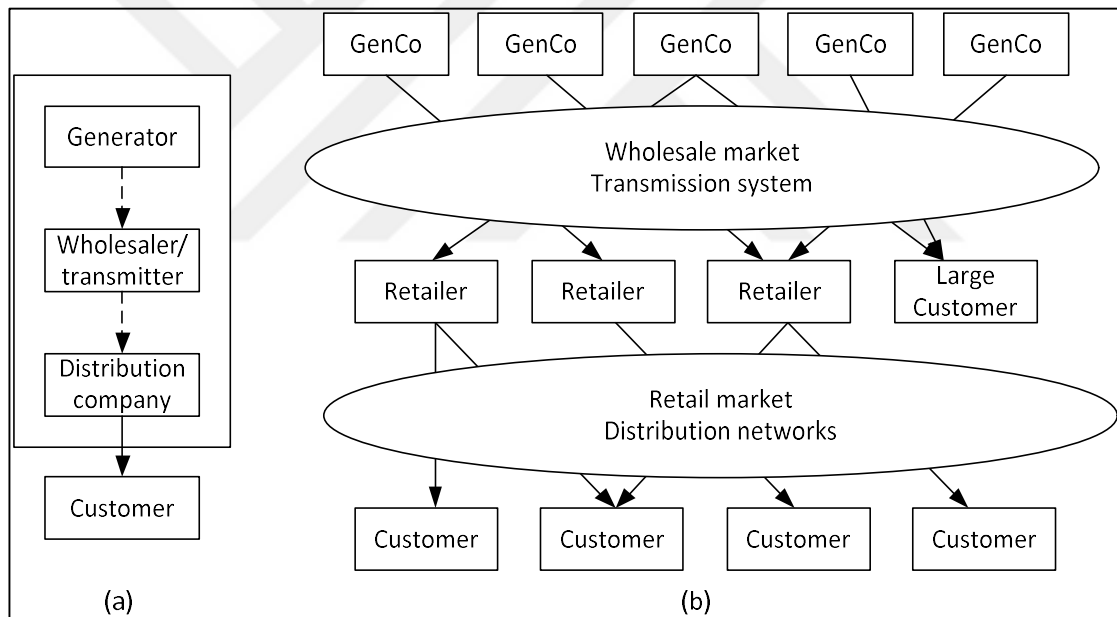
Figure 5.1. Structure of electric power industry (a) Monopoly, (b) Wholesale and retail competition

The regulative system's development and stability have caused the development of energy systems to become stagnant after a while [46]. After the changes in economic structure, the energy systems have begun to be privatized, and the private corporations have invested in energy generation. The primary challenge in the process of deregulation is to build a competitive market environment among other investors and systems managed by

monopolies. With increased competition, new trade routes between generation and retail services can be created. The energy produced by a generation company (GenCo) can be traded more than once before transmitted to the end-user in the market. Retailers earn revenue by purchasing large quantities of energy from wholesale markets and delivering them to the end consumer, which may vary from households to large manufacturing plants. However, end consumers do not always buy energy from retailers. While small and medium-sized consumers buy energy from retailers, large consumers may choose to participate directly in the wholesale market, as shown in Figure 5.1.b. Now that energy production is not under the control of a monopoly, market prices are not controlled and are determined in the wholesale market.

It is possible to classify today's electricity wholesale markets under three main structures as centralized markets (pool model), decentralized markets (bilateral agreements model) and hybrid model, which is shown in Figure 5.2. In the decentralized model, the participants can trade electric energy through agreements between themselves and at prices they specify. These agreements between the participants are called as bilateral contracts. The bilateral contracts include conditions that are not standardized such as start date, horizon, and delivery areas. The most remarkable benefit of this market is that supply and demand-side sign long-term contracts to avoid being affected by price fluctuations.
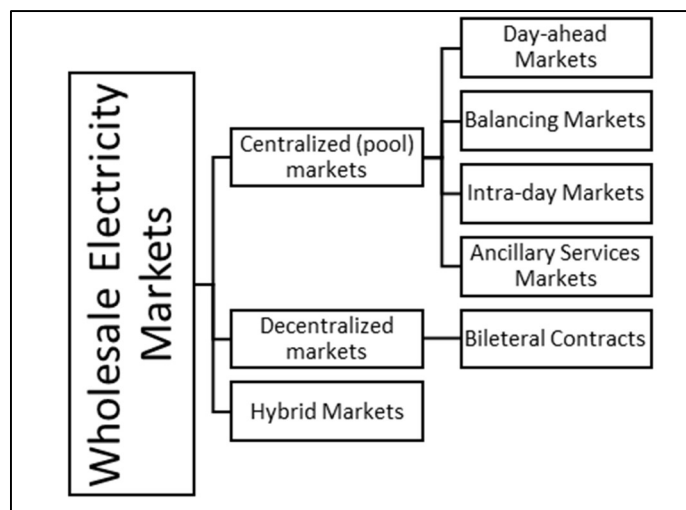
Figure 5.2. Structure of the wholesale market

In the centralized market structure, advanced power pool is operated by a central market operator. In pool-type markets, a GenCo can offer any price for the power that they want to sell. However, the offers should be reasonable; otherwise offering a high price may prevent the energy sale. Also, buyers such as end-users or retailers should set an appropriate price for purchasing power. The market operator matches the demand and supply quantity at the market-clearing process, and the energy prices are set, and the power is balanced. The clearing process will be explained in detail in Section 5.3, and there are many sources available for more detailed information on system price determination [47].

As shown in Figure 5.2, there are different types of centralized markets. They are used for trading energy in different time scales to ensure the energy generation meets the demand. These markets are summarized below.

- Day-ahead Markets: Most of the energy is traded in this market structure in which production and consumption in the energy system are balanced one day in advance. The Day-ahead market enables an opportunity to compensate their generation and consumption and take their place in the market more effectively while protecting themselves against the risky prices that may change. In this market, generators and consumers submit hourly bids for 24 hours of the next day. Supply and demand are matched, and price, which is also named as Market Clearing Price (MCP) is determined. However, since the future supply and demand cannot be forecasted perfectly, there will be imbalances. These imbalances are compensated in other markets having shorter time scales.

- Intra-day Markets: Intra-day markets is introduced recently to cope with renewable energy imbalances. It gives an opportunity to renewable GenCo to renew their bids based on the newly available information. Also, the intra-day market participants have the right to trade the capacities that they do not offer in day-ahead markets.

- Balancing Markets: Bids given in day-ahead and intra-day markets may not be met due to unforeseen events. Then, there is a need for balancing mechanism which is provided by balancing markets. In this market, participants who can provide their generation (consumption) energy immediately submit bids for reserve power. These bids are making reserve power available not using it. Whenever there is an imbalance in the energy system, these reserves will be used within minutes.

- Ancillary Services Market: This market has the shortest time scale and provides immediate correction for the imbalances to ensure safety operations. In addition, the ancillary market has an essential role in situations such as black start and secondary reserve service. In some energy markets, it operates as a single market with a balancing market.

5.1. HISTORY OF ENERGY MARKET IN TURKEY

The history of the Turkish electricity markets can be in three main periods: the monopoly period, deregulation period, liberalization period. Due to the need for increased production, distribution and transmission in the country, the Turkish Electricity Authority (TEK) was established with the TEK Law and started the operation in 1970. With the establishment of TEK, the interconnection system had been improved. Between 1970 and 1983, there was a public dominance in electrical energy investments. Law No. 3096, which came into force in 1984, allowed the private sector to make investments to energy generation that was totally state-controlled until that time. The model called Build - Operate - Transfer (BOT), which is also popular today, has begun to be used with this law. The purpose of this law was to eliminate the monopoly of the TEK by transferring the operating rights of the existing public electricity facilities to the private sector. TEK was divided into the Turkish Electricity Generation and Transmission Company (TEAŞ) and Turkish Electricity Distribution Corporation (TEDAŞ) on May 1994. TEDAŞ continued its electricity distribution activities until 2013, and as of that date, the operating rights of the distribution facilities have been transferred to the private sector in 21 distribution regions. After the transfer process, TEDAŞ undertook the mission of auditing these private sector companies.

The restructuring of TEAŞ for privatization occurred in 2001. The main aim of the program was;

- the establishment of separate public companies for electricity production, transmission, wholesale, and distribution,
- the privatization of public electricity companies,
- the restructuring of the electrical energy sector,
- the transition to the free electricity market system,

- the provision of the liberated competition environment.

With these goals, based on the Electricity Market Law dated 20.02.2001 and numbered 4628, TEAŞ was divided into Turkish Electricity Transmission Company (TEİAŞ), Electricity Generation Company (EÜAŞ) and Turkish Electricity Trading and Contracting Company (TETAŞ) and they organized as three separate state agencies. Figure 5.3 illustrates the evolution of state-owned energy companies over time.
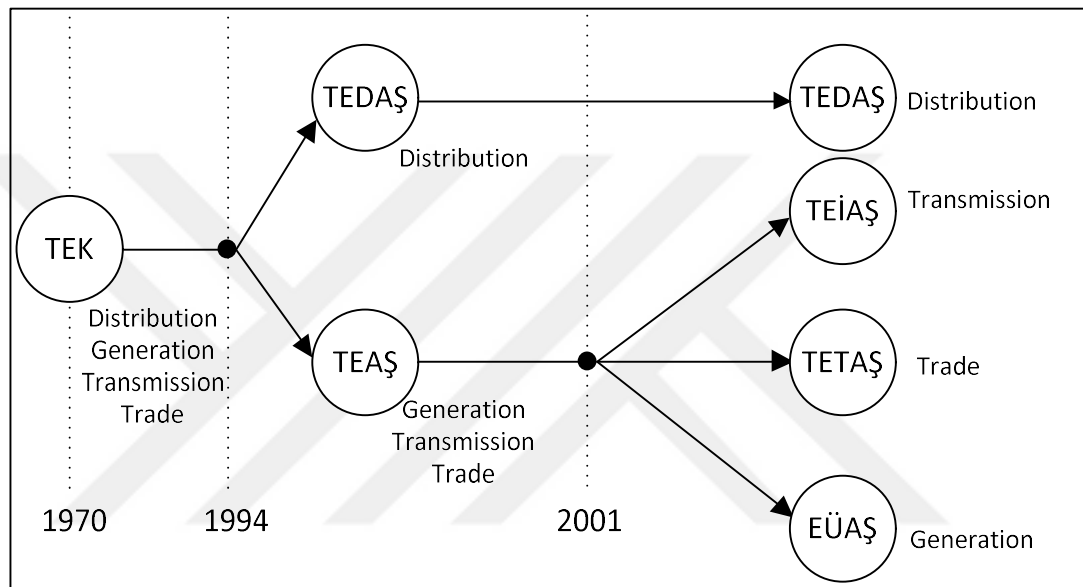
Figure 5.3. Disintegration of state-owned electricity companies

TEİAŞ conducted transmission activities as a state monopoly and operated balancing and ancillary services markets with its market operation license. Until the establishment of Energy Markets Operating Corporation (EPİAŞ) in 2013, it had also operated the day-ahead market. EÜAŞ has been operating the state-owned power plants which were not transferred to the private sector. As of the end of 2016, the total installed capacity of EÜAŞ was 20105.1 MW, while thermal and hydropower capacities were 6938.9 MW and 13166.1 MW, respectively. EÜAŞ installed capacity accounted for 26 percent of Turkey's installed capacity. The installed capacities of Turkey and EÜAŞ are presented in Figure 5.4. It is clear that the private energy generation sector has increased its share compared to the state-owned generation facilities.
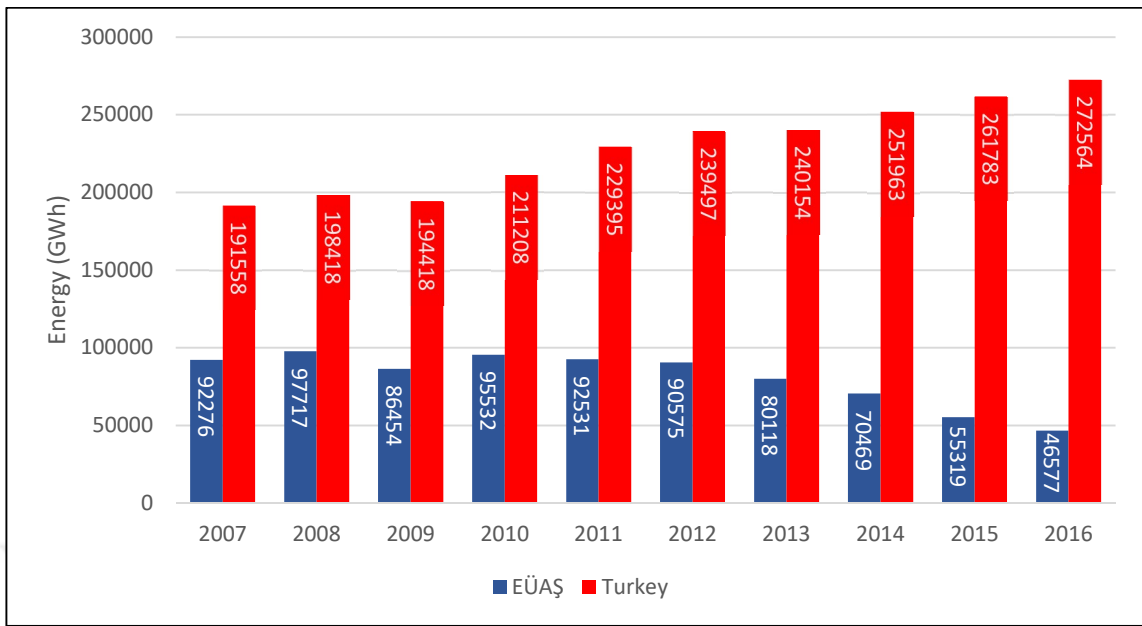
Figure 5.4. Comparison of energy generation of EUAŞ w.r.t Turkey

TETAŞ is a wholesale company that carries out sale and purchase. The primary duty of TETAŞ, which was established as the first electricity wholesale company, is undertaking the long-term, such as 15-20 years, energy trading commitments. These commitments are given to the power plants established as Build-Operate-Own (BOO), BOT and privatized power plants. The other responsibility of TETAŞ is selling the energy purchased with long-term contracts to distribution companies and its other customers. The share of TETAŞ in the market can be separated into three main periods, and it is presented in Figure 5.5. In 2001-2006, TETAŞ traded all the energy that had produced in the BOO, BOT, privatized power plants and EÜAŞ power plants. Thus, the market share of TETAŞ in the electricity sector in this period was averagely 76 percent. In 2007- 2012, a certain amount of electrical energy generated by EÜAŞ had been sold directly to distribution companies. Hence, TETAŞ market share in this period decreased to 40 percent. Market share in 2013-2016 had been increased to 45 percent after the establishment of EPİAŞ.
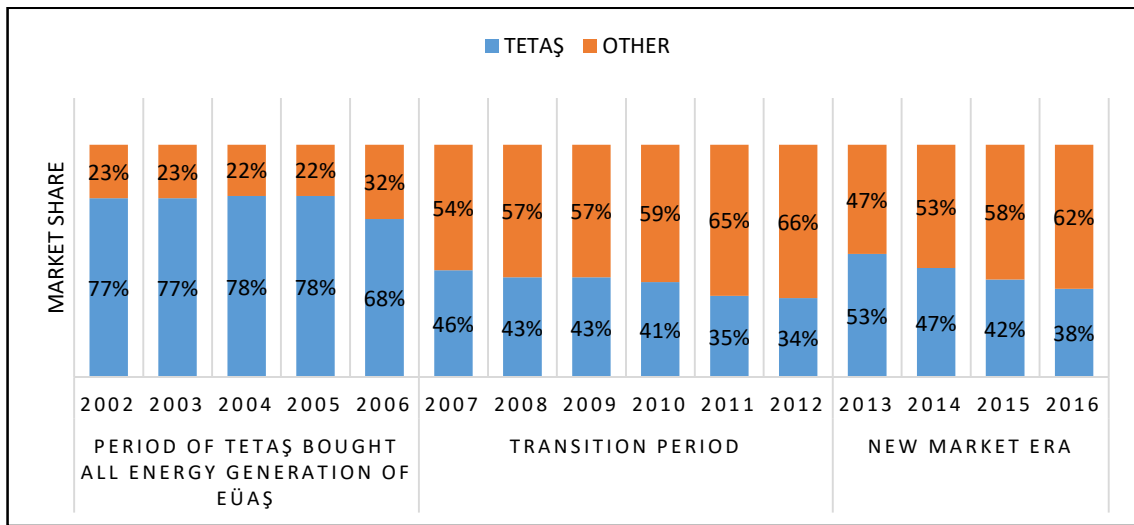
Figure 5.5. Share of TETAŞ in energy trading

Developments in the energy market were not only based on TEK but also supported by various laws and institutional changes. The changes in the energy market laws and institutions over the years are given in Figure 5.6. The law numbered 4628, which entered into force in 2001, can be considered as the milestone of the renovation in the Turkish energy market. This law covered the determination of the rights and obligations of the electricity generation, transmission, distribution, wholesale or retail sale, import and export, market operation and the establishment of the Energy Market Regulatory Authority (EMRA). Law No. 5346, which entered into force four years later, defined the principles and procedures for the protection of renewable energy resource areas, the certification of the electricity generated from these sources and the use of these resources. Moreover, the renewable energy support mechanism (YEKDEM), which is still in force, has been established with this law, and the economic support to be provided to the producer was determined. After this law, Turkey's wind power capacity of 51 MW in 2006 reached 6106 MW by the end of 2016, and 93 percent of this capacity is supported by YEKDEM. Law number 5784 has been enacted to update the Law No. 4628 in 2008. As a result of this law, some articles of Law no. 4628 had been amended, and the privatization of the distribution company and EÜAŞ had been provided. In addition, ancillary services regulation and automatic pricing mechanism had been settled. Even though the first steps for the settlement market were taken with the day-ahead planning in 2009, the day-ahead market mechanism, which is still in force today, has been introduced in 2011. The new Electricity Market Law No. 6446 entered into force on

March 30, 2013. The new law abolished all provisions of the Electricity Market Law No. 4628 except for the provisions of the EMRA regarding its organization, authorities and duties, and replaced them with new regulations. Under the new law, wholesale and retail licenses combined in a single license type under the name of supply license. In addition, a corporation named EPİAŞ was incorporated under this law to work on establishing new markets in organized wholesale electricity markets. On July 1, 2015, the intra-day market was put into operation to enable participants to provide a more balanced and active role in the Turkish electricity market, and a fully competitive market was established in 2016.
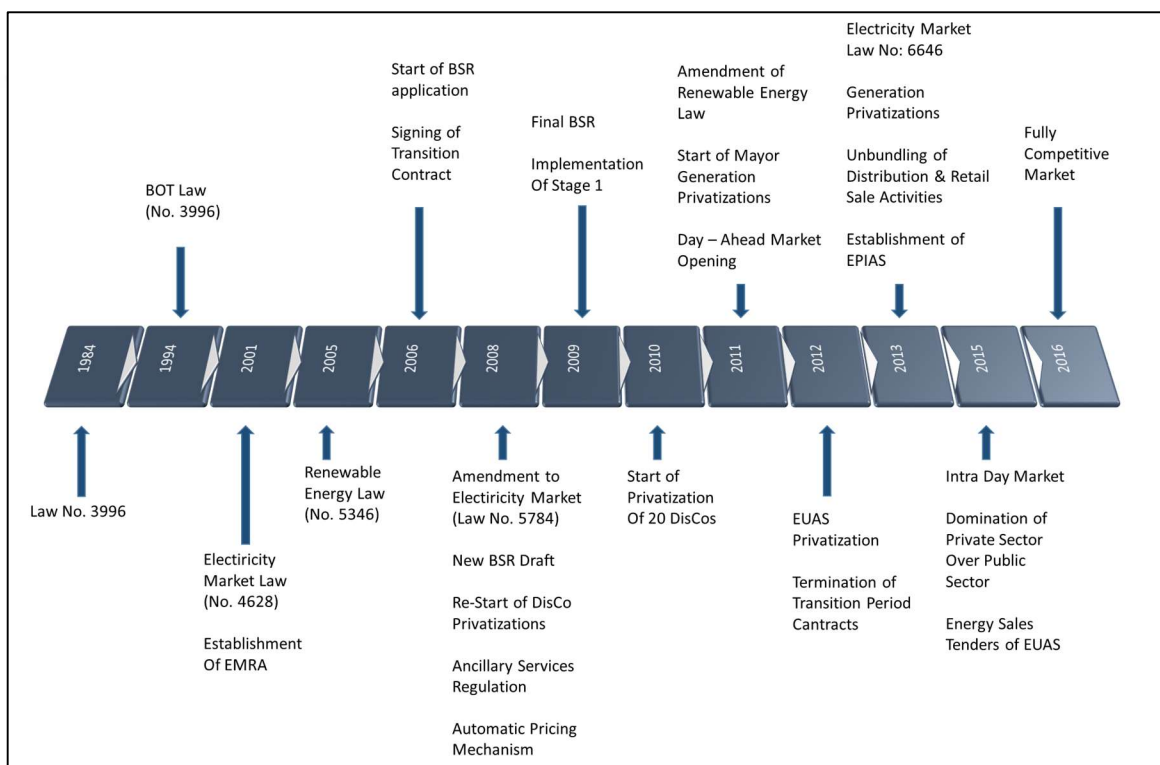
Figure 5.6. Milestones of Turkish electricity market reform

5.2. BALANCING AND SETTLEMENT MARKET HISTORY IN TURKEY

According to the provisions of the Law No. 4628 and Electricity Market Licensing Regulation, it is possible to perform electricity energy and capacity purchase-sale activities on the market through bilateral agreements between the parties, and supply and demand must continuously be balanced. To this end, the market model is based on the principle that the energy supplied to the system under the bilateral agreements is consumed in the same period.

Therefore, the simultaneous measurement of the generation and consumption side should be collected at a specific center to monitor the volume of the commitments with the bilateral agreements and the amounts to be borne by the parties causing the imbalance in the system can be determined. Thus, in order to provide the balance of electricity supply and demand during the day, the balancing and settlement market has been established with balancing and settlement regulation based on the Law No. 4628 at 3 November 2004. Although attendance of certain production facilities with certain capacities is obligatory in the first period, these necessities have now been repealed.

Although the balancing and settlement regulation had been established in 2004, it had gained functionality in 2006. This regulation permitted that accepted balancing energy offers were submitted monthly on hourly prices. Attendance of certain production facilities with certain capacities was obligatory in this first period. In 2009, a new regulation was issued that provided day-ahead planning and real-time balancing, which was formed for the first time. In this new market structure, offers were matched daily on an hourly basis. Attendance to the day-ahead planning and real-time balancing was mandatory to all generation /consumption facilities that can be activated within 15 minutes. In 2011, different from the day-ahead planning, the day-ahead market structure was introduced, which allowed the consumers (demand side) to submit bids. In addition, submission of bids within the day-ahead market can be made with a sensitivity of 0.1 MWh. The intra-day market was announced on 28 March 2015, which provided the opportunity for the supplier to update their generation schedule before the real-time operations. It is aimed to reduce the imbalances caused by suppliers like wind and solar power plants, whose forecast errors are high. Thus, the imbalance penalties which are paid by the GenCo's in the balancing market can be decreased. The evolution of the balancing and settlement market is shown in Figure 5.7.
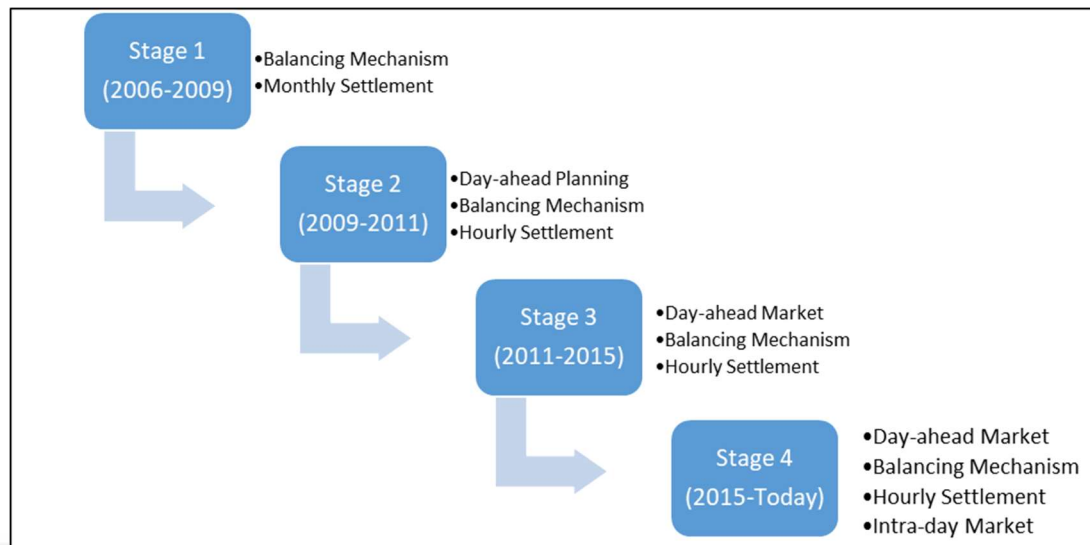
Figure 5.7. Timeline of Turkish balancing and settlement market

Today, balancing and settlement market is composed of the day-ahead, balancing and intra-day markets. As already mentioned, another way of selling electricity is bilateral agreements with a long-term contract which reduce the risk caused by price fluctuations. In addition to the reasons discussed above, since the balancing and settlement market is a relatively new trading tool, a significant portion of energy had been traded in bilateral agreements during the first years of these new markets. In 2009, when the day-ahead market first emerged, it had a share of 3.6 percent in total, while the bilateral energy trade had a rate close to 93 percent as shown in Figure 5.8. However, as the day-ahead market structure had been understood better, the share in the trade of energy was increased dramatically to 43 percent. Although the intra-day was established in July 2015, it was still a new market type and not preferred by the GenCo. The share of the intra-day market was 0.3 percent at the end of 2016, and it increased by 0.8 percent at the end of October 2017, which improves its share day by day.
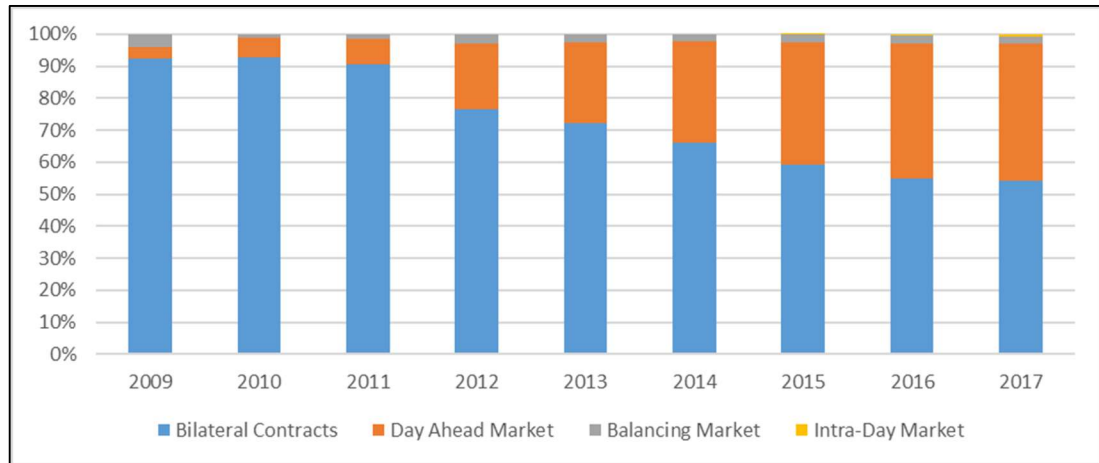
Figure 5.8. Evolution of Turkish wholesale market shares

5.3. STRUCTURE OF BALANCING AND SETTLEMENT MARKET IN TURKEY

5.3.1. Day-ahead Market Structure

The day-ahead market is the market in which energy trading is completed one day before the actual transfer of energy. From this point of view, the day-ahead market offers opportunities for market participants to reduce their risk to a minimum level by ensuring a predictable market nature. It also helps the system operator by providing a balanced system that enables to solve the problems caused by the continuous operation. Day-ahead market transactions are carried out within the following general guidelines.

- Day-ahead market operations are performed on a daily basis with hourly time steps, and each day begins at 00:00 and ends at 00:00 the following day.

- All bids submitted to the day-ahead market shall be valid for a specific day and a particular period of time within that day.

- Purchase-sale bids accepted in the day-ahead market have to be satisfied by the participants

- Each transaction concluded in the day-ahead period is completed by delivering the active electric energy to the settlement-based electric energy delivery point.

At this point, it will be useful to examine the structure of the bids in detail in order to better understand the day-ahead market. Market participants participating in the day-ahead market may offer either hourly, block or flexible or both offers within the context of the day-ahead market. It is essential that all bids submitted to the day-ahead market for a specific hour can be fulfilled at the same hour by the relevant market participant.

Hourly Buying / Selling Bids: It is a type of bidding option in which a market participant offers price and quantity information for each hour of the next day. These offers can be given in lots with a sensitivity of 0.1 MWh, and 32 bids can be formed in the direction of buying and selling.

An example of bids for a specific hour of the participant which may buy or sell energy is given in Table 5.1. According to the table, the trader decides that it is feasible to purchase energy if the price is less than or equal to 59 TL/MWh. The company may store this energy in order to use for arbitrage. Alternatively, if it has a bilateral contract for which energy price is higher than the market price, it can buy cheap energy from the market to satisfy the contracted energy. The GenCo submits generation bids which are represented with a negative sign when the price is higher than 100 TL/MWh.

Table 5.1. Sample bids for specific hour of a trader

Price (TL/MWh)	0	59	100	129	130	159	160
Quantity (MW)	20	20	-40	-40	-60	-60	-90

Block Purchase / Sale Bids: In addition to hourly bids, day-ahead market participants are also allowed to submit block bids. In block bids, an offer made by the participant will be used for more than one hour. The minimum length of a block can be three hours. A given bid cannot be accepted partially. Either it is rejected entirely, or it is approved for the whole period. Block bid offered to the day-ahead market cannot exceed 600 MWh.

A sample block bid is given in Table 5.2. As can be seen in the table, the length of the bids are more than three hours and has both energy purchase and sale.

Table 5.2. Sample block bids of a trader

Bidding Period	Price (TL/MWh)	Quantity (MW)
00:00-11:59	50	40
00:00-11:59	70	20
12:00-23:59	110	-50
12:00-23:59	200	-60

Flexible Sale Bids: Flexible bids can be submitted as a sale bid for an unspecified hour with a price and volume. These bids are either wholly rejected or entirely accepted. Market participants can notify up to 10 flexible sales bids to the market operator. The main goal of these bids is to reduce the energy price in an hour. It can be observed according to the given sample bid in Table 5.3. For example, if the energy price is higher than 100 TL/MWh at 6 am, then the bid number 1 will be accepted, and the GenCo will generate 10 MWh energy for that hour. However, in order to increase the profit of the participants, if the energy price is higher than 150 TL/MWh in any other hour of the day, then the first bid will be accepted in that higher price period.

Table 5.3. Sample flexible bids of a trader

Bid No.	Price (TL/MWh)	Quantity (MW)
1	100	-10
2	150	-30
3	170	-50
4	200	-60

As shown in Figure 5.9, after gathering the long-term bilateral contracts, the day-ahead bids are collected and matched by the market operator. The prices are determined in this bid matching operation, and two different methods are used in determining the price of electricity in the auction market model. In the first method, which is named as pay as bid, each bid is paid according to the offered price. However, in a market-clearing price method, all accepted bids are paid with a market-clearing price. In Turkey, the market-clearing price

method is used by the market operator, EPİAŞ. There is an example illustrated in Table 5.4 regarding the supply-demand balance in the day-ahead market auction structure for the one-hour interval with six participants.
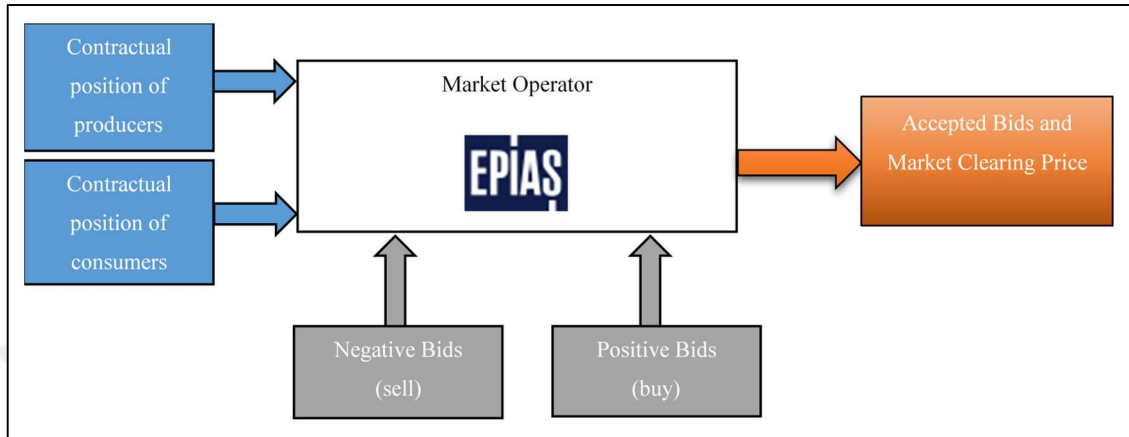
Figure 5.9. Inputs and outputs of the day-ahead market

The procedure starts with the ranking of prices in ascending order. Then, the bids for buying and selling are labeled with a positive sign a negative sign, respectively. The buying and selling energy bids are summed up separately and noted to total buying and selling rows for each price column. Finally, the energy balance can be calculated with a summation of entire buying and selling rows. To this end, an equilibrium point is obtained where energy balance is established with a zero value.

Table 5.4. Illustration of bids of market participants

Price (TL/MWh)	0	60	80	100	120	**140**	160	180	250	500
Quant.of firm A	-100	-100	-100	-100	-100	**-100**	-100	-100	-100	-100
Quant.of firm B	400	400	250	100	0	**-90**	-100	-130	-170	-170
Quant.of firm C	200	100	100	100	50	**50**	-50	-50	-50	-50
Quant.of firm D	200	150	150	110	110	**90**	90	50	30	0
Quant.of firm E	300	250	150	150	100	**100**	100	100	100	100
Quant.of firm F	-10	-20	-20	-30	-30	**-50**	-50	-50	-100	-100
Total Buying	1100	900	650	460	260	**240**	190	150	130	100
Total Selling	-110	-120	-120	-130	-130	**-240**	-300	-330	-420	-420
Energy Balance	990	780	530	330	130	**0**	-110	-180	-290	-320

The detailed procedure of the day-ahead market in Turkey is as follows:

- Until 12:30 each day, the day-ahead market participants shall submit the bids to the market operator through the system of the day-ahead market for the next day.
- Each submitted day-ahead market bid is verified by the market operator between 12:30-13:00.
- Confirmed bids are evaluated between 13:00 and 13:30 with the optimization tool and market clearing prices and quantities for each hour of the relevant day are determined.
- The accepted bids are notified to the relevant market participant at 13:30 each day. If there is an error in the content of these notifications, the market participant may submit their objections between 13:30-13:50.
- Objections are evaluated between 13:50- 14:00, and the result is reported to the participant. At 14:00, the prices and bids for the next 24 hours are finally announced.

5.3.2. Balancing Market Structure

After the closure of the day-ahead market auction, the operator determines electricity prices and accepted bids, which become fixed and do not change throughout the day. If there is a discrepancy between the actual energy produced, and the contract, it is compensated by trading energy in the balancing market. Even if the main task of the balancing market is to provide the energy balance of the system, it undertakes the services such as the elimination of system constraints, voltage control and ancillary services. The companies which are capable of changing the generation or load at least 10 MW in 15 minutes can participate in the balancing market.

The process of balancing power market starts at 14:00 each day with the completion of the day-ahead clearing and is carried out on a daily basis within the following steps;

- The market participant transmits daily regulation up and regulation down bids of balancing power market until 16:00 hours to the system operator. In addition, the system operator shall be informed with the strict daily production schedule, including the hourly production values for the production facilities registered in its name.

- Until 17:00 every day, the system operator checks the final day-ahead production/consumption program notifications and regulation up and down bids to determine if there are any errors in the notifications. The system operator will contact the relevant market participant for incorrect notifications and will make the necessary corrections until 17:00.

- The regulation up and regulation down bids submitted to the balancing power market are ordered with price by the system operator for each hour.
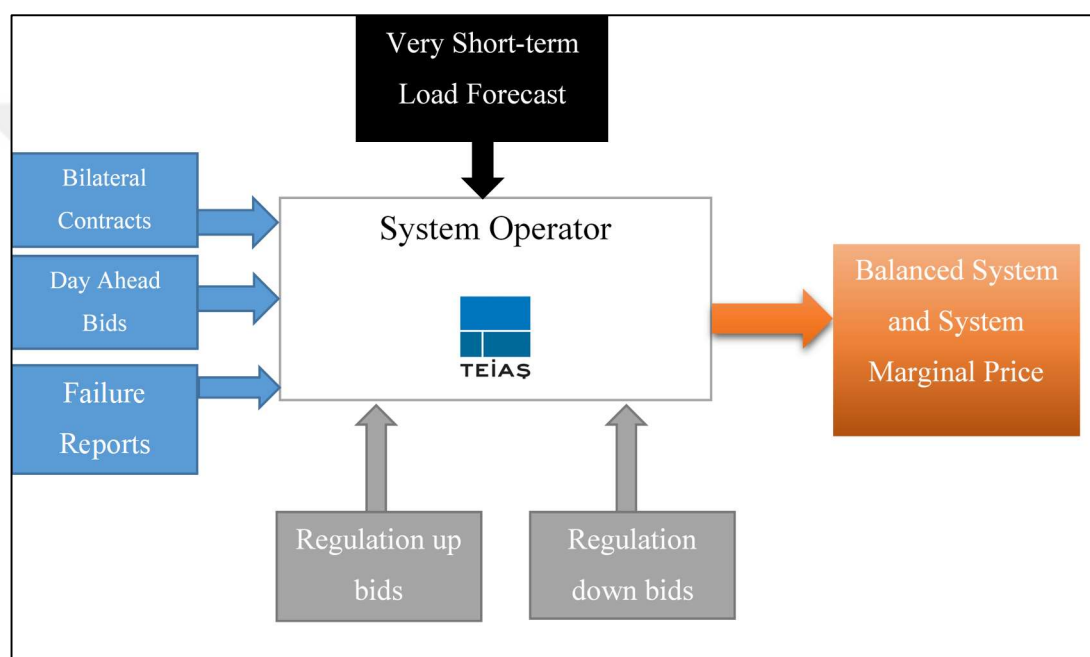
Figure 5.10. Inputs and outputs of Turkish balancing market

Figure 5.10 summarizes the real-time operation of a balancing market. Real-time operation begins at 00:00 and continues for that day until 23:59, and TEIAS is the system operator that ensures that the system remains balanced during this time. The system operator who has the fixed production schedule of all the participants in the balancing market takes into account the failure reports from the producers and consumers and decides whether the imbalance will occur by using the concise forecasting mechanism. In this case, if a supplier or consumer generated less or consumed more than its submitted bid, this energy will be bought at System Buy Price (SBP). In addition, a supplier or consumer generated more or consumed less than its submitted bid, this energy will be sold at System Sell Price (SSP).

In the case of imbalance, the System of Marginal Price (SMP) calculated with SBP and SSP in order to compensate for imbalance energy. This pricing can be calculated in two ways in the balancing markets, which are single imbalance pricing and dual imbalance pricing. Single pricing mechanism was the first method to calculate SMP until 2011 in balancing market in Turkey. In a single pricing structure, the party that causes imbalance has to be penalized whether the system is unbalanced or not. For the purpose of calculating the SMP in single pricing methodology, a constant which may change by region or country is multiplied with MCP.

$$SMP = \begin{cases} SBP = \alpha_b * MCP, & if\ shortfall\ exist \\ SSP = \alpha_s * MCP, & if\ extra\ energy\ exist \end{cases} \quad (5.1)$$

However, as a result of the introduction of the dual pricing structure in 2011, the system operator decreases deterrent SMPs to a reasonable level. Thus, imbalances have been observed to decrease by around 30 percent. [48]. In a dual pricing mechanism, SMP depends on the sign of an imbalance of the participant with respect to the sign of the overall system imbalance. Thus, where the transmission system has too much electricity, or in other term running long ($x > 0$), the supplier or consumer whose generate less or consumes more energy (short, $y < 0$), respectively, will not be penalized. However, the supplier which is running long ($y > 0$), will sell energy with SSP which is lower than MCP for the excess energy produced.

$$SSP = \begin{cases} SMP = \min\{MCP, SMP\}, if\ x > 0\ and\ y > 0 \\ MCP = \max\{MCP, SMP\}, if\ x > 0\ and\ y < 0 \end{cases} \quad (5.2)$$

In the case of the imbalance of the system is negative or network is running short ($x < 0$), then the SBP will be different than MCP if the supplier or consumer is running also short ($y < 0$), otherwise supplier will receive payment up to the MCP.

$$SBP = \begin{cases} MCP = \min\{MCP, SMP\}, if\ x < 0\ and\ y > 0 \\ SMP = \max\{MCP, SMP\}, if\ x < 0\ and\ y < 0 \end{cases} \quad (5.3)$$

6. STOCHASTIC OPTIMIZATION

On the contrary to the deterministic optimization problems, most of the real-world problems consist of parameters which are uncertain at the time when a decision should be made. Thus, it is essential to take into consideration the uncertainty, especially for problems in finance, supply chain, transportation, telecommunication, environment and energy [49]. With this in mind, Stochastic Programming (SP) was first introduced by Dantzig with the goal of making the best possible decision under given constraints in the presence of uncertainties affecting the decisions [50]. Stochastic programming consists of two main stages. The first one is the modeling of the optimization in which the objective function and constraints are determined. The second one is the modeling of the uncertainty used in the problem.

The modeling of a stochastic optimization can be grouped under four category, which is shown in Figure 6.1. Among the methods, expected value, risk-averse and chance-constrained methods are distribution-based methods. While expected value problems optimize the average of the objective function based on a distribution, risk-averse problems optimize the risk on the objective. Chance-constrained problems optimize the decision-making problems by ensuring that the probability of meeting constraints is above a certain level. On the other hand, robust optimization does not use probabilistic distributions as it optimizes the problem based on the worst case of the uncertainty.
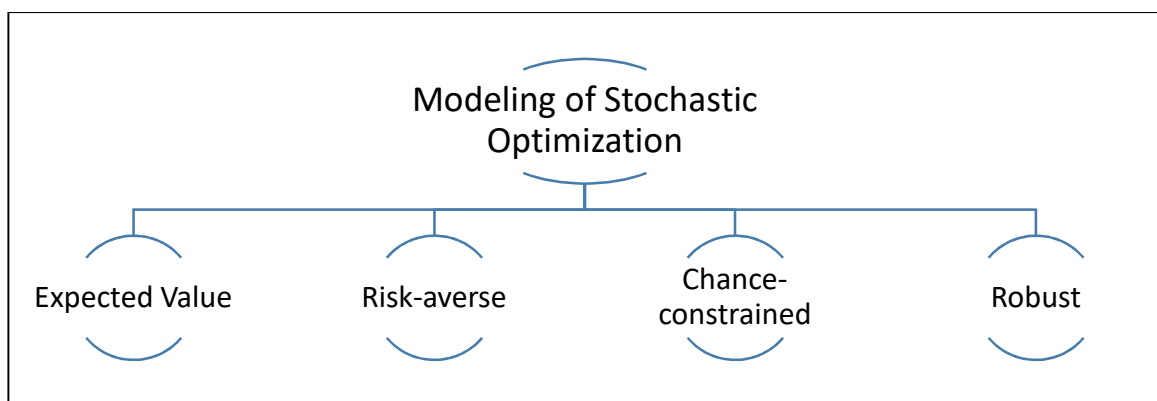
Figure 6.1. Categories of stochastic programming modeling

This section is organized as follows. Firstly, the modeling of the stochastic programs will be introduced with the different approaches used, and the comparison of these modeling

approaches is performed. Then, the modeling of the randomness is explained in detail with scenario generation and reduction techniques. Finally, the method used in this thesis is presented.

6.1. MODELING AND SOLUTION OF OPTIMIZATION

6.1.1. Expected Value Problems

One of the approaches for solving the stochastic optimization problems optimizes the expected value of the objective function. This kind of stochastic programming problems can be called as two-stage or in general multi-stage problems. In the following two sections, two and multi-stage expected value problems will be explained.

6.1.1.1. Two-stage Stochastic Optimization

Standard two-stage stochastic programming has different decision variables used for the first and second stages. The first-stage decision variables, which are also known as "here and now decisions," specify the decisions to be made before the occurrence of the uncertainty. The second-stage decision variables, which are also known as "wait and see decisions," state the decisions taken after the uncertainty is resolved. The general representation of two-stage stochastic programming is shown in Figure 6.2, and its linear formulation is as follows.

$$\min_{x} cx + \mathbb{E}\left[\min_{y} q(\omega)y(\omega)\right] \tag{6.1}$$

$$Ax = b \tag{6.2}$$

$$R(\omega)x + L(\omega)y(\omega) = h(\omega), \forall \omega \epsilon \Omega \tag{6.3}$$

$$x \in \mathbb{Z}_+^r \times \mathbb{R}_+^{m-r}, y \in \mathbb{Z}_+^d \times \mathbb{R}_+^{s-d} \tag{6.4}$$

where $\Omega = \{\omega^1, \omega^2, \omega^3, \dots, \omega^n\}$ is the set of uncertain outcomes with a certain probability distribution. In the above formulation, a two-stage optimization is performed, where x and y represent the first and second stage decision variables, respectively. In detail, the first part of Equation (6.1) identifies the profit obtained from the first stage, and the second presents

the expected income that can be obtained from the second stage. The second stage is an optimization problem where uncertainties, ω, are revealed by observations and recourse actions are taken. For a given realization, the second stage data $L(\omega)$, W, $q(\omega)$ and $h(\omega)$ become known. The term $q(\omega)y(\omega)$ is the profit of the recourse problem and the term $L(\omega)y(\omega)$ determines the compensation of the possible inconsistencies which can be modeled with $L(\omega)x$.
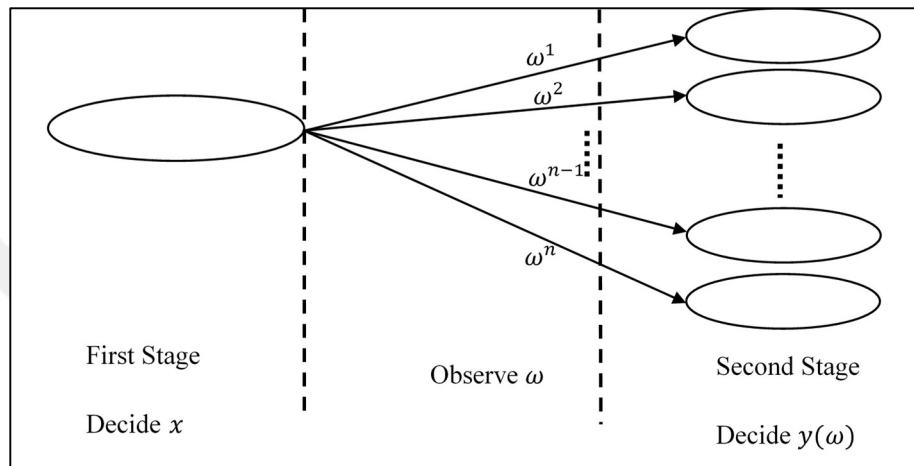
Figure 6.2. Two-stage stochastic programming

Constraints of the linear stochastic optimization mathematical model given in Equations (6.1)-(6.4) can be written in the matrix form as in the following equation.

$$min[c \quad q(\omega^1) \quad q(\omega^2) \quad q(\omega^3) \quad \cdots \quad q(\omega^n)] \begin{bmatrix} x \\ y(\omega^1) \\ y(\omega^2) \\ y(\omega^3) \\ \vdots \\ y(\omega^n) \end{bmatrix} \tag{6.5}$$

$$\begin{bmatrix} A & 0 & 0 & 0 & \cdots & 0 \\ R(\omega^1) & L(\omega^1) & 0 & 0 & \cdots & 0 \\ R(\omega^2) & 0 & L(\omega^2) & 0 & \cdots & 0 \\ R(\omega^3) & 0 & 0 & L(\omega^3) & \cdots & 0 \\ \vdots & \vdots & \vdots & \vdots & \ddots & \vdots \\ R(\omega^n) & 0 & 0 & 0 & \cdots & L(\omega^n) \end{bmatrix} \begin{bmatrix} x \\ y(\omega^1) \\ y(\omega^2) \\ y(\omega^3) \\ \vdots \\ y(\omega^n) \end{bmatrix} = \begin{bmatrix} b \\ h(\omega^1) \\ h(\omega^2) \\ h(\omega^3) \\ \vdots \\ h(\omega^n) \end{bmatrix} \tag{6.6}$$

By replacing Equations (6.1)-(6.4) with Equations (6.5) and (6.6), the optimization becomes a single linear programming model.

One of the critical weaknesses of a stochastic problem given in Equations (6.5) and (6.6) is that it can be challenging to find a solution if the number of realization of the random variables is large. Among different approaches that cope with this problem, the L-shaped method, which is proposed by the Van Slyke and Wets's [51] uses Benders' [52] and Dantzig-Wolfe [53] decomposition methods. These decomposition methods are based on the primal and dual structure of the mixed-integer models, respectively. In general, this method approximates the recourse function, which is the second part of Equation (6.1), in order to avoid numerous second-stage function evaluation. Therefore, the mathematical model of the problem is divided into the master problem and slave problems, which corresponds to deterministic and stochastic parts of the model, respectively.

The algorithm of the L-shaped method can be explained as follows briefly. Firstly, the master problem is solved and an optimal value of x^* is calculated. Then, this value is checked in the slave problem for each occurrence i in order to satisfy the feasibility condition. If the sub-problem is not feasible with x^*, then a feasibility cut is added to the main problem and the main problem is solved again with the newly added constraint. If the slave problem is feasible, optimality cut is calculated and added to in the main problem. This process is repeated until new optimality or feasibility cut cannot be generated. The overall process of L-shaped method and process of generating the feasibility and optimality cuts are explained in detail by Birge [54].

6.1.1.2. *Multi-stage Stochastic Optimization*

The two-stage stochastic programming model discussed so far has only one recourse problem. However, there are some cases where decisions must be taken consecutively for each period, depending on the information available at certain times on the horizon. The multi-stage stochastic programming models are used in such problems which can be considered as a multi-step extension of two-stage programming. In the multi-stage stochastic optimization, uncertainty information $\omega_1, \omega_2, \dots, \omega_t$ revealed is gradually over time and, the decisions should be made sequentially, as illustrated in Figure 6.3.

In the multi-stage stochastic programming models, instead of the first and second stage variables, which are defined as x and y as in two-stage stochastic programming model,

$x_0, x_1, \dots, x_t$ denotes the decisions at each stage. x_0 does not depend on uncertainity while x_t depends on past uncertainties $\omega_{\lfloor t \rfloor} = \{\omega_1, \dots, \omega_{t-1}\}$. Then, the decisions at any stage can be calculated with the following equation set.

$$\min_{x_0} c_0 x_0 + E\left[\min_{x_1} c_1(\omega_{\lfloor 1 \rfloor})x_1(\omega_{\lfloor 1 \rfloor}) + \dots + E\left[\min_{x_H} c_H(\omega_{\lfloor T \rfloor})x_H(\omega_{\lfloor T \rfloor})\right]\right] \tag{6.7}$$

$$\text{s.t. } Ax_0 = b \tag{6.8}$$

$$R_0(\omega_{\lfloor 1 \rfloor})x_0 + L_1 x_1(\omega_{\lfloor 1 \rfloor}) = h_1(\omega_{\lfloor 1 \rfloor})$$

$$\vdots \tag{6.9}$$

$$R_{T-1}(\omega_{\lfloor T \rfloor})x_{T-1} + L_T x_T(\omega_{\lfloor T \rfloor}) = h_H(\omega_{\lfloor T \rfloor})$$

$$x_t \in \mathbb{Z}_+^r \times \mathbb{R}_+^{m-r} \tag{6.10}$$

In above, c_0, A and b are deterministic while of c_t, R_t, L_t and h_t are random for $t = 1, \dots, T$. The objective function is the minimization of the first stage cost and minimization of the expected cost of the following stages. Equation (6.8) is the constraint for the first stage which is the deterministic part of the problem. The constraints of the following stages are given in Equation (6.9). The reader is referred to the [55] for details of creating the deterministic equivalent of Equations (6.8)-(6.10).

Figure 6.3. Multi-stage stochastic programming

In multi-stage stochastic programming, usually, uncertainties are modeled as scenario trees. A scenario tree is composed of nodes at each stage. At the first stage, there is one node which is called the root. At each time period, new nodes branch from the nodes of the previous time period forming a tree. Nodes at the last stage of the tree are called leaves. A path from the root to a leaf is called scenario.

A sample scenario tree with eight scenarios is given in Figure 6.4.a. As can be seen from the figure, all scenarios at $t = 1$, share the root node of the tree. After the branching at $t = 2$, two different nodes are created. While scenarios with index $i = 1,2,3,4$ share the first node, scenarios $i = 5,6,7,8$ share the second node at time $t = 2$. In order to illustrate how the scenarios are associated with the nodes, the relation between the scenarios and nodes are illustrated in Figure 6.4.b and shared nodes are put into ellipses. The mathematical equations of these share nodes for each stage are given in Equations (6.11)-(6.15). These equations are called as nonanticipativity constraints of the stochastic programming model.

$$x_1(\omega_1^1) = x_1(\omega_1^2) = x_1(\omega_1^3) = x_1(\omega_1^4) = x_1(\omega_1^5) = x_1(\omega_1^6) = x_1(\omega_1^7)$$
$$= x_1(\omega_1^8) \tag{6.11}$$

$$x_2(\omega_2^1) = x_2(\omega_2^2) = x_2(\omega_2^3) = x_2(\omega_2^4) \tag{6.12}$$

$$x_2(\omega_2^5) = x_2(\omega_2^6) = x_2(\omega_2^7) = x_2(\omega_2^8) \tag{6.13}$$

$$x_3(\omega_3^2) = x_3(\omega_3^3) = x_3(\omega_3^4) \tag{6.14}$$

$$x_3(\omega_3^6) = x_3(\omega_3^7) \tag{6.15}$$

where ω_t^i represesents the node of ith scenario at time t.
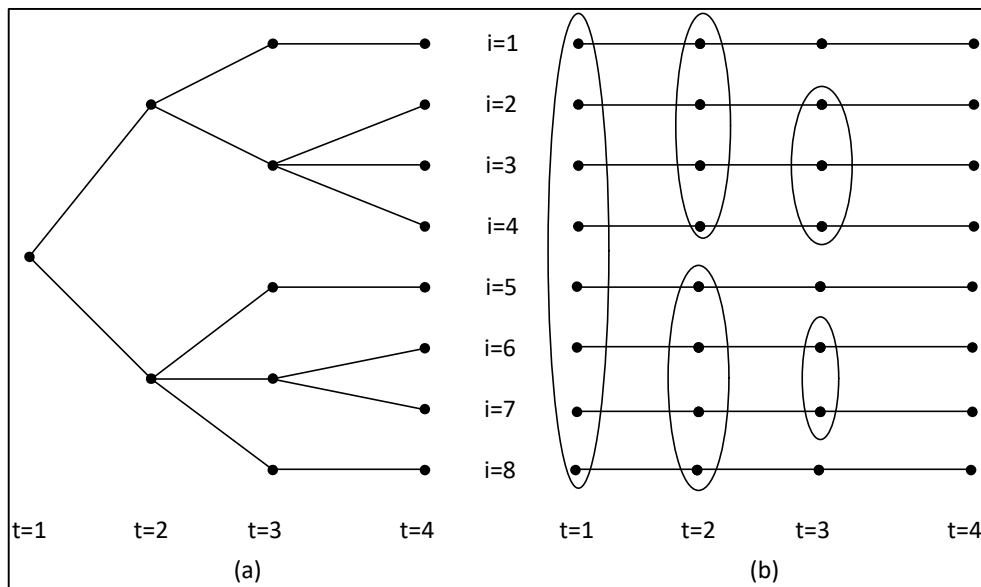
Figure 6.4. A sample scenario tree (a) Tree structure, (b) Non-anticipativity constraints

In general, the nonanticipativity constraints can be written as

$$x_t(\omega_{[t]}^i) = x_t(\omega_{[t]}^j), \forall i, j \text{ for which } \omega_{[t]}^i = \omega_{[t]}^j, \ t = 1, \dots, T \qquad (6.16)$$

As in two-stage recourse optimization, for large scale problems, it is necessary to use a decomposition method to solve multi-stage programming. To this end, the L-shaped method can be extended to a nested decomposition, which solves the problem with a forward step and a backward step in each iteration. The forward step solves the equations with an approximate expected cost-to-go function at each node n as in the L-shaped method from $t = 1, \dots, H$. When the algorithm reaches to H in iteration i, a feasible solution is obtained and an upper bound is calculated. Then, the backward step starts and update the lower bound for each node n from the last stage H until it reaches back to the root node of the tree. If the lower and upper bounds coincide, the nested decomposition terminates; otherwise, the algorithm continues with another iteration.

6.1.2. Risk-Averse Optimization

In robust optimization, the maximum loss is minimized with respect to the worst-case scenario to find the decision hedging against uncertainties. However, in general, this may lead to a too conservative solution that may result in low expected profit. One way to avoid this conservativeness is to introduce probabilistic risk measures into the objective function. One such measure is Value-at-Risk (VaR), which can be defined as the maximum possible loss within confidence interval α of the probability distribution. This definition is shown in Figure 6.5 and can be expressed for a specified probability level α as follows

$$VaR_\alpha^+ = min\{\zeta : \psi(x, \zeta) \geq \alpha\} \qquad (6.17)$$

where $\psi(x, \gamma)$ is the cumulative probability function associated with the decision variable x and the threshold ζ.

Using VaR, one can construct the following optimization problem

$$\min_{x} \beta_1 \mathbb{E}[c(\omega)x] + \beta_2 VaR_\alpha^+ \qquad (6.18)$$

$$A(\omega)x \leq b(\omega) \tag{6.19}$$

$$x \in \mathbb{Z}_+^r \times \mathbb{R}_+^{m-r} \tag{6.20}$$

The objective in Equation (6.18) is a weighted average of expected profit and VaR. By adjusting weights β_1 and β_2, one can adjust the trade-off between minimization of the expected loss and the minimization of VaR_α^+. The case $\beta_1 = 0$ and $\beta_2 = 1$ gives the most conservative solution. However, even this is less conservative when compared with robust optimization. This can be seen in Figure 6.5. VaR can not exceed maximum which corresponds to robust optimization objective.
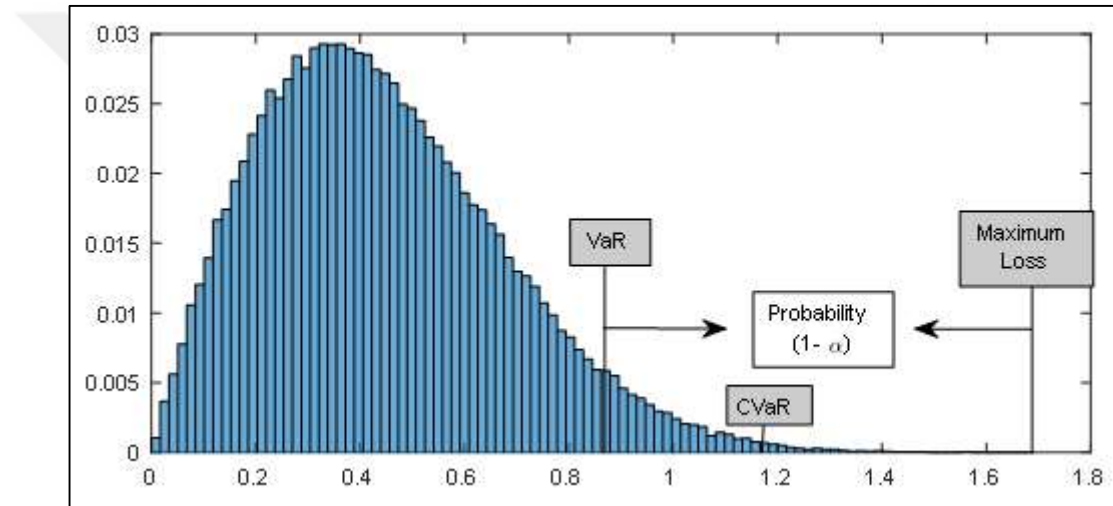
Figure 6.5. Illustration of VaR and CVaR [56]

Although the risk-averse formulation given above can be used to avoid conservativeness, it can lead to computational problems since it is not a coherent risk measure and non-convex in general. To avoid this problem, one may use Conditional Value at Risk (CVaR) instead, which can be defined as the weighted average over the losses greater than or equal to VaR. Thus, the $CVaR_\alpha$ can be defined as

$$CVaR_\alpha^+ = \frac{1}{(1-a)} \int_{f(x,y) \geq VaR_\alpha^+} f(x,y)\, p(y)dy \tag{6.21}$$

where $f(x,y)$ is the loss function with the decision variable x and a random variable y and $p(y)$ is the probability density function of random variable y.

Notice that $CVaR_\alpha$ uses the VaR_α which makes it difficult to handle in the optimization problems. Thus, Rockafellar and Uryasev [56] define an alternative formula for the $CVaR_\alpha$ as follows

$$CVaR_\alpha^+ = \zeta + \frac{1}{(1-a)}\int_y [f(x,y) - \zeta]^+ \, p(y)dy \tag{6.22}$$

However, in optimization problems, it is difficult to evaluate the integral in Equation (6.22). To alleviate this difficulty, one can use the following sampling-based approximation.

$$CVaR_\alpha^+ = \zeta + \frac{1}{(1-a)}\sum_{i=1}^{N} \pi^i [f(x,\omega^i) - \zeta]^+ \tag{6.23}$$

where ω^i is i^{th} sample and π^i is the probability of occurrence of the ith sample.

However, the Equation (6.23) can not be used in the linear optimization algorithms due to the discontinuity caused by $[\tau]^+$. To overcome this problem, Rockafellar and Uryasev [56] linearized the discontinuous terms of the equations and converted the problem to a linear programming problem as follows

$$\min_x CVaR_\alpha^+ = \min_x \left(\zeta + \frac{1}{(1-a)}\sum_{i=1}^{N}\pi^i\tau^i\right) \tag{6.24}$$

$$\tau^i \geq f(x,\omega^i) - \zeta \tag{6.25}$$

$$\tau^i \geq 0 \tag{6.26}$$

The formulation above is given for the minimization problem of the loss function $f(x,y)$. On the other hand, when one needs to maximize the minimum probable profit, then $VaR_{(1-\alpha)}^-$ should be used instead. The difference between VaR_α^+ and $VaR_{(1-\alpha)}^-$ is illustrated in Figure 6.6. Because of this difference, the derivation of the $CVaR_{(1-\alpha)}$ is not the same as Equation (6.24). Similar to $CVaR_\alpha^+$, the optimization of $CVaR_{(1-\alpha)}$ can be given as [56]

$$\max_x CVaR_{(1-\alpha)}^- = \max_x \left(\zeta - \frac{1}{(1-a)}\sum_{i=1}^{N}\pi^i\tau^i\right) \tag{6.27}$$

$$\tau^i \geq \zeta - f(x,\omega^i) \tag{6.28}$$

$$\tau^i \geq 0 \qquad\qquad (6.29)$$

Since profit maximization is interested in this thesis, $CVaR^-$ and VaR^- will be employed. To simplify the notation $CVaR^-$ and VaR^- will be denoted as $CVaR$ and VaR in the rest of the thesis.
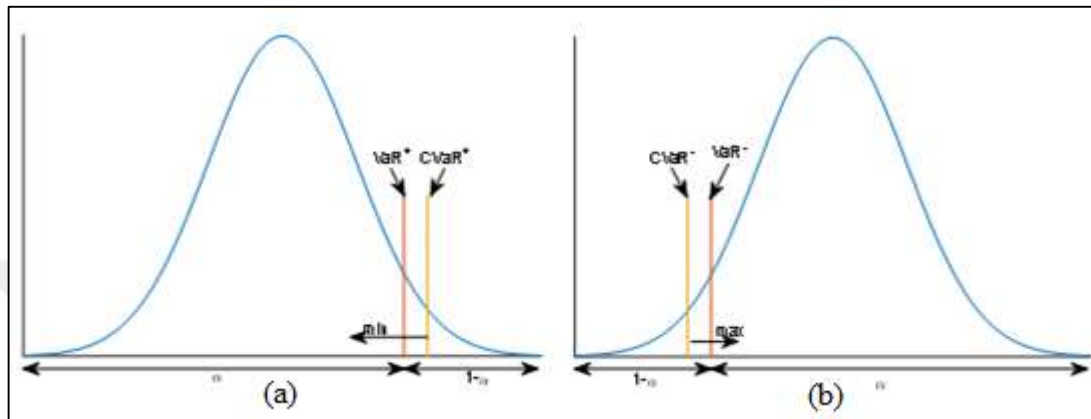
Figure 6.6. Illustrations for (a) $CVaR^{+/-}$, (b) $VaR^{+/-}$

6.1.3. Chance-Constrained Optimization

For the all optimization formulations explained so far constraints are expected to be satisfied for all realizations of uncertainties. However, in some applications, it would be allowable to violate constraints as long as the occurrence of the violation is rare. In this case, one may replace constraint satisfaction with less conservative probability constraints and use the chance-constrained method. This method was proposed by Charnes et al. [57] and ensures that the probability of fulfilling a particular constraint is above a certain level [58].

Chance-constrained optimization mathematical models are based on probability (or chance) constraints which may have the form as given in Equation (6.30).

$$P\{T(\omega_i)x \geq h(\omega_i)\} \geq \beta_i \quad i = 1,2,\dots n \qquad (6.30)$$

where $0 \leq \beta_i \leq 1$.

The deterministic equivalent of Equation (6.30) can be developed with different approaches. One of them is using the sample average approximation, which can be acquired by substituting the real distribution in chance-constrained optimization by an empirical

distribution corresponding to a random sample [59]. The sample average approximation formulation of the probabilistic constraint can be written as follows. Suppose that $g_i(x, \hat{\xi}^j) = T^j(\omega_i)x - h^j(\omega_i)$ and the uncertain variables are defined as $\hat{\xi}^j = \{T^j(\omega_i), h^j(\omega_i)\}$. Then

$$g_i(x, \hat{\xi}^j) \geq 0 \quad i = 1, 2, \dots n, j = 1 \dots N \tag{6.31}$$

where $\hat{\xi}^1 \dots \hat{\xi}^N$ are independent and sampled from a distribution, which gives a discrete approximation of Equation (6.30). If the probability distribution function is replaced with Monte Carlo samples of ξ, then the Equation (6.31) transforms to the following deterministic constraint.

$$\frac{1}{N} \sum_{j=1}^{N} \mathbb{I}(g_i(x, \hat{\xi}^j) \geq 0) \geq \beta_i, i = 1, 2, \dots n \tag{6.32}$$

where $\mathbb{I}(\mathcal{A})$ is an indicator function which is one when the $\mathcal{A}$ is true and zero otherwise. Finally, if the big-M method is employed, the following MILP equivalent of Equation (6.32) can be obtained.

$$g_i(x, \hat{\xi}^j) + M_i^j y^j \geq 0, i = 1, 2, \dots n, j = 1 \dots N \tag{6.33}$$

$$\frac{\sum_{j=1}^{N} y^j}{N} \leq 1 - \beta_i \tag{6.34}$$

$$y^j \in \{0,1\} \tag{6.35}$$

where M_i^j is big enough constant. In general, except for some special cases, it is difficult to solve chance-constrained problems, since they are non-convex.

6.1.4. Robust Optimization

Robust optimization (RO) is another stochastic optimization approach developed for the solution of optimization problems under uncertainty. This optimization technique aims to find the solution for the best objective function value under the worst-case uncertainty. The solution is mostly conservative because it hedges against the worst-case realization. The RO

may not be ideal for some applications due to this conservative nature; however, the RO is used in various sectors like inventory management, logistics, finance, machine learning, energy systems, safety systems, and healthcare systems [60].

The robust approach entered into the optimization literature by Soyster addressing the problem of linear programming with uncertain data [61]. In this study, small perturbations are applied to the data, and a reformulation which is feasible under all possible perturbations to the original problem was found. Mulvey et al. proposed the robust optimization method to cope with the trade-off between solution and model robustness by integrating goal programming formulations and scenario-based optimization [62].

RO problems are transformed into a deterministic format called robust equivalence using strong duality arguments and are solved using standard optimization algorithms[63]. A static RO problem can be formulated as follows.

$$\min_{x} \max_{\omega \in \Omega} c(\omega)x \tag{6.36}$$

$$A(\omega)x \leq b(\omega) \tag{6.37}$$

$$x \in \mathbb{Z}_+^r \times \mathbb{R}_+^{m-r} \tag{6.38}$$

where Ω is the uncertainty set. This formulation optimizes the objective for the worst-case realization of $\omega \in \Omega$.

The mathematical model given in Equation (6.36) is a static model which does not consist of multiple stages. Similar to multi-stage recourse problems mentioned in Section 6.1.1.2, multi-stage robust optimization, i.e., adjustable robust optimization, concentrate on the cases when the decisions can be separated into multiple different cases. The term "adjustable" refers that decision-makers can adjust their decisions when the uncertain parameters are realized in each stage. Adjustable robust optimization is less conservative than the classic RO approach as it calculates more flexible solutions which can be adjusted at any stage. Ben-Tal et al. [64] introduced the adjustable robust solution and formulated for two-stage as in the Equation (6.39)-(6.42).

$$\min_{x} cx + \max_{\omega \in \Omega} \min_{y} q(\omega)y(\omega) \tag{6.39}$$

$$Ax = b \tag{6.40}$$

$$R(\omega)x + L(\omega)y(\omega) = h(\omega), \forall \omega \epsilon \Omega \tag{6.41}$$

$$x \in \mathbb{Z}_+^r \times \mathbb{R}_+^{m-r}, y \in \mathbb{Z}_+^d \times \mathbb{R}_+^{s-d} \tag{6.42}$$

In this formulation, x is the here-and-now decisions and y is the wait-and-see decisions. The difference between the stochastic recourse problem described in Section 6.1.1 and adjustable recourse problem can be seen in this formulation. While Equation (6.1) minimizes the expected cost for the second-stage, the expectation operator is switched with a maximization operator in Equation (6.39). Note that the expectation operator is a linear operator while the maximization is another optimization problem. The Equation (6.1) can be extended to multi-stage similar to stochastic optimization in the Equation (6.7) by replacing the expectation operator with a maximization operator.

In early studies on RO, the uncertainty was modeled with the scenario trees by Mulvey et al. [62]. However, using scenario trees may not contain the worst-case scenarios because sampling methods are used for scenario generation. In order to solve this problem, uncertainty sets are used. Thus, the solution of the robust formulation is guaranteed to be optimal and feasible for the entire uncertainty set. Commonly used uncertainty sets are as follows; box uncertainty set [61], ellipsoid uncertainty set [65], polyhedral uncertainty set [66], and combinations of these sets.

6.2. SAMPLING BASED APPROXIMATION OF STOCHASTIC PROCESSES

Solving stochastic problems with continuous variables is intractable in general. Thus, to make such problems traceable, one needs to use discrete approximations to these continuous variables. For multistage problems, such discrete approximation takes the form of a scenario tree due to the dependence of past observations. This approximation process of the scenario tree includes some or all of the following steps, which are also shown in Figure 6.7 [49].

- The collection of past observations of variables and preprocessing the collected data,

- Determining the assumptions of the model describing the behavior of random variables and estimation of the model using historical data,

- Generation of data trajectories consistent with the discretization of the distribution

- Reduction of the scenarios in order to generate a scenario tree with desired features
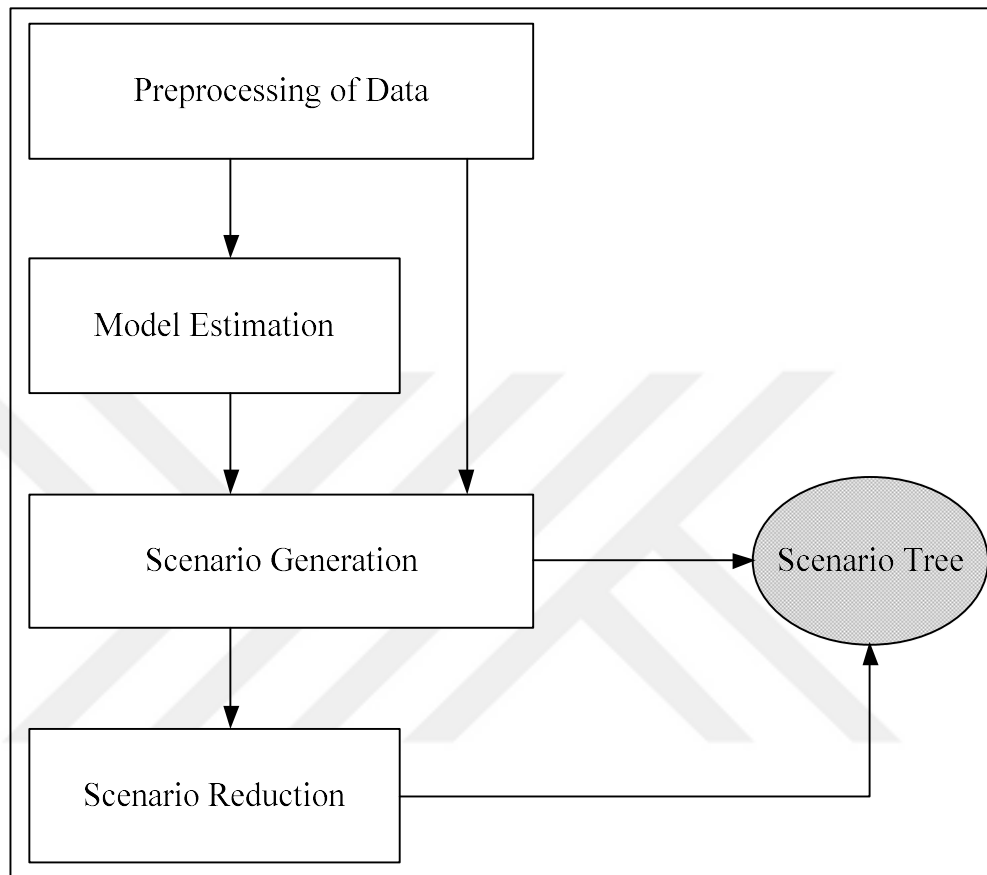
Figure 6.7. Modeling of randomness

In data preprocessing, data is transformed into a new format with cleaning, transformation and reduction techniques after the data collection. In data cleaning, the missing values are filled, and outliers are identified and removed. Transformation routine work for normalization, aggregation and conversion of the data. Data reduction is used for reducing the data set into a smaller size to make the data more convenient. Model estimation, scenario generation and scenario reduction techniques will be explained in detail in the following part of this section.

6.2.1. Model Estimation

A model from the collected data can be created with different methods. The forecasting methods are one of the most common techniques used for model estimation. In literature, there exist numerous research results about the electricity price and wind speed forecasting methods. Forecasting techniques for wind speed are classified by Soman et al. [67], and Weron [68] summarizes the electricity price forecasting methods in five categories. The classification methods that can be used for the modeling of the randomness of wind and price data are shown in Figure 6.8. As can be seen from Figure 6.8, some methods are common to both wind and price forecasting problems, and some others are specific to each problem. In below, all forecasting techniques shown are explained briefly.

6.2.1.1. Techniques Specific to Wind Speed Forecasting

As can be seen from Figure 6.8, forecasting techniques specific to wind speed forecasting can be classified into two groups, namely, Numeric Weather Prediction (NWP) and persistence method. Persistence method assumes that the wind speed in the future is the same as the current time instant. This method is an effective way of forecasting for the ultra-short-term (seconds to several minutes), and it can be used to benchmark other methods [67].

NWP method solves complex mathematical models by using ambient properties like surface roughness, obstacles, temperature and pressure. These models need lots of computations and information which should be rendered with supercomputers. Thus, these calculations can be made by the central governmental institutions. Moreover, NWP is adequate for medium and long terms since the wind speed can be forecasted one or two times in a day. On the other hand, unstable atmospheric conditions result in bad weather predictions that reduce the accuracy of wind speed forecasting.
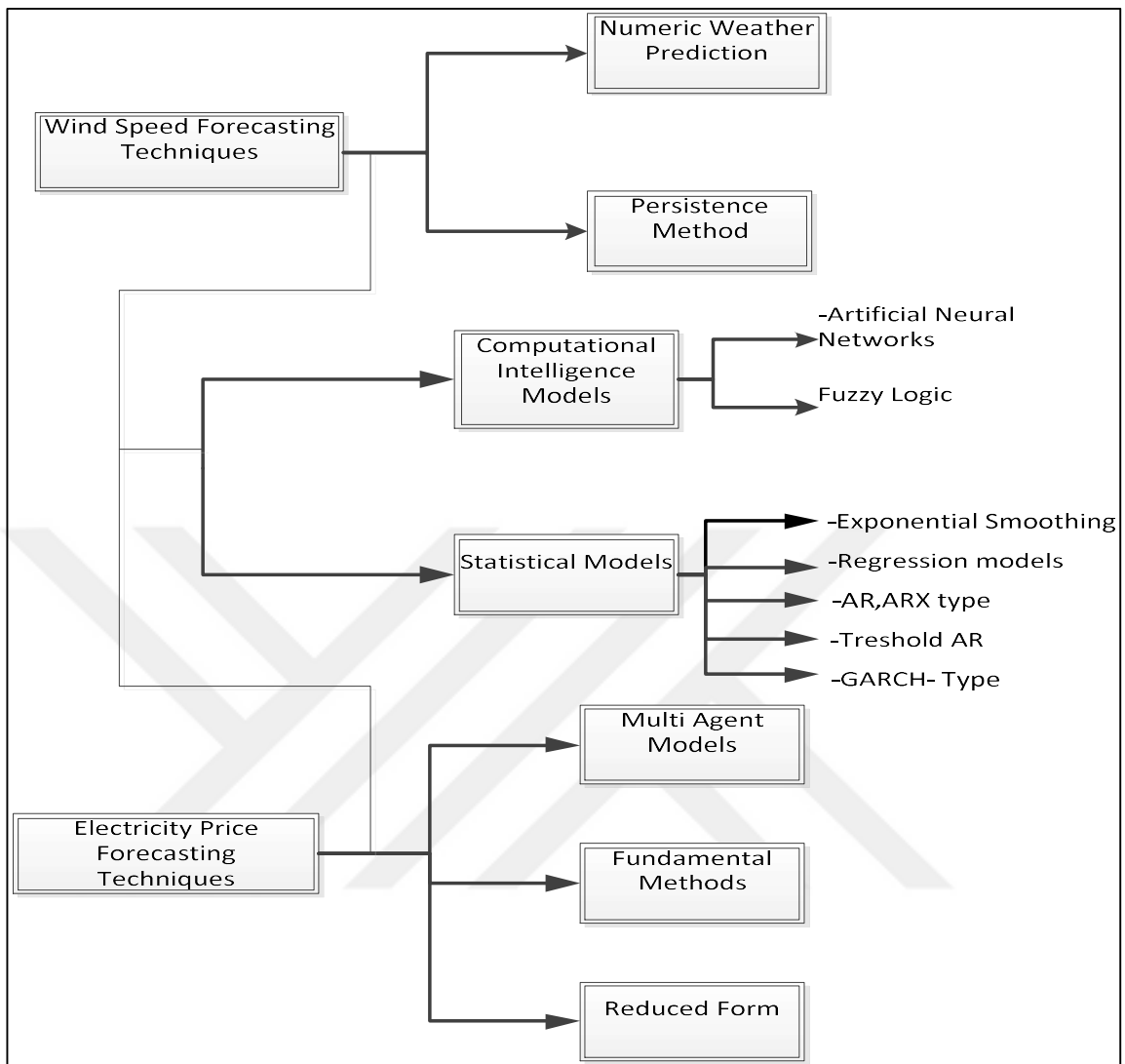
Figure 6.8. Forecasting methods for wind speed and electricity prices

6.2.1.2. *Techniques Specific to Electricity Price Forecasting*

There are three approaches specific to the energy price forecasting, namely, multi-agent models, fundamental methods and reduced-form models. Multi-agent systems simulate the whole electricity generation and transmission system to estimate the prices by mimicking the actual procedures carried out by the system in determining the electricity prices. A review of the methods for price estimation by simulation can be found in [68] and [69]. These methods constitute an incredibly flexible framework for analysis, which may also be a weakness as all assumptions in the model should be justified. Unlike the other techniques, it

focuses on mostly qualitative issues. Thus, it has a lower prediction accuracy than the other methods.

Fundamental methods, which are reviewed by Weron [68], use fundamental drivers like loads, fuel prices and weather conditions and tries to model the primary relationship between these drivers and energy price. Many approaches of fundamental methods in the literature are considered as hybrid solutions with other methods. Medium-term forecasts are more accurate than short-term because fundamental driver data is often collected in weekly or monthly scale. Therefore, the practices of this method are usually limited to risk management. Also, in the fundamental methods, the price forecasts are very sensitive to the variations which need too much effort to adjust.

Reduced-form models which are reviewed in detail by Benth et al. [70], determine the demographic characteristics of electricity prices over time, usually for risk management purposes. Some of the few studies conducted to estimate daily energy prices either with mean-reverting jump-diffusion [71] or Markov regime-switching models [72], however, Benth et al. [70] confirm that poor results have been achieved with these methods.

6.2.1.3. *Techniques Common to Wind Speed and Electricity Price Forecasting*

As can be seen from Figure 6.8, the forecasting methods common to both price and wind speed forecasting can be categorized as computational intelligence and statistical models.

Computational intelligence-based techniques forecast the electricity prices and wind speed by learning, evaluation, and fuzziness approaches. The greatest strength of the computational intelligence-based methods is that they can model inherent complexities and nonlinearities of the data by learning. This allows them to build a useful model to make short-term predictions. Also, these models are simpler to construct as it is not necessary to define the mathematical expressions explicitly. Artificial Neural Networks (ANN) and fuzzy logic models are the primary techniques in this category.

Artificial Neural Networks (ANN) is based on learning the relationship between input and output using historical data. They are composed of neurons which form networks. Two different types of network can be used, which are feed-forward and recurrent networks for

forecasting. Each network is composed of an input layer, hidden layer(s) and an output layer.ANNs can be classified by different aspects such as network structure, learning algorithm, etc. Also, fuzzy logic based ANNs are used for forecasting because it allows outputs to be deduced from noisy or fuzzy inputs, which eliminates the necessity of mapping of input and output.

Different network structures can be used for price forecasting like radial basis functions [73], multi-layer perceptron [74, 75], recurrent network [76] and self-organizing maps [77]. Some of the existing ANN models used in the wind forecasting are radial basis functions [78], multi-layer perceptron [79], and recurrent network [80]. Also, fuzzy-neural ANNs are applied for both wind speed [81, 82] and electricity price forecasting [83]. However, since there exists a wide variety of rich methods in computational intelligence, it is challenging to decide which one will yield a better result.

Statistical methods use historical data or external factors or both to forecast with a mathematical model. Mathematical models of the algorithms are composed of a combination of critical fundamental factors. Also, the structure of the analyzed data influences the accuracy of the prediction. Although this approach is still questioned in some studies, it is preferred due to the seasonal structure of electricity markets and wind speed in nature.

As can be seen from Figure 6.8, statistical methods can be classified into five categories. Exponential smoothing predicts future observations with a weighted average of past observations. These weights are exponentially decreasing depending on a parameter. Also, it can handle seasonal and trend components. Taylor [84] and Jonsson et al. [85] employed Holt-Winters exponential smoothing for energy price forecasting and Cadenas et al. [86] forecasted the wind speed with a simple exponential smoothing.

Regression methods are based on the relationships between predictor variables and a dependent variable. While predictor variables used for electricity price forecasting can be gas prices, temperature or rainfall, the wind speed forecasts may use temperature, pressure, and humidity. Among different alternatives, linear regression models are the most popular forecasting methods. In the literature, Wan der Walt and Botha [87] implemented ordinary least squares and Bayesian ridge regression models to wind forecasting, and Schmutz and Elkuch [88] forecasted energy prices with multiple regression model which uses gas prices, nuclear capacity, temperatures and rainfall as predictor variables.

AutoRegressive Moving Average (ARMA) models are one of the most popular forecasting technique that uses time-series data. The ARMA model has several variations depending on the structure of the data used. ARMA models are suitable if the time-series data is stationary. These models are used for energy price forecasting by Cuerasma et al. [89] and wind speed forecasting by Torres [90]. However, if there is non-stationary (or trend) data, then Autoregressive Integrated Moving Average (ARIMA) should be employed. Conejo et al. [91] forecasted the energy price with ARIMA technique and Palomares-Salas et al. [92] implemented an ARIMA model for wind speed forecasting.

On the other hand, Seasonal Autoregressive Integrated Moving Average (SARIMA) models are employed when the time series exhibits seasonality. Mainly, wind speed and energy price data exhibits a seasonal structure mostly. Thus, the SARIMA model is suitable for these data. Many studies in the literature used SARIMA models for wind speed [93–95] and energy price [96–99] forecasting. ARX-type time series models use past values of the output variable together with exogenous variables like gas price, generation capacity and weather conditions.

Threshold autoregressive models are proposed by Ambach and Schmid [100] for the medium-term forecast of the wind speed and Lucheroni [101] for the energy price forecasting. For ARX type models having non-constant variance or covariance function, Bollerslev [102] proposed a model named the Generalized AutoRegressive Conditional Heteroscedastic (GARCH). Jiang et al. [103] and Garcia et al. [104] forecasted wind speed and energy prices with GARCH method, respectively.

6.2.2. Scenario Generation

Scenario generation is the process of sampling trajectories of a stochastic process characterized by discrete or continuous distribution. In scenario generation, scenario trees, which are discrete possible outcomes in the future, are obtained. They can be used as a representation of future uncertainties in a stochastic programming model. In a scenario tree, the starting node shows the initial value, and the branches from that node express the values that the random variables in the following period can take. At the end of each branch, there are nodes which represent the values of the next period. This continues based on the stages

in which the statistical programming is determined. This tree is composed of several scenarios. Scenarios can be found by starting from the root node and following the next node till the end. The number of scenarios is equal to the total nodes at the last stage. A sample scenario tree, which is composed of 18 scenarios, is given in Figure 6.9.

t=0   t=1   t=2   t=3   t=4
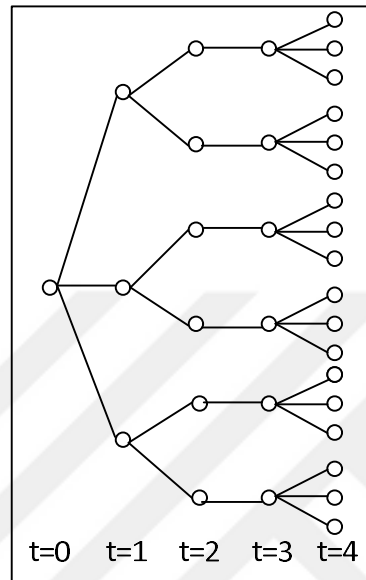
Figure 6.9. Sample scenario tree

Among different scenario tree generation methods mentioned in the literature [49, 105], the sampling method is one of the most appropriate ones for the generation of wind speed and energy price scenario trees. The basic principle of the sampling method is to take a sample from the probability density function, which will give the value of the scenario node and its probability. Among different sampling techniques, random sampling [106], stratified sampling [106], bootstrapping [107] and Monte Carlo [108] are the most common methods in the literature.

6.2.3. Scenario Reduction

In scenario generation, while some techniques may directly generate scenario trees with few scenarios, some of them generate a rich set of trajectories. Nevertheless, the number of scenarios should be kept small to be able to attain a tractable problem. Moreover, if there exists more than one stochastic variable in the problem than the total scenario number will

be all combinations of them, which leads to an exponential growth of the number of scenarios. Thus, there is usually a need for reducing the number of scenarios. There exists different scenario reduction technique like Barycentric approximation [109], sequential clustering [110, 111] and backward and forward reduction [112].

6.3. SCENARIO TREE GENERATION APPROACH USED IN THE THESIS

In this thesis, the steps depicted in Figure 6.7 are applied for scenario tree modeling. Different methodologies can be used for the implementation of each step, as described in Section 6.2. In this study, the following methods are chosen for each step.

Firstly, the preprocessing of the data stage is realized for the collected wind speed data by adjusting to the required height level, as mentioned in Section 2.2. Also, outliers of wind speed and electricity price data are cleared at this stage. SARIMA method is employed for modeling. The simulations were performed using SARIMA models of wind and price data to generate scenarios. Finally, the generated scenarios are reduced by means of a k-means clustering-based reduction technique. Details of the methods and reasons for choosing them are described in the following section.

6.3.1. Estimation of Forecast Model and its Parameters

The time-series methods were described briefly in Section 6.2.1.3. In this thesis, ARMA type models are employed because it is a well-established method that can be modeled easily. A general ARIMA model can be represented as ARIMA(p,d,q), where q is the order of Moving Average (MA) part, d is the order of differencing used, and p is the order of AutoRegressive (AR) part. It can be formulated as follows.

$$(1 - \varphi_1 B - \varphi_2 B^2 - \cdots - \varphi_p B^p)(1 - B)^d x_t$$
$$= (1 - \theta_1 B - \theta_2 B^2 - \cdots - \theta_q B^q)e_t \tag{6.43}$$

where x_t and e_t are time-series data and residuals, respectively. On the other hand, $\varphi_i(i = 1,2,\dots,p)$ and $\theta_i(i = 1,2,\dots,q)$ represent the parameters of the AR and MA parts of the

model, $(1 - B)^d$ shows the differencing operation where B is a backward shift operator, i.e., $Bx_t = x_{t-1}$.

In addition to dependence on past values and residuals, one also needs to take seasonalities in the data into account if they are present. One way to achieve this is to add an additional term into the standard ARIMA model. This leads to well known Seasonal ARIMA model which can be represented as SARIMA$(p, d, q)(P, D, Q)_s$. The P and Q represent seasonally autoregressive and seasonal moving average orders. In order to ensure the stationarity of the series, a seasonal difference of order D can be taken. In this representation, s corresponds to the period of the seasonal part.

If the differenced series is represented as $Y_t = (1 - B)^d (1 - B)^D x_t$ SARIMA model can be defined as

$$\varphi(B)\Phi(B^s)Y_t = \theta(B)\Theta(B^s)\, z_t \tag{6.44}$$

where φ and θ are non-seasonal AR and MA polynomials which are given in Equation (6.43), respectively. Φ and Θ represent seasonal AR and MA polynomials, respectively. These polynomial are similar to non-seasonal polynomials however they are composed of seasonal terms as expressed in the following equations.

$$\Phi(B^s) = 1 - \Phi_1 B^s - \Phi_2 B^{2s} - \Phi_3 B^{3s} \ldots - \Phi_P B^{Ps} \tag{6.45}$$

$$\Theta(B^s) = 1 - \Theta_1 B^s - \Theta_2 B^{2s} - \Theta_3 B^{3s} \ldots - \Theta_P B^{Qs} \tag{6.46}$$

After a brief introduction to the SARIMA model, the estimation of the SARIMA model parameters needs to be explained. This process consists of many stages, which are shown in Figure 6.10. First, the model's seasonality is determined by inspecting time-series Autocorrelation Function (ACF) and Partial Autocorrelation Function (PACF). If a periodic behavior is observed in corresponding plots, a seasonal difference is added to the model until the elimination of the seasonal pattern. Following the determination of the seasonality, the degree of the model is determined by inspecting the ACF and PACF lags. If the model has no seasonality, then p and q are determined. Otherwise, the P and Q are determined firstly in order to eliminate the effect of seasonal AR and MA. After the degree of the model is determined, the coefficients of the model polynomials are estimated with the help of a software. Finally, residuals are analyzed to validate the model. In the analysis of the

residuals, firstly, their independence is tested with statistical and graphical methods. Finally, the statistical test for the validation of the models is performed.
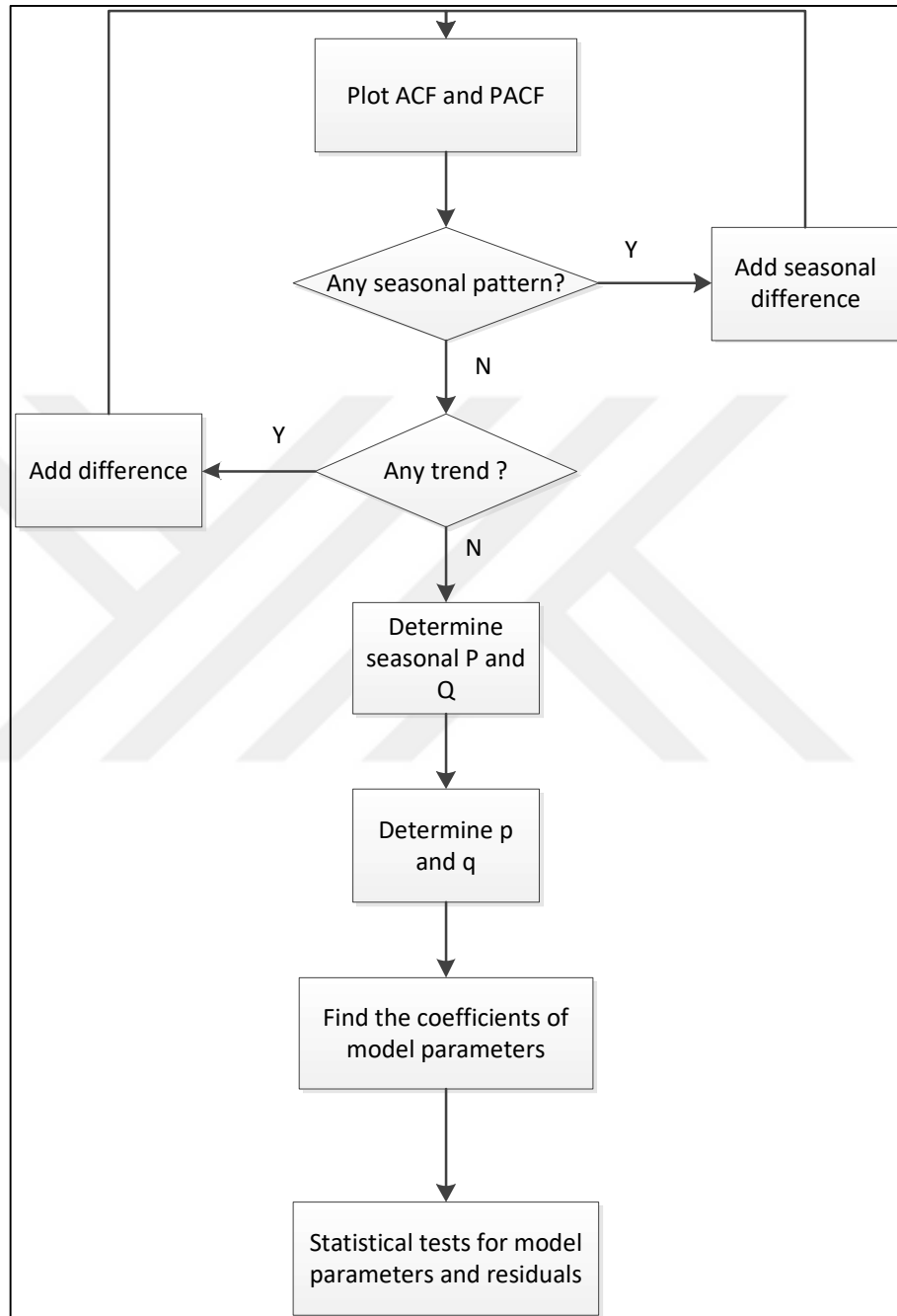
Figure 6.10. Stages of SARIMA model parameter estimation

6.3.2. Monte Carlo Simulation

Among different scenario generation technique, the Monte Carlo simulation is used in this thesis in order to generate scenarios. To this end, the SARIMA model developed is fed by independently and randomly generated residuals to obtain sample paths of the underlying stochastic process. Example scenario fans are presented in Figure 6.11 and Figure 6.12 for wind speed and energy prices, respectively. In the scenario generation, 10,000 scenarios are generated with equal probabilities. However, 100 samples are selected randomly from the generated scenario fans to illustrate the scenarios clearly.
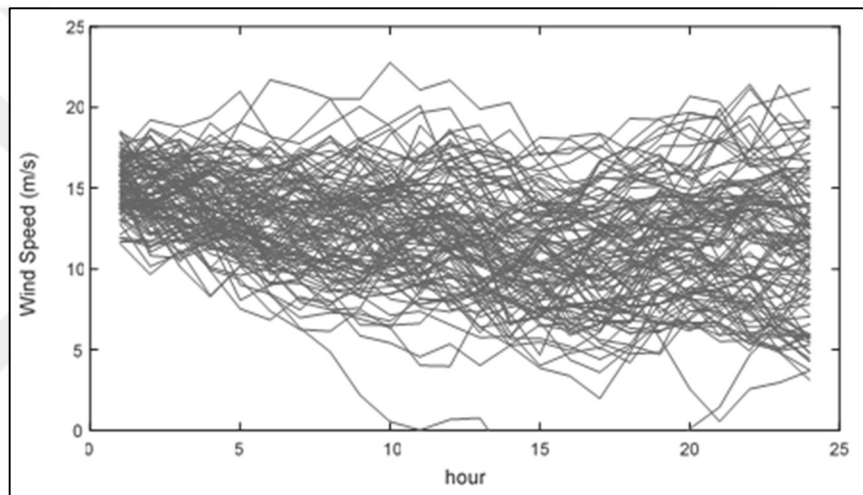
Figure 6.11. Sample Monte Carlo simulation output of 100 scenarios for wind speed
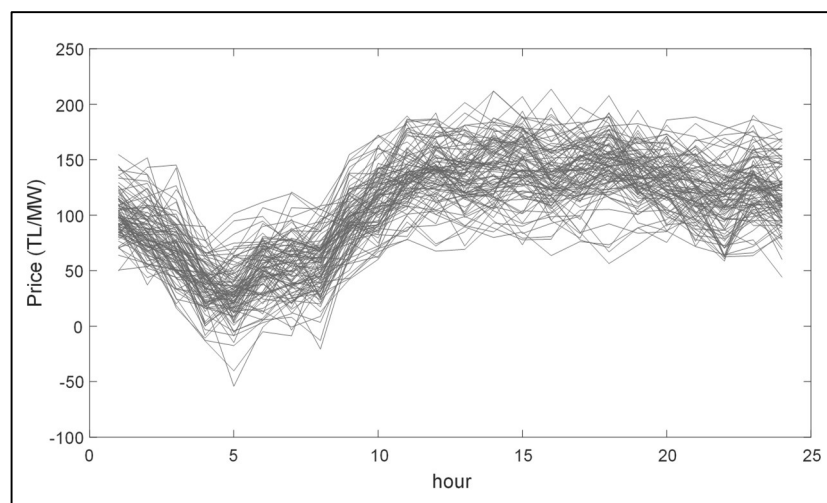
Figure 6.12. Sample Monte Carlo simulation output of 100 scenarios for energy price

6.3.3. Clustering-based Scenario Reduction

In order to obtain realistic results, a rich set of prediction trajectories are usually generated in the scenario generation stage. Nevertheless, for a large number of scenarios, there is a need to perform reduction to make corresponding stochastic optimization problem tractable. Towards this end, reduction algorithms were employed to construct scenario trees of moderate sizes, which contain the essential information associated with the underlying stochastic process.

There are different methods for the scenario reduction in the literature [110, 113]. In this work, the method proposed by Sutiene et al. [114] is employed, and the detailed flow chart is presented in Figure 6.13. This method is an iterative algorithm that starts by creating a root node to which all the scenarios are assigned. Then, repeatedly, for each node, scenarios associated with it are divided into smaller sets using the clustering algorithm, and a node is created for each cluster (Step 2 and Step 3). The value of a newly created node and its probability is calculated based on the scenarios assigned to it (Step 4 and Step 5). This procedure is repeated until the end of the horizon to construct the tree that expands as one moves forward in time. The procedure in each step can be explained as follows.

Suppose that the initial scenario set, which is denoted by $\xi^s = (\xi_0^s, \xi_1^s, \dots \xi_t^s, \dots, \xi_T^s)$, $s = 1, \dots, S$ has K scenarios where t is the stage. b_t is the branching structure at time t which means the scenarios passing through the node at time $t - 1$ will be divided into b_t clusters $C^1, \dots, C^{b_t}$. Each scenario which was assigned to the node k_t at time t is represented by $\xi_t^k = \left(\xi_{t+1}^k, \dots, \xi_T^k\right)$, $k = 1, \dots, NC^{k_t}$ where NC^{k_t} is the number of scenarios assigned to a node k_t. The total number of nodes at time t is denoted by N_t where $N_t = \prod_1^t b_t$, $t = 1, \dots, T$ and $N_0 = 1$ as there will be only one node at root node.

Step 1: Collect generated scenarios, determine b_t, $t = 1, \dots, T$, set $t = 0$ and create the root node ξ_0^1 by calculating the mean of generated scenarios at time $t = 0$.

Step 2: Calculate cluster centroids, which is shown as $\bar{\bar{\xi}}^i = (\bar{\bar{\xi}}_{t+1}^i, \dots, \bar{\bar{\xi}}_T^i)$, $i = 1, \dots, b_{t+1}$ of the b_{t+1} branches passing through the current node k_t. The cluster centroids are calculated by minimizing the following objective function

$$\min \sum_{i=1}^{b_{t+1}} \sum_{k=1}^{NC^{k_t}} d(\xi_t^k, \bar{\xi}^i) \qquad (6.47)$$

where $d(\xi_t^k, \bar{\xi}^i)$ changes according to the clustering method used.

Step 3: For each scenario ξ_t^k passing through the current node, assign it to the cluster C^l such that ξ_t^k is closest to $\bar{\xi}^i$. The value l is determined with

$$l = \arg \min_{i \in \{1, \dots, b_t\}} d(\xi_t^k, \bar{\xi}^i) \qquad (6.48)$$

Step 4: For each node calculated at time t, calculate the ratio between the number of scenarios in C^i and the total generated scenario.

Step 5: Assign $\bar{\xi}_{t+1}^i$ as the value of the node for each node calculated at time t.

In the method mentioned above, different clustering techniques can be applied. In order to find out an appropriate method for scenario reduction, two different techniques are applied, namely k-means clustering and Fuzzy C-Means (FCM) clustering. These techniques differ in cluster assignment and centroids update stages. While k-means assigns the scenarios to the clusters with the minimum distance function as in Equation (6.49), FCM uses a distance function, which is given in Equation (6.50), by calculating the membership value of each scenario before the distance calculation.

$$d(\xi^k, \bar{\xi}^i) = \left\| (\xi_{t+1}^k, \dots, \xi_T^k) - (\bar{\xi}_{t+1}^i, \dots, \bar{\xi}_T^i) \right\|_2 \qquad (6.49)$$

$$d(\xi^k, \bar{\xi}^i) = (u_t^{ik})^m \left\| (\xi_{t+1}^k, \dots, \xi_T^k) - (\bar{\xi}_{t+1}^i, \dots, \bar{\xi}_T^i) \right\|_2 \qquad (6.50)$$

where m is the fuzzifier and $m > 1$. The value of u_t^{ik} is calculated at each time and for each scenario by the following equation.

$$u_t^{ik} = \left(\sum_{s=1}^{b_t} \left(\frac{\left\| (\xi_{t+1}^k, \dots, \xi_T^k) - (\bar{\xi}_{t+1}^i, \dots, \bar{\xi}_T^i) \right\|}{\left\| (\xi_{t+1}^k, \dots, \xi_T^k) - (\bar{\xi}_{t+1}^s, \dots, \bar{\xi}_T^s) \right\|} \right)^{\frac{2}{m-1}} \right)^{-1} \qquad (6.51)$$
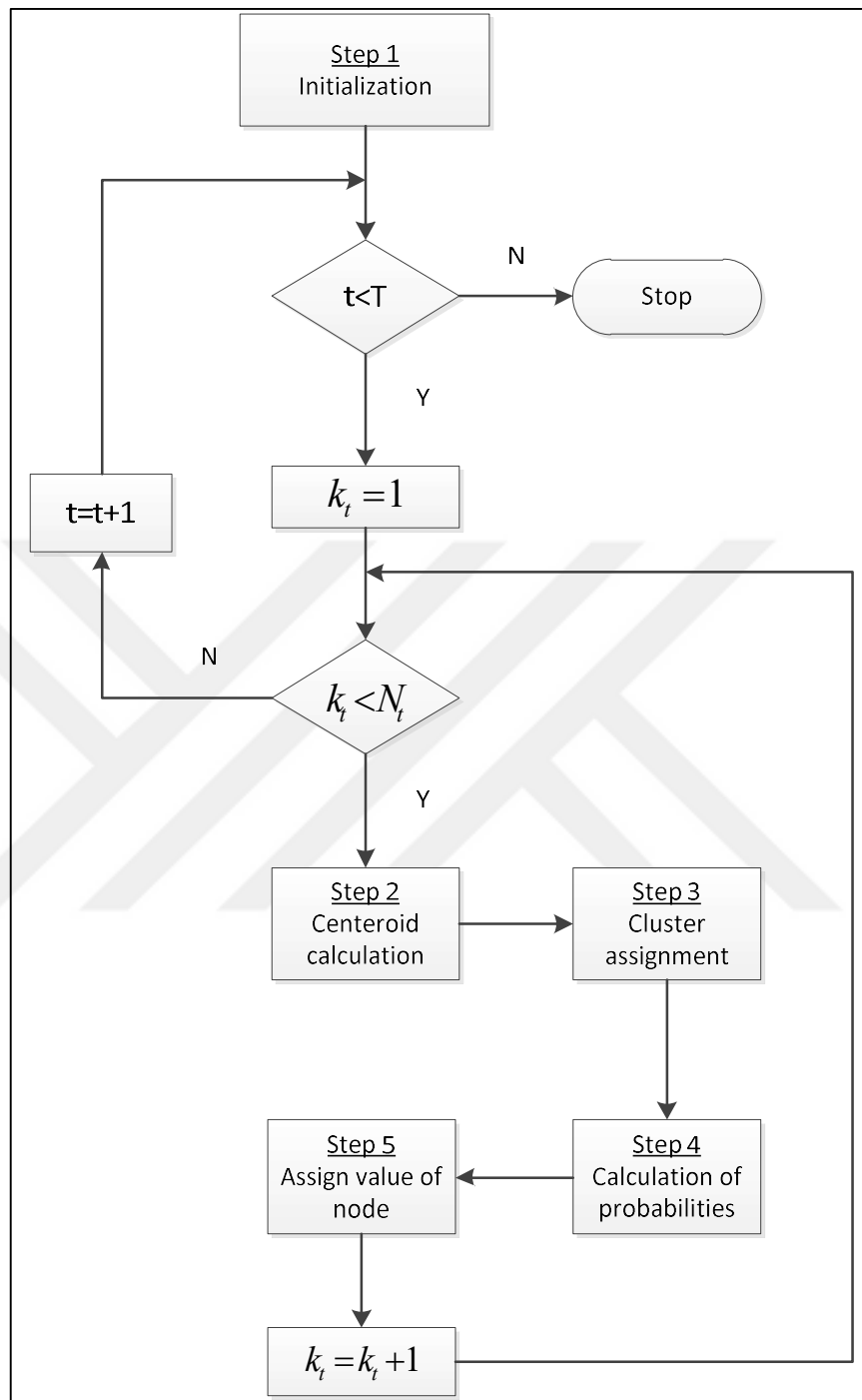
Figure 6.13. Flow chart of the scenario tree reduction

In order to show how the reduction algorithm depicted in Figure 6.13 performs, the methods are applied to a set of wind and price scenarios given in Figure 6.11 and Figure 6.12. Both clustering methods described above are used separately. The reduced scenarios for energy price and wind speed are presented in Figure 6.14 and Figure 6.15. As can be seen from the

figures, the reduced scenarios are slightly different for each method. Hence, it is not clear which method performs better based on these figures.
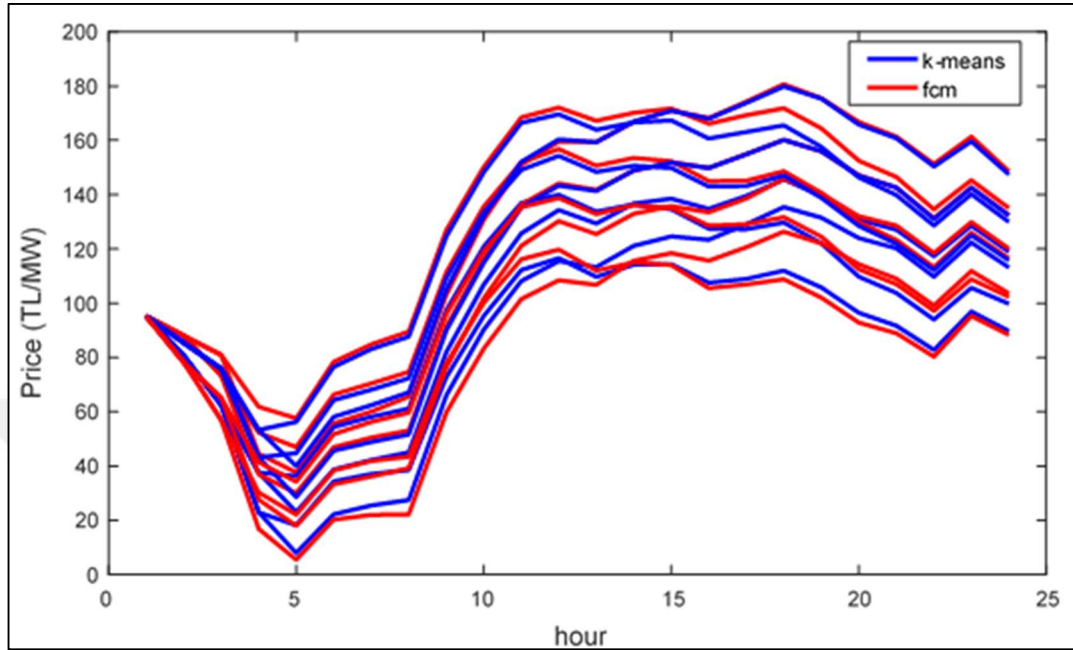
Figure 6.14. Sample scenario trees of energy price that reduced with two clustering algorithm
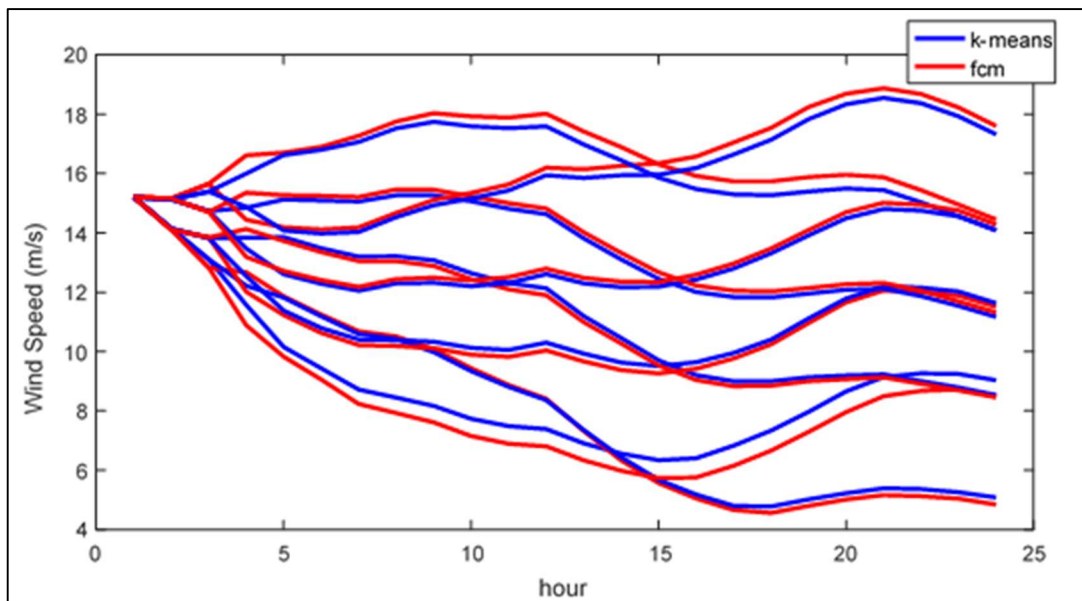
Figure 6.15. Sample scenario trees of wind speed that reduced with two clustering algorithm

Therefore, the scenario reduction process is repeated for 60 different days with two clustering algorithm in order to determine which clustering method will be used in this thesis. During the simulations, computation times are recorded, and the weighted distances between the scenarios and real data are calculated by using scenario probabilities. Then, a paired samples t-test is conducted for the distances and computation times as both methods are tested for the same days. The test statistics of the paired samples t-test, mean and standard deviation of all results are given in Table 6.1. As can be seen from the table, all comparisons are significant as the p values are less than 0.05. It can be concluded that the k-means algorithm generates scenarios closer to the real data and has a better computation time than the FCM algorithm. Thus, k-means is preferred in this thesis.

Table 6.1. Test statistics of compared algorithms

		Wind		Price	
		k-means	FCM	k-means	FCM
Distance	Mean	59.54	61.85	318.86	333.32
	Std.Dev	17.41	16.77	109.75	104.79
	p	0.000		0.000	
Speed	Mean	0.43	0.92	0.44	1.08
	Std.Dev	0.16	0.28	0.13	0.08
	p	0.000		0.000	

7. PROBLEM FORMULATION AND LITERATURE REVIEW

The penetration of wind energy has increased rapidly all over the world in the last decades. Environmental concerns along with decreasing capital costs, low operation costs and improvements in turbine efficiencies constitutes the driving forces behind this growth. However, higher utilization of wind leads to significant challenges due to its intermittent nature, constituting a significant problem for both market operators and GenCos.

As long as wind energy producers are concerned, currently there are incentives in many countries in which energy is bought with the feed-in tariff. This policy ignores the variations in the production for the GenCo. However, the support mechanism is valid for a limited time after which GenCo should trade in deregulated markets. In the market environment, deviations from energy schedules are penalized, reducing the income of the company.

A viable approach to mitigating this problem is to support wind generation with a storage unit. Storage systems can perform energy shifting, arbitrage and imbalance reduction. Several technologies, which are mentioned in detail in Section 3, can be used, such as batteries, compressed air energy storage systems, supercapacitors and Pumped Hydro Storage (PHS) reservoirs. Among these energy storage systems, PHS technology is one of the most important solutions for large-scale wind energy integration with fast response time, high efficiency and large capacity, as mentioned in Section 4.3 [115].

Thus, in this work, a system composed of wind farms and a PHS unit is considered. This hybrid power plant can participate to day-ahead market and compensates its real-time operation deviations in the balancing market. An overall block diagram of the bidding and real-time operation for a wind-powered PHS system and a timing diagram of the market structure are depicted in Figure 7.1 and Figure 7.2, respectively. It can be seen that at day D-1 energy contracts for the next day are computed based on the wind and day-ahead price forecast scenarios. These bids must be submitted to the day-ahead market before the gate closure time. However, there is a significant delay between the gate closure and operation times. This implies that contracts need to be made under a high level of uncertainty since the accuracy of wind energy forecasts diminishes with time significantly, as illustrated in Figure 7.2 [116, 117]. There are different approaches proposed in the literature for computing profitable bidding decisions. A review of these methods is given in the next section.

After the submission of the bids to the day-ahead market, market clearing is performed by the system operator. This is followed by the real-time operation period, which starts considerably later. At this phase, the company is expected to meet its contracts at each hour. Throughout the day D, the real-time operation algorithm controls the systems by calculating operation decisions of PHS. The decisions are computed for each hour making use of the day-ahead bids determined, announced market prices and actual wind power when the decisions are calculated. As can be seen in Figure 7.2, there is a significant certainty gain about wind production at this stage when compared with the bidding phase. The new measurements of wind energy are available at each hour, which can be exploited to obtain better forecasts for the rest of the operation horizon. Also, the amount of energy in the storage device is known at each time step. All this information can be used to make more informed decisions in real-time when compared with the bidding stage.
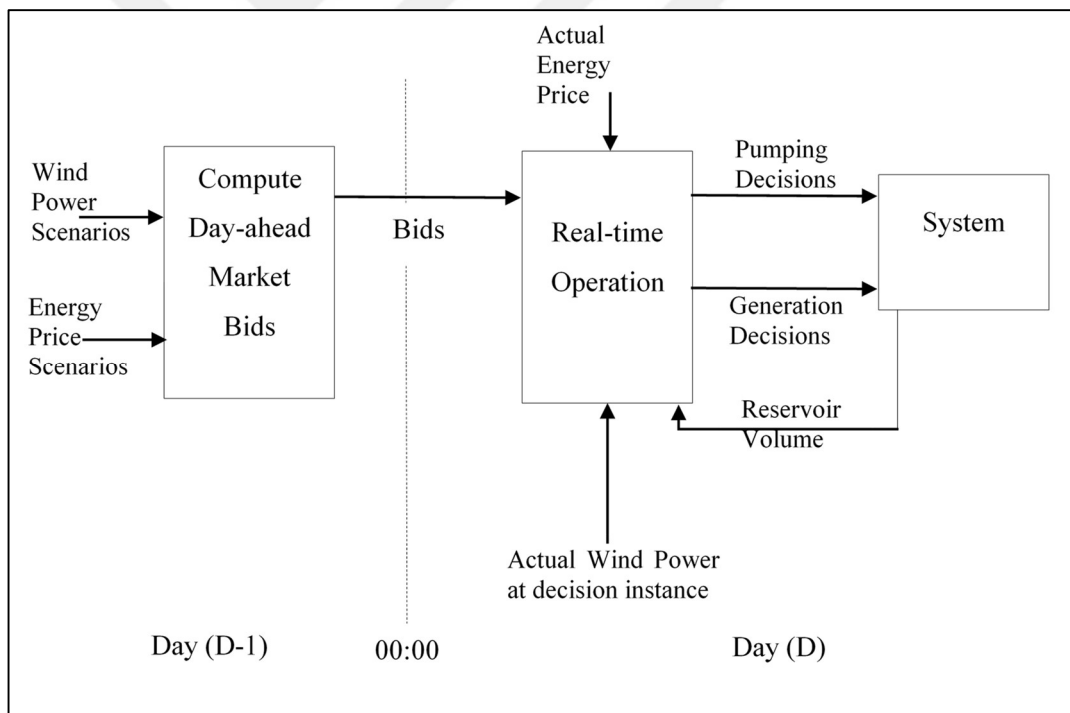
Figure 7.1. Block diagram of bidding and real-time operation of one day
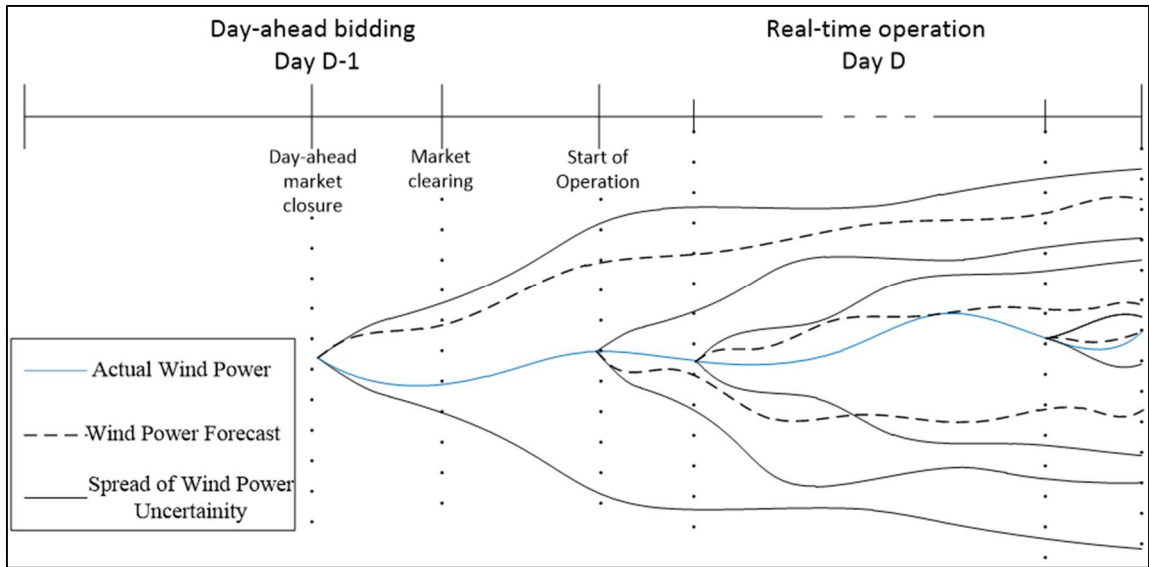
Figure 7.2. Diagram showing wind forecast uncertainty and timing of energy trading in day-ahead and balancing markets

In the following sections, firstly, the mathematical model of the joint wind-PHS system and market trading are introduced. Then, the detailed literature survey for the bidding and real-time operation is given. Finally, the contribution of the thesis is explained.

7.1. WIND-PHS SYSTEM

The system considered in this thesis is composed of wind farms and a PHS system, as depicted in Figure 7.3. In this system, the main objective is to sell the energy generated by the wind farm to the grid. PHS system, on the other hand, provides a buffering capability by storing energy drawn from the network or wind farm and supplying it to the grid when deemed necessary. PHS plant is equipped with several reversible turbines, which are capable of generating energy and pumping water.
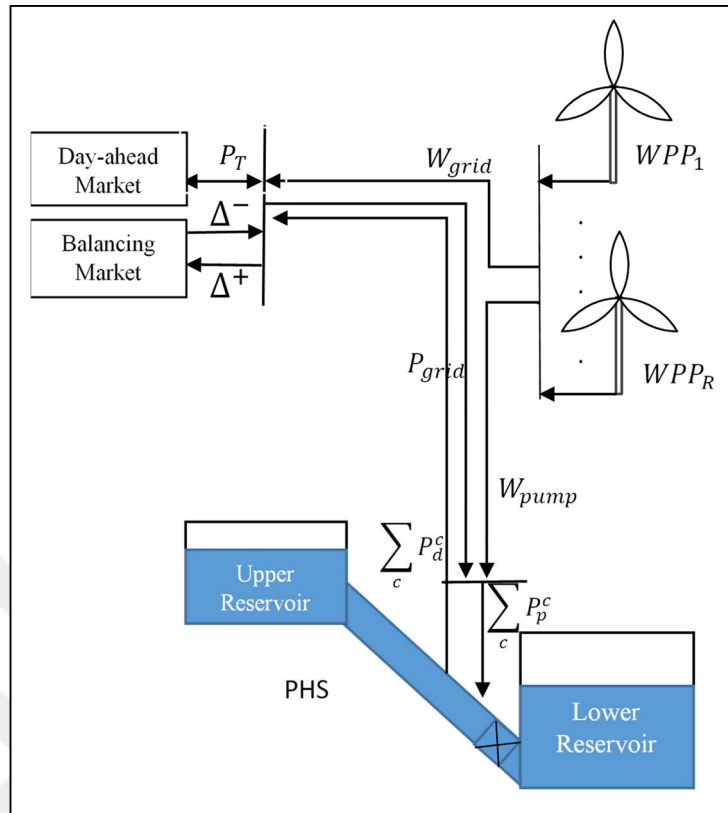
Figure 7.3. Schematic representation of the wind–PHS system.

The energy flow in the system is governed by the following equations

$$P_T(t) = \sum_c P_d^c(t) + W_{grid}(t) - P_{grid}(t) \tag{7.1}$$

$$\sum_c P_p^c(t) = P_{grid}(t) + \eta_T W_{pump}(t) \tag{7.2}$$

$$W(t) = W_{pump}(t) + W_{grid}(t) \tag{7.3}$$

where P_T is the net power exchange with grid, P_d^c is the power generated by the turbine c, P_p^c is the power consumed by the turbine c, W is the wind power generated by the wind farms, W_{grid} is wind energy sold to the grid, W_{pump} is the wind energy consumed by the turbines, P_{grid} is the energy bought from the day-ahead market, η_T is the transmission efficiency between wind farms and PHS system.

Equation (7.1) shows that the net power exchange with the grid is given by the difference between the energy supplied by the wind farm and the PHS, and the energy drawn from the network. The left-hand side of Equation (7.2) is the total energy consumed by the turbines for pumping. This energy is supplied by the wind farm and the grid as can be seen from the right-hand side. Equation (7.3) shows that the total wind power generated is distributed to turbines for pumping and to the grid.

7.2. MARKET MODEL

In this thesis, the wind-PHS power generation company participates to the day-ahead market and compensates their imbalances occurred in the real-time operation in the balancing market. In the day-ahead market, it receives a payment $\lambda \times P_T$, where λ is the day-ahead market price, for the energy it supplies to the system. Deviation of the supply from the contract, $\Delta = P_T - B$, leads to an imbalance cost which result from compensating the deviation in the balancing market. The imbalance cost can be expressed as

$$IC = \lambda \times \begin{cases} r^- \times \max(-\Delta, 0), & reg.\,up \\ r^+ \times \max(\Delta, 0), & reg.\,down \end{cases} \tag{7.4}$$

To understand the formulation above, first, suppose that system is in the regulation-up state (there is an energy deficit). If $\Delta > 0$, the company is not penalized since it is helping the system but in a contrary situation cost incurred becomes $\lambda \times r^- \times \Delta$. Similarly, provided that system is in the regulation-down state if $\Delta > 0$ imbalance cost becomes $\lambda \times r^+ \times \Delta$ while if $\Delta < 0$ there is no associated cost because the company consumes the excess energy of the system. Here, r^+ and r^- are penalty ratios which can be computed from the ratios of the positive and negative imbalance market prices to the day-ahead market price. More specifically, $r^+ = 1 - \lambda_{ib}^+/\lambda$ and $r^- = \lambda_{ib}^-/\lambda - 1$, where λ_{ib}^+ and λ_{ib}^- are positive and negative imbalance market prices, respectively.

7.3. LITERATURE REVIEW OF BIDDING AND REAL-TIME OPERATION

7.3.1. Literature Review of Bidding

The most straightforward approach to the day-ahead bidding problem for a wind producer is to compute point forecasts of wind generation and submit them as generation bids. The success of this method depends on the accuracy of the predictions. There is a rich literature on wind forecasting [118, 119] and the proposed methods range from primitive persistence forecasts to more advanced techniques, as mentioned in Section 6.2.1. However, there is a limit on the accuracy of these tools [120]. Although improvements have been achieved over time, according to recent figures, the estimation errors of the state of art methods are no less than 10 percent for day-ahead timescales [118, 121].

Another idea is to make use of probabilistic methods [122]. Instead of point forecasts, the probability distribution of uncertainty, such as the Weibull distribution [123], can be employed to formulate the bidding as an expectation maximization problem. For simple systems, only composed of wind farms, analytical solutions that provide optimal contracts can be found [124–126].

Aforementioned analytical solutions can be derived when there is no time couplings and limiting constraints as in the case of the systems composed of only wind energy generation units. However, with the involvement of energy storage or some other aspects such as risk-control, this becomes a challenging task if not impossible. Stochastic programming methods, which converts the bidding problem into a numerical optimization by approximating uncertainties with scenario trees, constitute a remedy to this difficulty [127]. Representative papers in which stochastic programming is used can be found in Table 7.1. As can be seen from the table, these studies mainly differ in energy generation and storage devices used. The stochastic approach was used for bidding of price-taker wind energy companies [128–131], wind farms supported by PHS plants or hydro reservoirs [42, 132–135], and standalone PHS systems [95]. Moreover, in [136], a system having multiple wind farms and battery storage units was investigated. In [137] and [138], this technique was applied to virtual power plants.

Apart from the energy generation and storage, studies differ in forecasting technique. While time series forecasting method is the dominant approach in the literature, ANN is also used for forecasting the price and wind speed. In most of the studies, the scenario trees are generated by adding the forecast error to the point forecasts of wind power. Also, historical data is used directly instead of applying a forecasting method in some studies.

Table 7.1. Stochastic bidding methods employed in the literature

	Storage	Energy source	Optimization Technique	Forecasting			Scenario generation	Risk aversion
				Imbalance Cost	Energy Price	Wind Speed		
[128]	-	Wind	MIP	Ratio of price	Historical data	ARMA	Additive error	No
[129]	-	Wind	LP	SARIMA	SARIMA	AR	Additive error	Yes
[130]	-	Wind	LP	SARIMA	SARIMA	SARIMA	Additive error	Yes
[131]	-	Wind	LP	ANN	ANN	ANN	Additive error	No
[42]	PHS	Wind	MILP	Ratio of price	ANN	ANN	IOHMM	No
[132]	PHS	Wind	MINLP	Historical data	Historical data	ANN	Additive error	No
[133]	-	Wind + Hydro	MILP	ARIMA	ARIMA	ARMA	Additive error	No
[134]	-	Wind + Hydro	NLP	Historcial data	Historcial data	Historical data	Historical data	No
[95]	PHS	-	MINLP	-	SARIMA	-	-	No
[136]	Battery	Wind	LP	-	Historical data	-	Probability distribution	No
[135]	-	Wind+Hydro	MILP	Ratio of price	Historical data	Historical data	-	Yes
[137]	Battery	Wind+PV+ Diesel	MILP	-	-	-	Probability distribution	Yes
[138]	PHS	Wind+CPP	MILP	Historical data	Historical data	Historical data	Historical data	Yes

Although maximizing the expected profit is a desirable target, companies are usually sensitive to risks encountered due to contingencies. They want to avoid the worst-case low probability scenarios that can lead to significant losses in case such events occur. With this in mind, a stochastic programming-based risk-averse bidding strategy for a wind energy producer was developed in [129, 130]. Similarly, [135] considered the day-ahead bidding of a combined wind-hydro plant by incorporating risk-control. Also, the risk-aversion approach was discussed for the virtual power plants in [137, 138]. Conditional Value at Risk (CVaR) was chosen as the risk measure, which was optimized in conjunction with the expected profit by taking their weighted average as the objective. This provides a trade-off between the

expected profit and unexpected substantial losses. The detailed information about CVaR was given in Section 6.1.2.

7.3.2. Literature Review of Real-time Operation

In contrast to day-ahead bidding, the real-time operation is a dynamic decision-making problem [139]. The company should make a decision on the amount of energy to supply to the grid at each hour based on new information available. If the only energy source is wind, there is nothing much that can be done because weather conditions determine the generation entirely. To alleviate this problem, the wind generation can be supported by a storage unit, which can be used to adjust the energy injected into the grid by storing and supplying it when deemed necessary. At this stage, the decision-maker has a certain advantage compared to the day-ahead bidding because new information on wind measurements is available. This leads to a substantial reduction in wind uncertainty, as can be observed from Figure 7.2. Moreover, the stored energy can be measured in case there is a storage device, and the spot market prices are known along with the accepted bids.

Until recently, the real-time operation problem had not drawn enough attention. Most of the works concentrated on the bidding phase without considering this aspect rigorously. The underlying stochastic optimal control problem was either ignored entirely or employed with simple heuristics. For example, a popular approach appeared in several works including [140–143] is to determine a fixed schedule at the beginning of the day and apply it for the whole horizon, which, herein, is referred to as the open-loop strategy. This strategy, however, is blind to the information that becomes available up to the present time within the day. To benefit from this information, [144] proposes a ratio-based heuristic that adapts the precomputed plan to actual wind power realizations by preserving ratios of individual variables, which are derived from the open-loop decisions. An alternative idea appeared in [145] and also used in [146] utilizes the storage device to minimize deviations from the bid instantaneously. This method is called as bid-following heuristic throughout the thesis. All these methods will be explained in detail in the following section.

In the last few years, several works appeared that focuses on real-time operation more systematically. Representative papers can be found in Table 7.2. As can be inferred from the

table, deterministic model predictive control (DMPC) is the dominating approach for real-time operation. The underlying algorithm is a rolling horizon method in which an optimization problem depending on point forecasts of random variables is solved repeatedly. The real-time performance can be improved significantly as a result of the certainty gain arising from the repeated computation (recall Figure 7.2).

The studies using DMPC mainly differ in the energy generation and storage technologies utilized. In [147], a Concentrated Solar Power Plant (CSPP) supported by a thermal storage unit was considered. The DMPC optimization objective is imbalance minimization instead of financial losses while bidding model considered is deterministic. [148] investigated a system involving solar, wind, and Combined Heat and Power (CHP) sources and having a thermal storage unit. Bidding is taken as a two-stage stochastic program, and imbalance cost minimization is performed both in bidding and operation phases. In [149], a plant composed of a micro-CHP, PhotoVoltaic (PV), and thermal storage units was studied. The bidding model is deterministic and does not involve imbalances. Imbalances are only considered in the operation phase. The system investigated in [150] consists of a wind farm and a thermal generator as the energy sources while batteries maintain storage. Bidding is formulated as a stochastic mixed-integer nonlinear programming problem having the imbalance cost in the objective. Real-time operation considers only deviations from the day-ahead contracts. In [151], a wind energy source supported by a battery storage system was investigated. Only real-time operation aspects are considered ignoring the bidding phase. In [152], a PV system coupled with a generic energy storage device was studied. Day-ahead contracts were assumed to be given, and only the operation part was analyzed. Lastly, the system investigated in [153] comprises a wind farm and a PHS plant. Generation contracts were taken as point forecasts of wind production while the objective of the real-time operation was imbalance cost minimization.

Although the DMPC approach benefits from certainty gain with updated computations, the probability distribution of uncertainties are not exploited since the underlying algorithm is based on point forecasts. Moreover, it is not amenable to incorporating risk control because of the deterministic formulation. Similar to stochastic programming based methods proposed for the bidding problem, one may naturally think about making use of the uncertainty information to compute better decisions and bring the risk-control into the operation phase.

There are just two studies covers the stochastic approach. The methods shown in Table 7.2 are based on Stochastic Model Predictive Control (SMPC) and Linear Decision Rules (LDR). SMPC can be regarded as an extension of DMPC in which instead of a point forecast, a scenario tree is used to model the effects of uncertainties. [154] introduced a risk-neutral SMPC method for the real-time operation of a system composed of a wind farm and a PHS. The proposed approach involves risk control, neither in bidding nor operation phases. LDR, on the other hand, obtain risk-averse bidding and operation strategies for a wind energy producer having a generic storage device by employing local linear approximations of decision functions which depend on uncertainties [155].

Table 7.2. Real-time operation methods employed in the literature

	Storage	Energy source	Day-ahead Bidding	Real-time operation	Imbalance cost		Forecasting	Scenario generation	Risk Aversion
					DAB	RTO			
[147]	thermal	CSPP	Deterministic MIQP	DMPC MIQP	Deviation	Deviation	Historical data, linear regression (AR type)	NA	no
[148]	thermal	PV + wind + CHP	Stochastic MILP	DMPC MILP	IB cost	IB cost	Historical data	Additive error	no
[149]	thermal	CHP+PV	Deterministic MILP	DMPC MILP	No	IB cost	ARIMA, historical data, linear regression	NA	no
[150]	Battery	Wind + Dist. thermal	Stochastic MINLP	DMPC MINLP	IB cost	Deviation	Historical data	Additive error	no
[151]	Battery	Wind	NA	DMPC MILP	No	Income from IB market	Historical data	NA	no
[152]	Generic	PV	Given	DMPC LP	No	IB cost	Historical data, solar model	NA	no
[156]	PHS	Wind	Stochastic MILP	SMPC MILP	IB cost	IB cost	ANN time series	Additive error	no
[153]	PHS	wind	Point wind forecast	DMPC LP	No	IB cost	NWP	NA	no
[155]	Generic	Wind	Stochastic LDR	Stochastic LDR	IB cost	IB cost	Historical data	Additive error	yes

7.4. CONTRIBUTION OF THE THESIS

This work aims to introduce a combined method for bidding and real-time operation, the main focus being on the latter, of a wind farm equipped with a PHS system. Bidding is based on MILP stochastic programming model of the problem. For real-time operation, an SMPC

strategy is proposed. Compared to previous works employing the DMPC approach, the distinguishing aspect of the proposed method is the incorporation of uncertainty information and risk control into real-time operation computations. The proposed algorithm differs from the other stochastic operation methods proposed in [43] and [44] in that the former does not consider risk control while the latter is based on a completely different technique and uses a different type of storage unit.

Different real-time operation methods in the literature were implemented along with the proposed SMPC algorithm and their performances were compared under changing market conditions. This is the first study that gives such a detailed comparison between available operation methods.

Also, although real-time operation decisions and their consequences depend on the bidding strategy, this was not elaborated in all of the works. In some of them, the bidding stage is ignored completely ([151, 152]). However, the actual performance achieved is determined by the outcomes of the real-time operation. Thus, the gap between the profits given by bidding and operation-based analyses is investigated in order to demonstrate how important the latter is for a realistic evaluation of the actual performance. There have been no studies in the literature which perform this analysis.

Another aspect, which was not treated well, is imbalance costs. Imbalance cost is taken into account realistically both in bidding and operation phases in just a few of the papers. In the rest, instead of incorporating the imbalance cost, either deviation from the bids are penalized, or imbalances are entirely ignored in the bidding phase. Moreover, the mathematical model utilized in this study involves several characteristics of a PHS plant, which were not taken into account completely in previous works.

For the forecasts of uncertain variables, the majority of the papers directly make use of historical data instead of employing a forecasting mechanism, which is not realistic. Furthermore, in all of the works using a stochastic model for bidding or operations phases, scenarios are generated by simply adding a noise component to the point forecasts. This does not model the temporal relations of the random variables well. A more appropriate approach would be to use advanced time series techniques for this purpose. Thus, scenarios utilized in bidding and operation phases are generated by Monte Carlo simulations, which are performed by a well-developed SARIMA based time-series models of wind and price data.

8. PROPOSED METHOD FOR BIDDING AND REAL- TIME OPERATION

In this section, firstly, the proposed mathematical model for the bidding is presented with the scenario tree structure used. Then, the proposed real-time operation approach is explained in detail. Finally, the real-time operation methods in the literature, which are employed for the performance comparison of the proposed method are explained briefly.

8.1. BIDDING IN DAY-AHEAD MARKET

The bidding phase aims to determine the energy contracts for the next day that maximizes the expected profit. Due to uncertainties involved, the bidding is modeled as a stochastic programming problem in which the wind farm and the PHS systems are assumed to cooperate. This coordinated planning results in utilizing PHS for two purposes, namely, energy shifting and arbitrage. The former means that the excess wind energy is stored and used in a later time when the wind energy source is insufficient. The latter implies that energy bought from the grid in a low price period is sold back to the network when energy prices are high to make a profit out of this difference.

In stochastic programming formulation, the different realizations of the random data are represented, as a scenario tree as depicted in Figure 8.1, which shows the spread of the random information over time. Each node is represented by a pair of integers, the second of which is the time. The first enumerates the nodes at each time instant starting from one to K, where K represents the number of nodes at time t. Each scenario has a certain probability which is shown as $\pi(k)$, such that the summation of node probabilities for a fixed time adds up to one.

In order to construct the optimization problem, one needs to combine the objective with the constraints arising from the physical model described in Section 7.1 and from physical and operational limitations. The constraints are required to be satisfied for all possible scenario nodes at every time instant. The following MILP gives the overall optimization problem.
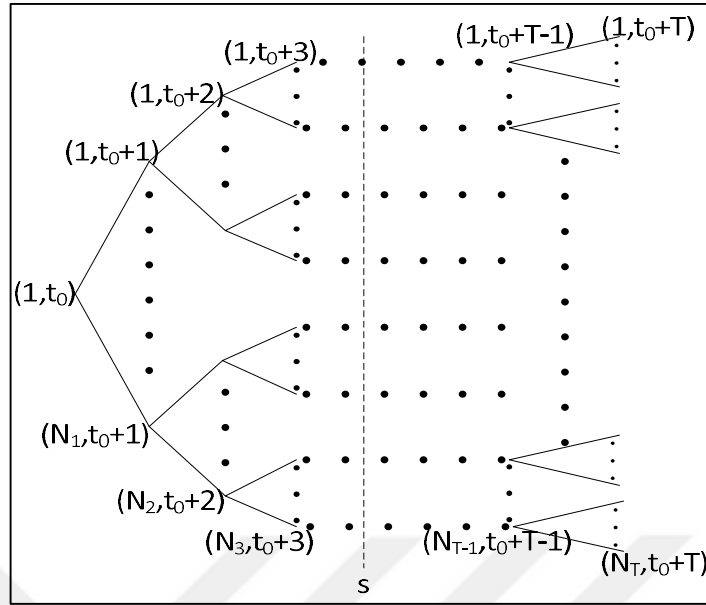
Figure 8.1. Scenario tree structure used in bidding model

$$max \sum_{k=1}^{K} \sum_{t=s}^{T} \pi(k)(\lambda(k,t)P_T(k,t) - IB(k,t) - SUSD(k,t)) + \beta \cdot CVaR_\mu \qquad (8.1)$$

$$IB(k,t) = r^+ \lambda(k,t)\Delta^+(k,t) + r^- \lambda(k,t)\Delta^-(k,t) \qquad (8.2)$$

$$\Delta^+(k,t) - \Delta^-(k,t) = P_T(k,t) - B(t) \qquad (8.3)$$

$$SUSD(k,t) = \alpha_d^{up} \sum_{c=1}^{C} y_d^c(k,t) + \alpha_p^{up} \sum_{c=1}^{C} y_p^c(k,t) + \alpha_d^{down} \sum_{c=1}^{C} z_d^c(k,t)$$

$$+ \alpha_p^{down} \sum_{c=1}^{c=C} z_p^c(k,t) \qquad (8.4)$$

$$y_d^c(k,t) - z_d^c(k,t) = u_d^c(k,t) - u_d^c(k,t-1) \qquad (8.5)$$

$$y_p^c(k,t) - z_p^c(k,t) = u_p^c(k,t) - u_p^c(k,t-1) \qquad (8.6)$$

$$CVaR_\mu = \zeta - \frac{1}{1-\mu} \sum_{k=1}^{K} \pi(k)\tau(k) \qquad (8.7)$$

$$-\sum_{t=s}^{T}\left(\lambda(k,t)P_T(k,t) - IC(k,t) - SUSD(k,t)\right) + \zeta - \tau(k) \le 0 \tag{8.8}$$

$$V(k,t) = V(k,t-1) + \sum_{c=1}^{C}\left(q_p^c(k,t) - q_d^c(k,t)\right) \tag{8.9}$$

$$V(k,0) = V_{initial} \tag{8.10}$$

$$\underline{V} \le V(k,t) \le \overline{V} \tag{8.11}$$

$$q_d^c(k,t) = u_d^c(k,t)\underline{q}_d(c) + q_\delta^c(k,t) \tag{8.12}$$

$$P_d^c(k,t) = u_d^c(k,t)\underline{P}_d^c + q_\delta^c(k,t)\delta^c \tag{8.13}$$

$$q_\delta^c(k,t) \le u_d^c(k,t)\left(\overline{q}_d^c - \underline{q}_d^c\right) \tag{8.14}$$

$$P_p^c(k,t) = u_p^c(k,t)\tilde{P}_p^c \tag{8.15}$$

$$q_p^c(k,t) = u_p^c(k,t)\tilde{q}_p^c \tag{8.16}$$

$$\sum_{c=1}^{C}u_d^c(k,t) - l(k,t)C \le 0 \tag{8.17}$$

$$\sum_{c=1}^{C}u_p^c(k,t) + l(k,t)C \le C \tag{8.18}$$

$$P_T(k,t) = W_{grid}(k,t) + \sum_{c=1}^{C}P_d^c(k,t) - P_{grid}(k,t) \tag{8.19}$$

$$\sum_{c=1}^{C}P_p^c(k,t) = W_{pump}(k,t)\eta_T + P_{grid}(k,t) \tag{8.20}$$

$$W(k,t) = W_{pump}(k,t) + W_{grid}(k,t) \tag{8.21}$$

$$l(k,t), u_d^c(k,t), u_p^c(k,t), y_d^c(k,t), y_p^c(k,t), z_d^c(k,t), z_p^c(k,t) \in \{0,1\} \tag{8.22}$$

$$P_d^c(k,t), P_p^c(k,t), q_d^c(k,t), q_p^c(k,t), q_\delta^c(k,t), W_{grid}(k,t), P_{grid}(k,t),$$
$$W_{pump}(k,t), \quad \tau(k), \Delta^+(k,t), \Delta^-(k,t) \geq 0 \tag{8.23}$$

where all constraints are satisfied for $k = 1:K, t = s:T$ and constraints Equations (8.5),(8.6), (8.12),(8.16), (8.22)and (8.23) are satisfied for $c = 1:C$.

In the objective function (8.1), the first term is the expected net profit. It is the average of the difference between the income from the energy exchange with the grid and penalties paid for the imbalance and startup/shutdown costs. The second term is the CVaR at probability level μ $(CVAR_\mu)$ that imposes the risk control [56]. It is weighted by the factor β to adjust the degree of risk aversion. The imbalance cost is computed using Equation (8.2) as the summation costs for positive and negative deviations from the day-ahead contracts, which are obtained using Equation (8.3). Equations (8.4)-(8.6) are for startup and shutdown costs of the turbines while constraints Equation (8.7) and (8.8) compute the CVaR.

The time evolution of the water volume in the upper reservoir and its initial value and limits are given by Equations (8.9), (8.10) and (8.11), respectively. Constraints Equations (8.12)-(8.18) describe the operation of turbines, as explained in Section 4.5. Turbine c is in generation mode if the associated logic variable u_d^c is one. In that case, Equation (8.12) implies that the discharged water is the sum of its technical minimum and the deviation from this minimum (q_δ^c). Similarly, the produced power is given by Equation (8.13) as the technical minimum power plus the additional energy produced by q_δ^c. The deviation q_δ^c is limited by Equation (8.14) If the turbine c is not in generation mode, u_d^c becomes zero, which, in turn, enforces q_δ^c, q_d^c, and P_d^c to become zero. On-off operation in the pumping mode is represented by Equations (8.15) and (8.16). Equations (8.17) and (8.18) are for preventing simultaneous pumping and discharging.

The energy balance of the system is formulated by the constraints (8.19)–(8.21). Equation (8.19) implies that the total energy exchange with the grid is equal to the energy provided by the wind and PHS turbines minus the energy drawn from the network. Equation (8.20) indicates that the wind turbines and the grid provide the energy consumed for pumping. Here, losses encountered while transmitting wind power to the PHS system are taken into account by multiplying the power with the transmission efficiency η_T. As can be observed from Equation (8.21), the total wind power generated is transferred to the turbines and the

grid. Equation (8.22) defines binary variables while nonnegativity constraints are imposed by Equation (8.23).

Also, the following nonanticipativity constraints must be satisfied

$$P_d^c(i,t) = P_d^c(j,t), P_p^c(i,t) = P_p^c(j,t) \; \forall c \text{ and } \forall (i,j) \in \Omega(n,t) \text{ and } \forall n,t \qquad (8.24)$$

$$B(i,t) = B(j,t) \; \forall i,j,t \qquad (8.25)$$

The nonanticipativity constraints were explained in Section 6.1.1.2 in detail. To be able to formulate nonanticipativity constraints in the mathematical model used, the set of indexes of all scenarios passing through a node (n,t) as $\Omega(n,t)$ is denoted. The purpose of nonanticipativity constraints is to ensure that variables of the scenarios corresponding to the same non-leaf node take the same values. By this way, one can make sure that a decision made at a specific time instant does not depend on the future realizations of the random data (see [157] for further details).

It should be noted that the actual values of random data are only known for the times coming before the beginning of bidding computations (t_0). On the other hand, bids should be determined for the operation period, which starts considerably at a later time (s). Therefore, although the scenario tree is constructed starting from the beginning of the bidding phase, only the part of it corresponding to the operation interval $(t = s:T)$ is used, as can be observed from Figure 8.1a and Equations (8.1)–(8.25).

8.2. PROPOSED APPROACH TO REAL-TIME OPERATION

The proposed approach, which is depicted in Figure 8.2, is an SMPC based real-time operation optimization method that also optimizes the day-ahead bids. As mentioned in Section 2, the day-ahead bids of day D are determined with wind $\widehat{W}$ and price forecast $\hat{\lambda}$ scenarios in day D-1. As the bids are calculated and submitted to the market, the real-time operation starts at 00:00 for day D. At day D, the SMPC algorithm regulates the operation of the PHS system by calculating pumping (p) and generation (d) decisions. Decisions are calculated every hour using bids, and declared electricity prices determined before the start of the operation, and updated balancing market price ratios, amount of energy in reservoirs

and wind scenarios generated for the rest of the day. The price and wind scenarios used in the operation phase are generated with Monte Carlo simulations that use SARIMA forecast models. During operation, these historical data are updated every hour with a new wind measurement, and the data is stored in a memory unit. The oldest wind data is deleted when the new one is written to memory. Using the most recent of wind measurements, the generation of wind scenarios to be used in the SPMC is repeated at each hour.
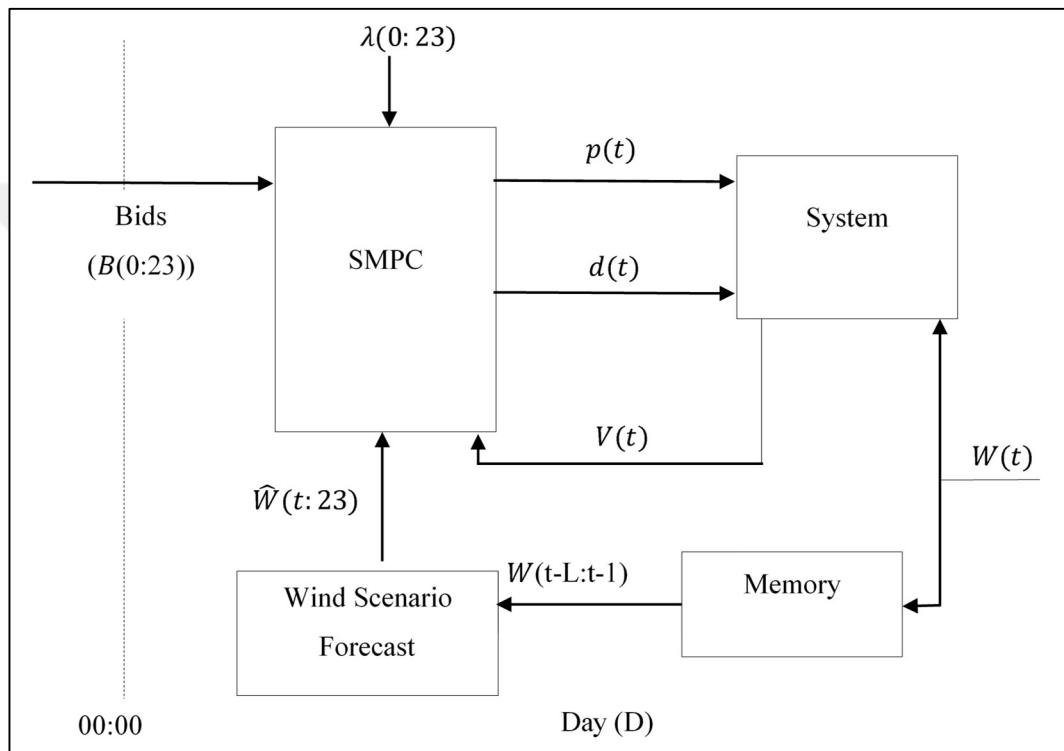
Figure 8.2. Block diagram of the proposed real-time approach

The flow chart of the SMPC-based operation algorithm is depicted in Figure 8.3. In this algorithm, in contrast to that of bidding, t_0 refers to the current hour within the operation day for which the decisions are computed. At $t = t_0$, the storage level of the PHS plant and the wind realization are measured, wind scenarios are forecasted for the rest of the day, and a scenario tree is created employing a scenario reduction algorithm. Then, a stochastic MILP problem is solved to calculate the decision variables p and d for the rest of the horizon. Only the values corresponding to the first time instant are taken as the decisions and the rest are discarded.
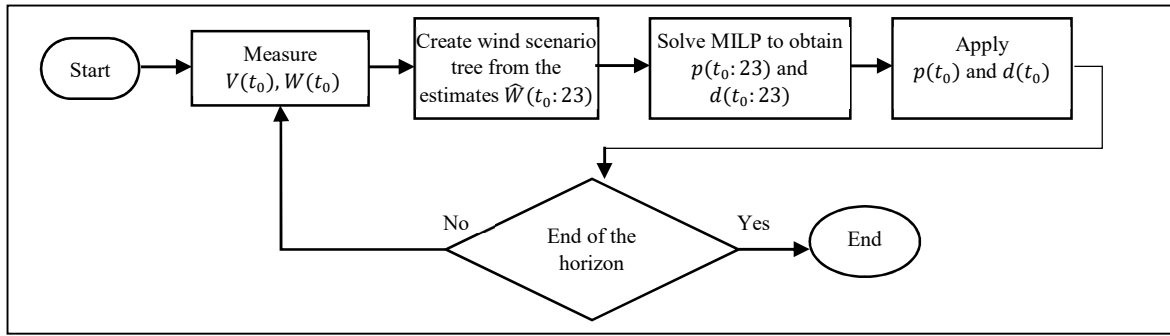
Figure 8.3. Flowchart of the SMPC algorithm

The optimization problem of the SMPC strategy is very similar to that of bidding with the difference that bids and energy prices become known. This implies that the only random information remaining in the problem is the wind generation for the following hours. Hence, the SMPC control law can be computed by solving Equations (8.1)-(8.24) by replacing bids with their known values in Equation (8.3), employing cleared market prices in Equations (8.1), (8.2) and (8.8), and constructing the scenario tree only from wind data. The start time should be taken as $s = t_0$ because, unlike bidding, there is no gap among the times at which computations are performed and decisions are applied. Note that because the optimization problem is stochastic, p and d normally take different values for different nodes of the scenario tree. For $t = t_0$, however, it is necessary to have a single solution to be able to make a decision. To achieve this, the scenario tree used in the operation phase is constructed so that branching starts at $t = t_0 + 1$. In other words, there is only one node at $t = t_0 + 1$, which is connected to the root at $t = t_0$ with a single edge (see Figure 8.4). The risk-averse operation can be achieved by choosing a β value different from zero.
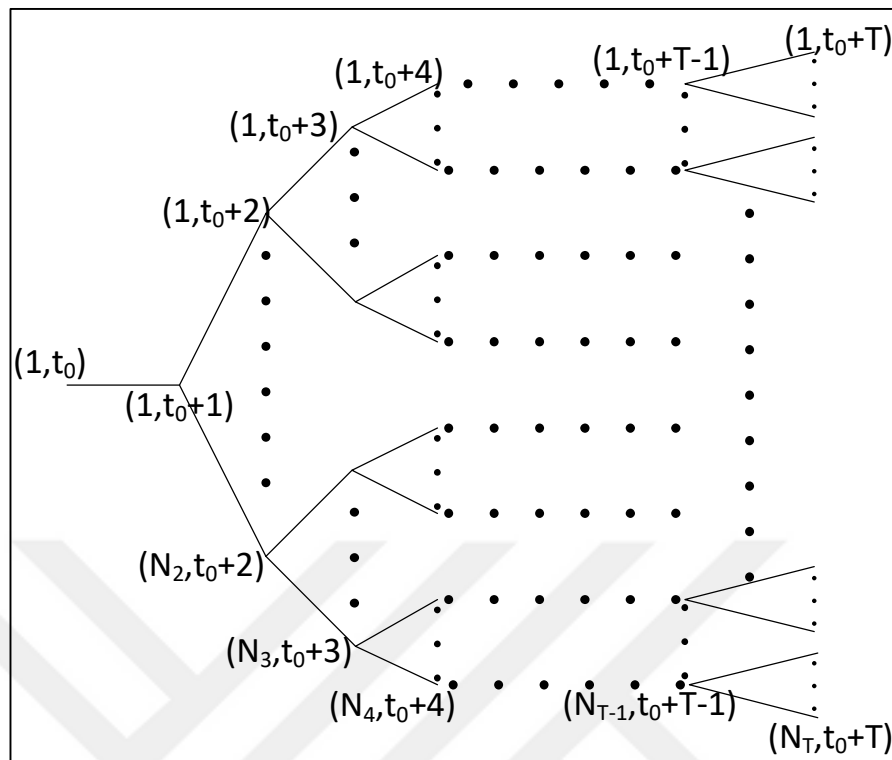
Figure 8.4. Scenario tree structures used in SMPC model

8.3. ALTERNATIVE   APPROACHES   PROPOSED   FOR   REAL-TIME OPERATION IN LITERATURE

In order to demonstrate the importance of the choice of the real-time operation method, several alternative algorithms described in Section 7.3.2 were analyzed and compared with the proposed SMPC approach. These methods are summarized in this part and implemented to demonstrate the performance of the SMPC strategy.

8.3.1. Bid-following Heuristics

The basic idea of this method, which is employed in [155] and [146] is to satisfy the bid as much as possible. In other words, it is an instantaneous imbalance minimization with the most recent wind information which is shown in Figure 8.5.
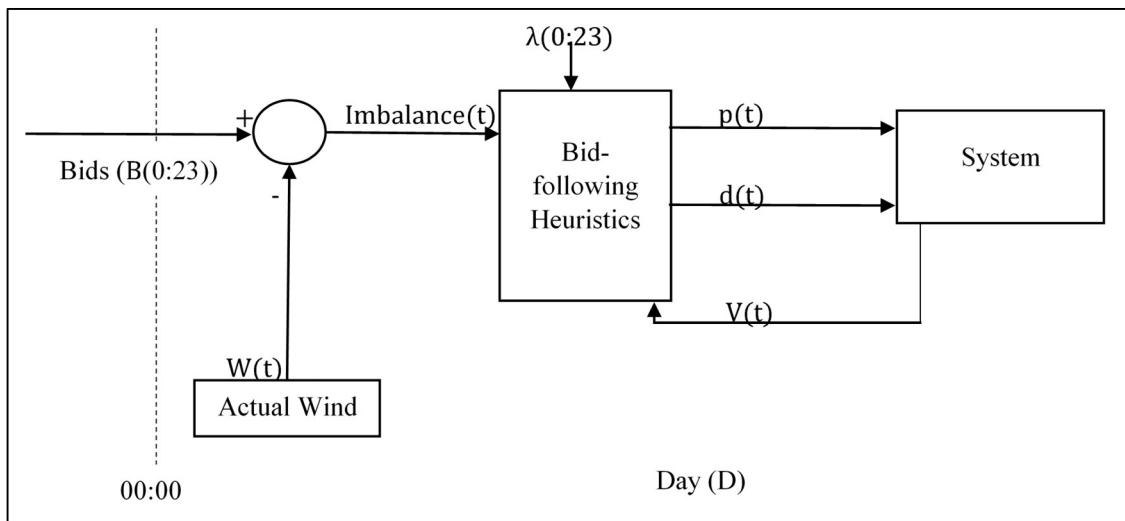
Figure 8.5. Block diagram of bid-following heuristics algorithm

In this method, firstly, the imbalance is calculated with a difference of bid and actual wind power for a specific hour. According to the sign of imbalance, the decisions of the PHS units are calculated based on the flow chart given in Figure 8.6. In the case of the negative imbalance, the excess energy needs to be pumped to the upper reservoir, while water needs to be discharged to the lower reservoir as the imbalance is positive. However, if the imbalance is zero, then the PHS system will be in idle mode. In both cases, system constraints are taken into account, and the decisions need to be modified to comply with them whenever necessary. Thus, after the pumping and generation decisions are calculated, they are checked if they are higher than the operational limits of the turbine for generation and pumping. Then, volume for the following hour is calculated to check the volume that should be between the upper and lower limits of the reservoir. If it is not in the operation limits, then corrections are calculated, and the decisions are sent to the PHS system. This process is repeated until the end of the day for each time step. While utilization of the actual wind power is the main advantage for this method, this heuristic strategy only considers the current time without taking into account what may happen in the future about wind power realizations.
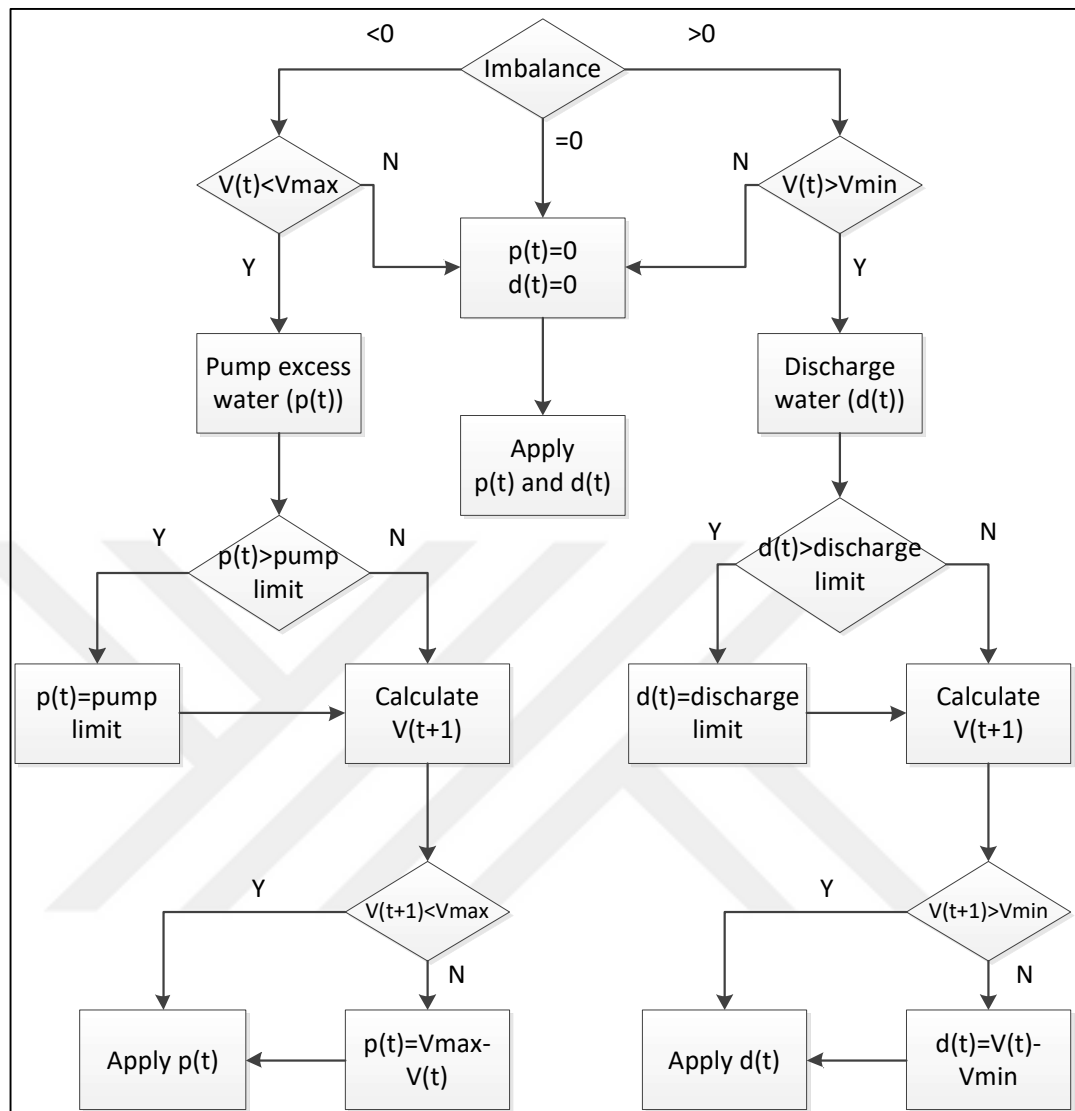
Figure 8.6. Flow chart of bid-following heuristics algorithm

8.3.2. Open-loop Method

This real-time operation method is one of the most common techniques employed in the literature [140–143]. The optimization model, which is explained in the bidding phase with the Equations (8.1)-(8.23) is implemented without a scenario structure and the risk aversion. The wind power is forecasted for the whole horizon in order to compute an optimal plan which decides the operation of the PHS units from the start of the operation till the end of the day with the submitted day-ahead bids. The decisions are applied without any change

independent of wind energy realizations through the day. Since the actual wind power will possibly be quite different from its initial forecasts, that approach leads to suboptimal results.

8.3.3. Ratio-based Heuristics

It is a real-time operation method implemented in [144], and this can be considered as a closed-loop adaptation of an open-loop strategy which is shown in Figure 8.7 with the flow chart of the algorithm presented in Figure 8.8.
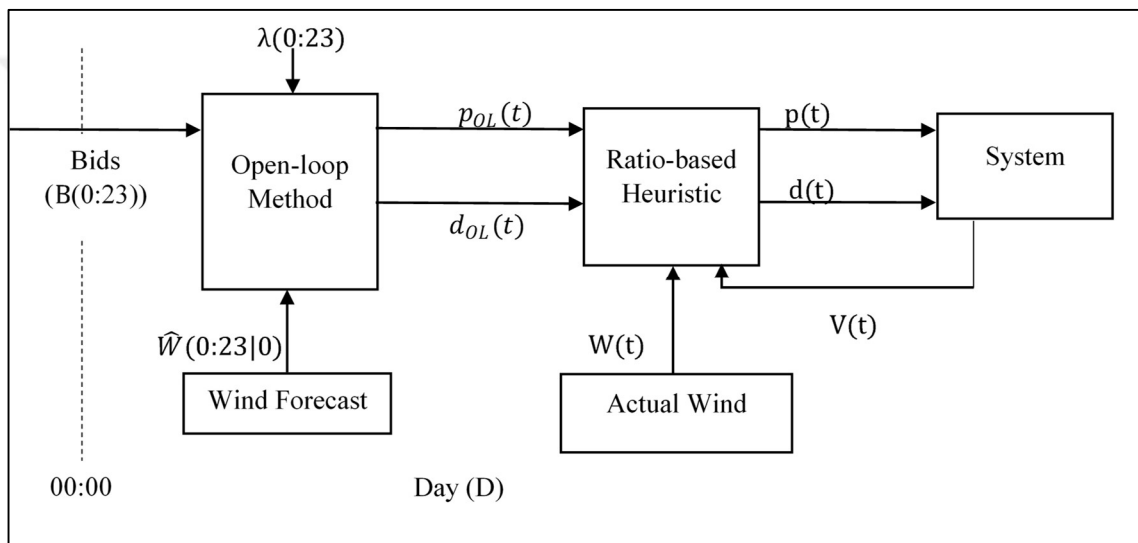
Figure 8.7. Block diagram of ratio-based heuristics method

Firstly, the generation, d_{OL}, and pumping, p_{OL}, decisions obtained and wind power used in the open-loop method are collected. By using this information, the stored energy in the open-loop algorithm, E_{OL}, is calculated for each hour. Then, at the start of each hour, the decision of open-loop algorithm is checked that if it is pumping or generating. If a pumping action is decided in the open-loop algorithm, then the sign of total power sent to the grid is checked. According to the sign of total power sent, the ratios of wind power delivered to the grid, R_{wind}^{grid}, or wind power used in the pumping operation, R_{pump}^{wind}, in the open-loop method are calculated. On the other hand, if the open-loop method decides to generate energy, ratio of energy generated by the turbine, R_{tur}^{cap}, in the open-loop method is calculated. Then, based on the newest information of wind speed, new decisions are computed, which preserves the precomputed ratios. After the update of the decisions, the new volume and new energy

capacity,E_{ratio}, that will occur after the updated decisions are calculated in order to check that the PHS will be in the operating limits. As in the bid-following heuristics algorithm, if operating limits are exceeded, the PHS decisions are updated again to take within limits.
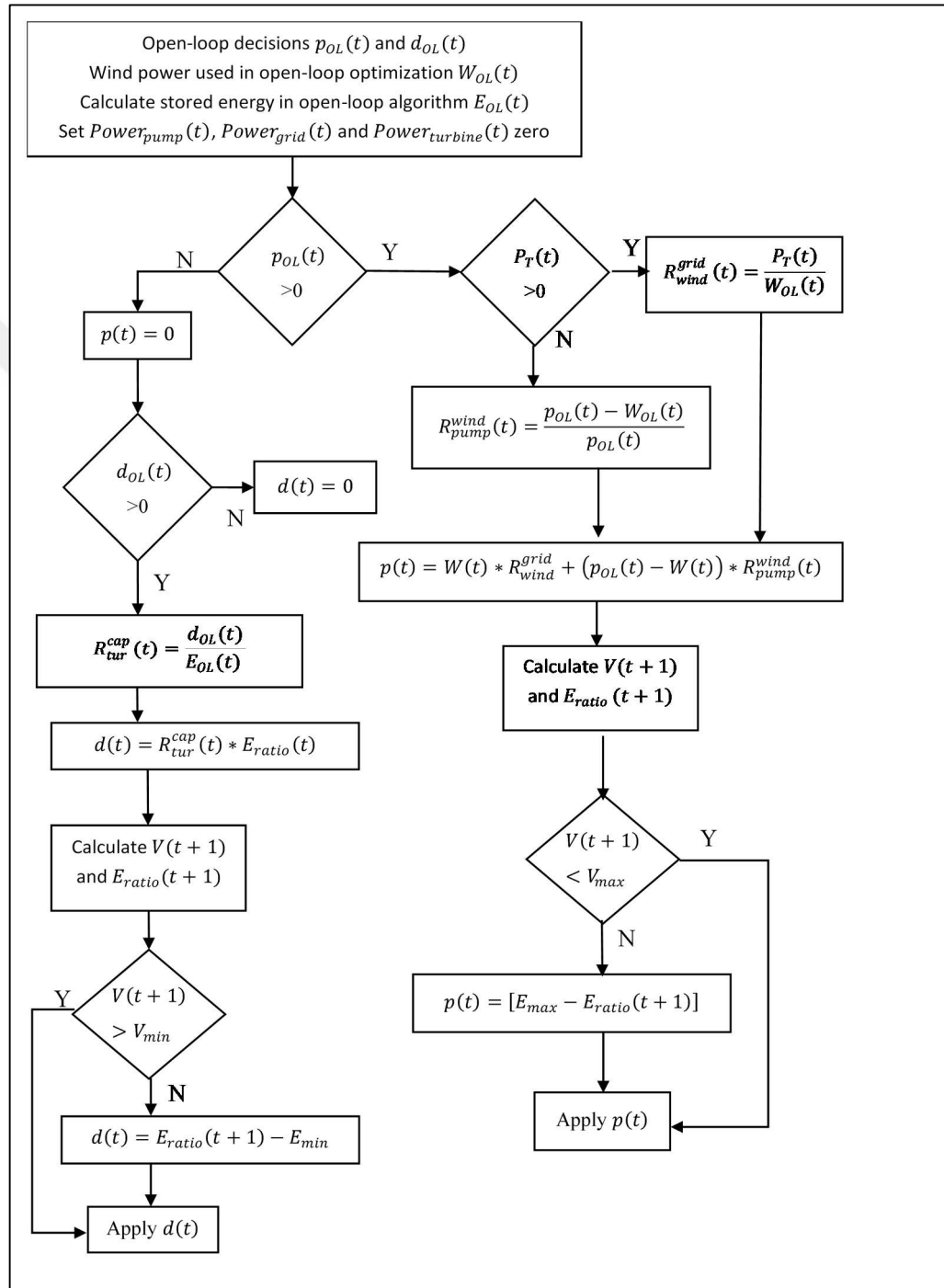
Figure 8.8. Flow chart of ratio-based heuristics algorithm

8.3.4. Deterministic Model Predictive Control (DMPC) Method

It is a rolling horizon method studied in [147–152] which uses a point forecast of future wind power realizations. It constitutes a special case of SMPC in which scenario tree is just a single trajectory without any branching.

8.3.5. Perfect Information Solution

In this strategy, the actual wind power is used as the forecast in the open-loop method. Since the future wind power generation is known perfectly, it provides the best possible solution, and no other method can give a better result. Although this method cannot be realized in practice, it is used as a reference to show how close the other methods are to the ideal case.

9. CASE STUDY

In this section, numerical results for the proposed bidding and operation strategies are investigated, comparing their performance with the other methods available in the literature. The methods contrasted with SMPC are open-loop scheduling, ratio-based heuristic, bid-following heuristic and DMPC. These methods were described briefly in Section 8.2 by giving references to the related works. In addition, for the SMPC method, two variants are implemented with different tree structures, in order to understand the effects of the scenario tree structure on the performance.

The first set of simulations were carried out for a specific day, i.e., April 8, 2011. First, day-ahead bids were computed and a Pareto analysis was performed to investigate the tradeoff between expected profit and CVaR. Second, for these bids, daily schedules of all operation methods were obtained and compared. Third, a Monte Carlo analysis was conducted to investigate the Pareto optimality of the operation methods and bidding results. This analysis also verifies observations made based on the daily schedules statistically. In all these simulations, positive and negative imbalance ratios were set as $r^+ = 0.44$ and $r^- = 0.44$, which are averages of values calculated from actual imbalance and spot market prices for 2011.

The purpose of the second set of simulations is to justify the observations made for a single day in the long run and investigate the sensitivity of the economic performance to imbalance market conditions. The time span was taken from April 1, 2011, to April 30, 2011. Optimization problems were solved using CPLEX 12.6.1, and high-level algorithms were implemented in MATLAB.

9.1. SPECIFICATIONS OF WIND FARM AND PHS SYSTEM

The system investigated comprises two wind farms and a PHS plant as depicted in Figure 9.1 and Figure 9.2. Wind Power Plants (WPP), namely Soma and Sayalar, are operated by the same company and approximately 20 km apart. Due to their close proximity, they experience very similar weather conditions.
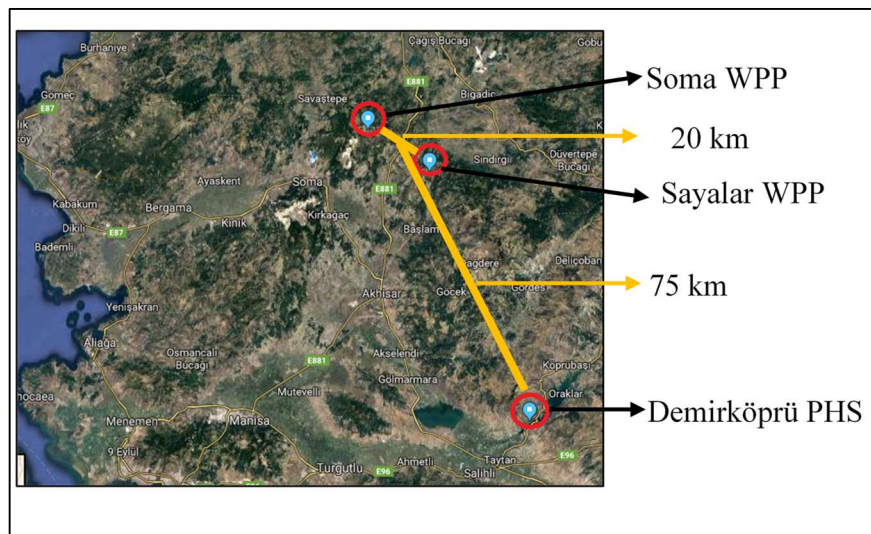
Figure 9.1. Locations of wind farms and the PHS plant
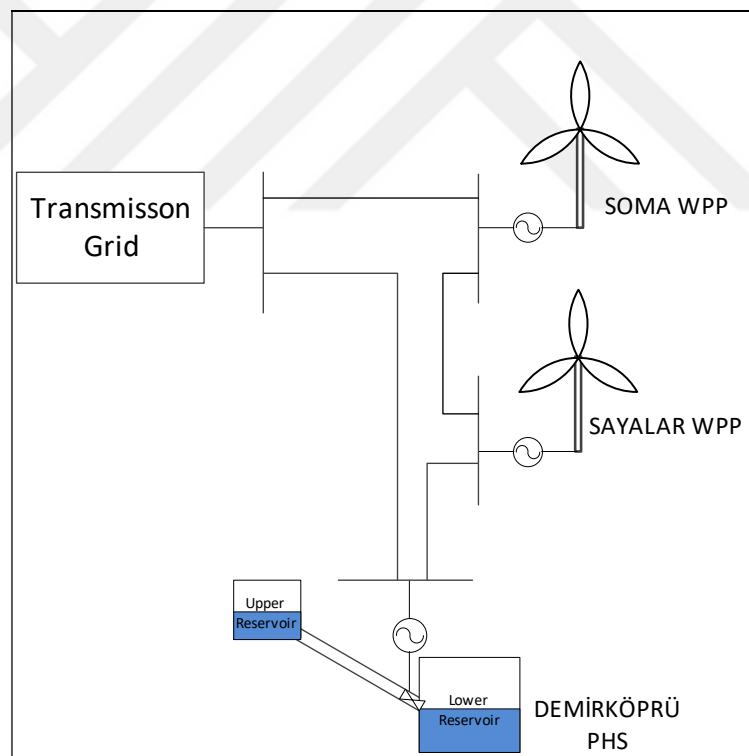
Figure 9.2. Schematic representation of the wind-PHS system

As described in Section Section 2.3, Soma WPP has a total installed capacity of 240.1 MW provided by 169 ENERCON (80 E-70,89 E-44) turbines while Sayalar WPP has 48 ENERCON (10 E-70, 38 E-44) turbines of the total capacity of 57.2 MW, the combined

capacity being 297.3 MW. As for the PHS plant, its all parameters are given in Table 9.1 which includes start-up and shut-down costs and transmission losses in addition to the ones given in Section 4.

Table 9.1. Parameters of the PHS plant

$\overline{V}$	$3\ hm^3$	$\overline{\eta}_d^c$	0.87
$\underline{V}$	$0\ hm^3$	$\overline{\overline{P}}_p^c$	130.9 MW
$\overline{h}$	$215\ m$	$\overline{\overline{q}}_p^c$	$55.3\ m^3/s$
$\underline{h}$	$205\ m$	$\overline{\overline{\eta}}_p^c$	0.87
$\underline{P}_d^c$	37.3 MW	η_T	0.98
$\overline{P}_d^c$	99.1 MW	α_d^{up}	525 TL
$\underline{q}_d^c$	$23.8\ m^3/s$	α_p^{up}	325 TL
$\overline{q}_d^c$	$55.3\ m^3/s$	α_d^{down}	52.5 TL
$\underline{\eta}_d^c$	0.78	α_p^{down}	32.5 TL

9.2. SARIMA MODELS OF WIND POWER AND ELECTRICITY PRICE

Stages of model estimation were described in Section 6.3 and applied as follows. Firstly, in order to determine the seasonality of the SARIMA model, ACF and PACF are plotted as in Figure 9.3 and Figure 9.4 with the raw data of wind speed and electricity price. The periodicity of the lags in the ACF plots of the raw data exhibits the 24-hour seasonality as can be seen from Figure 9.3 and Figure 9.4.
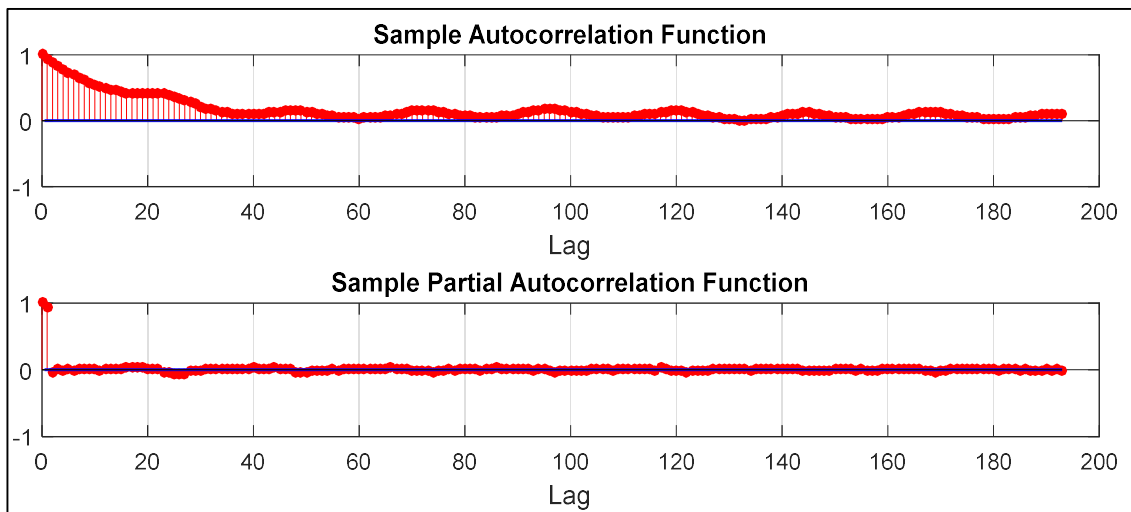
Figure 9.3. ACF and PACF of wind speed raw data
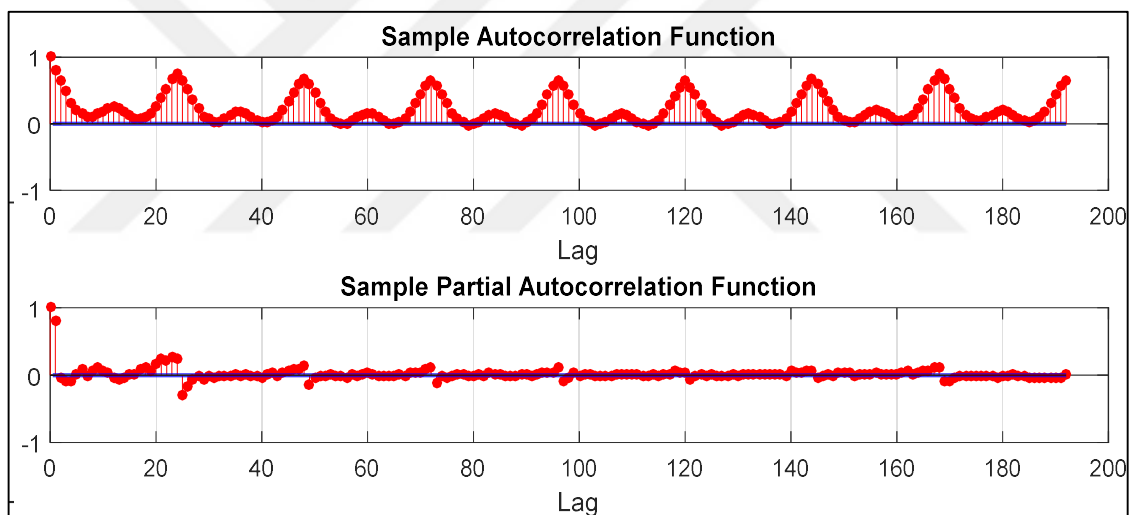
Figure 9.4. ACF and PACF of energy price raw data

After determination of the seasonality, the SARIMA models for wind speed and electricity price were estimated by applying all stages of the method explained in Figure 6.10. The models used for both variables are presented in Table 9.2 and Table 9.3. As can be seen from tables, both models are complicated, which may result in inaccurate model estimation. Therefore, SPSS Time Series Module, which can identify the best-fitting for SARIMA model estimation was used to check the proposed SARIMA models if they are correct or not.

Table 9.2. SARIMA model parameters of wind speed

Wind Power Model		Value	t	p
AR	Lag 2	0.893	125.7	0
Difference				1
MA	Lag 1	0.056	4.6	0
	Lag 2	0.996	171.2	0
	Lag 4	-0.051	-4.6	0
AR. Seasonal	Lag 1	0.909	87.1	0
	Lag 2	0.034	-2.7	0.01
MA. Seasonal	Lag 1	0.853	211.5	0
$(2,1,4)(2,0,1)_{24}$				

Table 9.3. SARIMA model parameters of energy price

Price Model		Value	t	p
AR	Lag 1	0.957	132.9	0
MA	Lag 1	0.421	32.1	0
	Lag 2	0.077	5.81	0
	Lag 3	0.053	3.9	0
	Lag 4	0.083	6.4	0
	Lag 5	0.063	5.1	0
AR. Seasonal	Lag 1	0.078	8.3	0
Seasonal Difference				1
MA. Seasonal	Lag 1	0.864	149.0	0
$(1,0,5)(1,1,1)_{24}$				

The best-fitting parameters can be calculated with different measures like normalized Bayesian information criterion, R^2, MAPE and MAE. The model fit statistics for both models are presented in Table 9.4 and the model fit statistics are higher than 0.5 which shows the 50 percent of the dependent variable variance is explained by the independent variables. In a SARIMA model, the dependent variable is the forecasted value and the independent variables are the historical data which is used by the SARIMA model parameters.

After the model specifications, a statistical test for autocorrelation should be applied to the residuals. Ljung-Box Q tests the overall randomness of a specified number of lags instead of testing at each distinct lag. It generally tests the autocorrelation of residuals of an ARIMA model that is different from zero or not. If the significance value of this test is less than 0.05, then the correlations of the residuals are zero. Table 9.4 shows that the residuals are uncorrelated in both wind speed and electricity price SARIMA models.

Table 9.4. Residual and model fit analysis

Wind Speed					Electricity Price				
Model Fit Statistics	Ljung-Box Q		Residual Descriptive Statistics		Model Fit statistics	Ljung-Box Q		Residual Descriptive Statistics	
R^2	χ^2	p	μ	σ	R^2	χ^2	p	μ	σ
0.896	35.4	0.0	0.005	1.47	0.826	25.6	0.004	0.07	19.5

The statistical results of the residuals can be supported with the graphs, which show whether autocorrelation of residuals is within specified limits. Figure 9.5 and Figure 9.6 show that the ACF and PACF are decreased below the desired limits for wind speed and electricity price residuals, respectively. The outliers of residual lags, which is higher than the limits, are so close to the limits, and these can be neglected. Moreover, the histogram of the residuals for both wind speed and electricity price forecasting shows that these residuals are normally distributed. Normality is an essential measure for the Monte Carlo simulation because the residuals in the simulation need to be normally distributed.
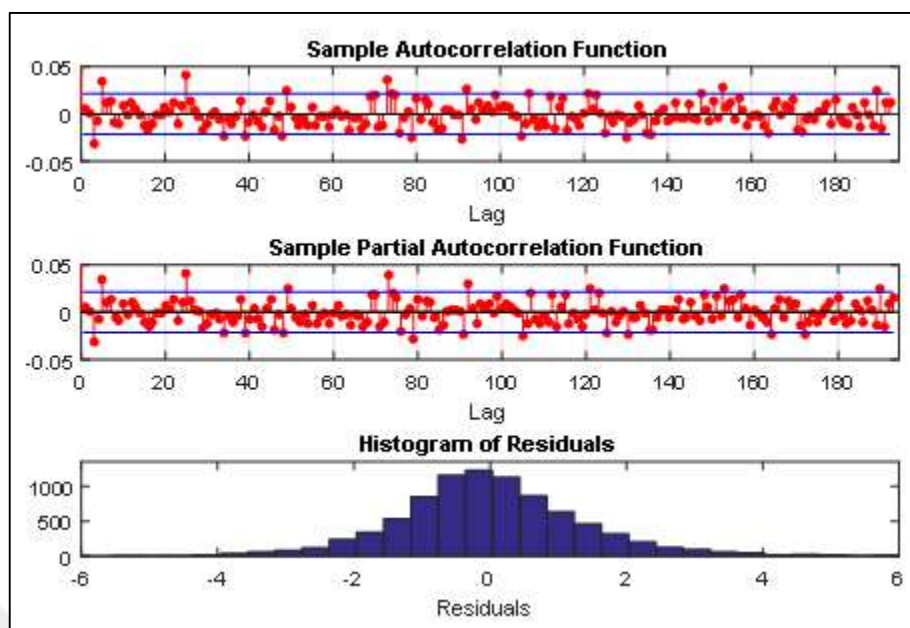
Figure 9.5. ACF, PACF and histogram of residuals after SARIMA model of wind speed forecasting
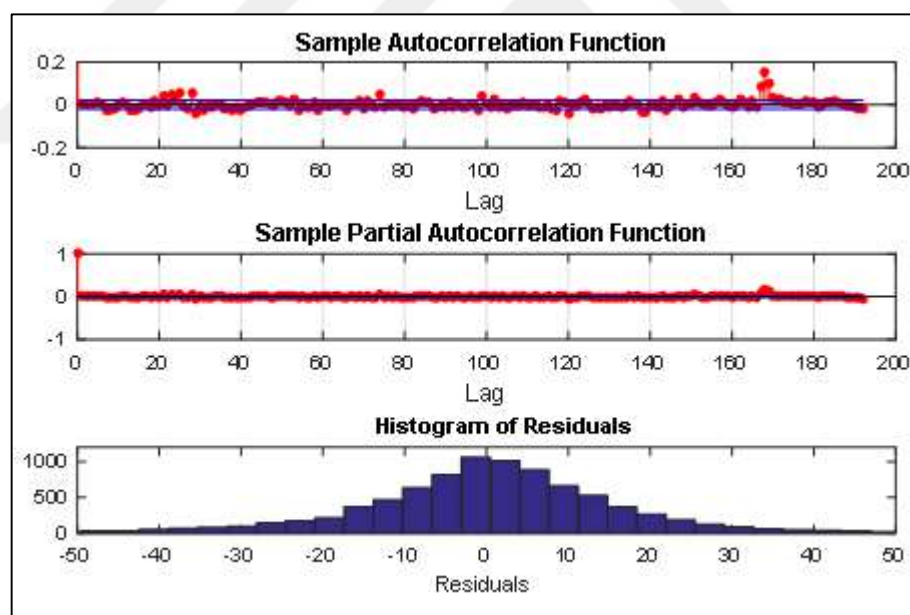

Figure 9.6. ACF, PACF and histogram of residuals after SARIMA model of electricity price forecasting

After the assumptions for a statistically valid model are satisfied, the validity of SARIMA model parameters should be tested. In order to conclude that the model parameters are statistically valid, the t-test values of all estimated parameters should satisfy the statistical

conditions, $p < 0.05$. In accordance with this information, the test results of SARIMA model parameters can be analyzed in Table 9.2. The p-values in Table 9.2 for both model wind speed and electricity price respectively, satisfy this statistical condition. Thus, the model is valid and the SARIMA models of both variables are presented in the last row of the table.

Lastly, a SARIMA model can be expressed in two forms. The first one is a multiplicative model which is formulated as in Equation (6.43) and the results presented in Table 9.2 are the parameters shown in Equation (6.43). Then, the multiplicative model for wind speed and electricity price can be expressed, respectively, as follows

$$
\begin{aligned}
(1 - 0.893B^2)&(1 - B)(1 - 0.0344B^{24} - 0.9091B^{48})W_t \\
&= (1 - 0.0556B - 0.9959B^2 + 0.05148B^4)(1 - 0.8531B^{24})e_t
\end{aligned} \tag{9.1}
$$

$$
\begin{aligned}
(1 - 0.9572B)&(1 - 0.0782B^{24})(1 - B^{24})\lambda_t \\
&= (1 - 0.4207B - 0.0774B^2 - 0.0531B^3 - 0.0825B^4 \\
&\quad - 0.0626B^5)(1 - 0.8636B^{24})e_t
\end{aligned} \tag{9.2}
$$

where B^i is the lag operator.

The second method is the additive model representation of SARIMA. It can be derived by multiplication of the parameters of Equation (6.43) and the additive model for wind speed and electricity price can be expressed as follows

$$
\begin{aligned}
W_t = {}& 0.8120\,W_{t-51} - \\
0.8120\,W_{t-50} &- 0.9091W_{t-49} + 0.9091W_{t-48} + 0.0307W_{t-27} - 0.0307W_{t-26} - \\
0.0344&W_{t-25} + 0.0344W_{t-24} - 0.8932W_{t-3} + 0.8932W_{t-2} - \\
W_{t-1} &- 0.0439e_{t-28} + 0.8495e_{t-26} + 0.0475e_{t-25} - 0.8531e_{t-24} + \\
&0.0515e_{t-4} - 0.9958e_{t-2} - 0.0556e_{t-1} + e_t
\end{aligned} \tag{9.3}
$$

$$
\begin{aligned}
\lambda_t = {}& -0.0749\lambda_{t-49} + 0.0782\lambda_{t-48} + 0.8823\lambda_{t-25} - 0.9218\lambda_{t-24} + \\
0.9572&\lambda_{t-1} + 0.0540e_{t-29} + 0.0712e_{t-28} + 0.0458e_{t-27} + 0.0667e_{t-26} + \\
0.3629&e_{t-25} - 0.8626e_{t-24} - 0.0626e_{t-5} - 0.0825e_{t-4} - 0.0531e_{t-3} - \\
&0.0774e_{t-2} - 0.4207e_{t-1} + e_t
\end{aligned} \tag{9.4}
$$

9.3. DAILY ANALYSIS OF DAY-AHEAD BIDDING

The first simulation was conducted to analyze the results of the day-ahead bidding. In this simulation, three different analysis were realized. In the first one, the effect of scenario number on expected profit and CVaR was analyzed to determine the number of scenarios that will be used. Then, by changing the confidence interval of the risk aversion, the Pareto frontier's were calculated to determine the most suitable the confidence interval value. Finally, the effects of risk-aversion on daily bids were investigated for the confidence interval and the number of scenarios found.

In all bidding analysis, the wind and price scenarios were derived from SARIMA models Equations (9.3) and (9.4). To be more specific, 10,000 price and wind trajectories were generated by Monte Carlo simulations. By reducing these trajectories into a different number of scenarios having smaller sizes, two different sets of scenarios were created for the first analysis. In the first of these scenario sets, the trajectories were reduced into ten wind and five price scenarios using the reduction method described in Section 6.3.3. Then, 50 pairwise combinations of these scenarios were taken as bidding scenarios. In the second scenario set, scenarios in the first scenario set were reduced into 6 wind and 4 price scenarios, and a total of 24 scenarios were generated with the pairwise combination of these scenarios. Finally, the values between day-ahead market closure time ($t = 0$) and the start of the operation ($t = 12$) were clipped in the both scenario sets. After the scenario generation, the expected profit and CVaR of both sets were calculated for the values of β between 0 and 1. In addition, the Pareto frontier's of the scenario sets were plotted.

As can be seen from Figure 9.7, using a higher number of scenario increases the expected profit and CVaR significantly. On the other hand, the computation times of the 50 scenarios and 24 scenarios were averagely 38.2 and 7.2 minutes, respectively. This shows that raising the number of scenarios increased the computation time considerably, and if more than 50 scenarios were used, the calculations would take longer than the time available for computing the day ahead bids. Thus, 50 scenarios were used in the bidding phase analysis.
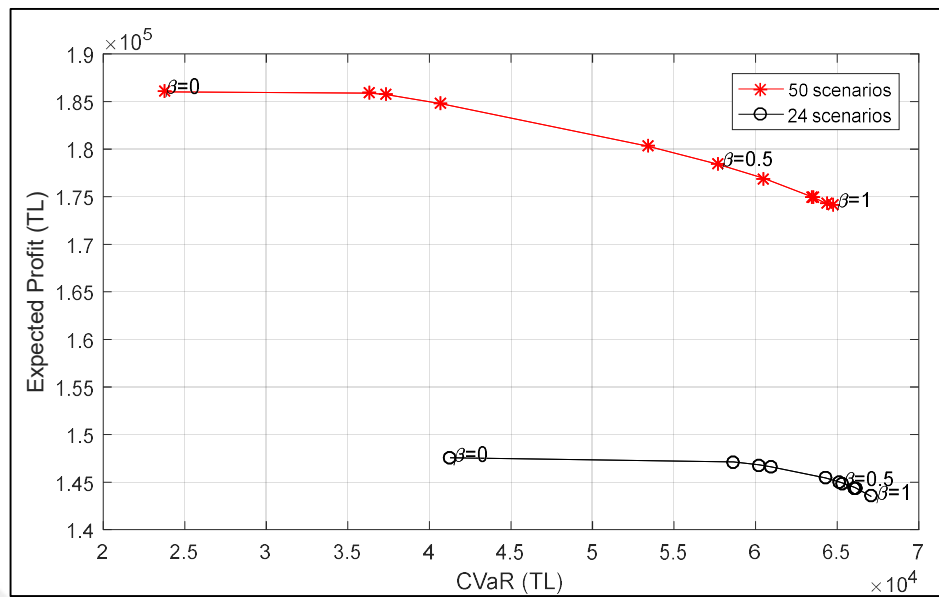
Figure 9.7. Comparison of expected profit and CVaR with respect to the different number of scenarios

After the number of scenarios that should be used in the bidding phase was determined, the next stage is to decide the confidence interval level, μ. To accomplish this, three different confidence levels, $\mu = 0.7$, $\mu = 0.8$ and $\mu = 0.9$, were selected and the expected profit and CVaR values were calculated with 50 scenarios. Based on these calculations, the Pareto frontiers were plotted as Figure 9.8. In this figure, it is expected that the increase in the confidence interval level will decrease the CVaR because of a decrease in the number of risky scenarios. Thus, it can be concluded that the CVaR and expected profit calculations are consistent based on the change of confidence interval level. In the literature, three different confidence interval level is used which are 0.99, 0.95 and 0.90. On the other hand, 0.99 and 0.95 are suitable when the number of scenarios is very high. Thus, 0.90 is selected as the confidence level in this thesis.

Figure 9.8. Expected profit vs. CVaR frontier for different values of μ and β

Figure 9.9. Wind power scenarios and actual wind power generation
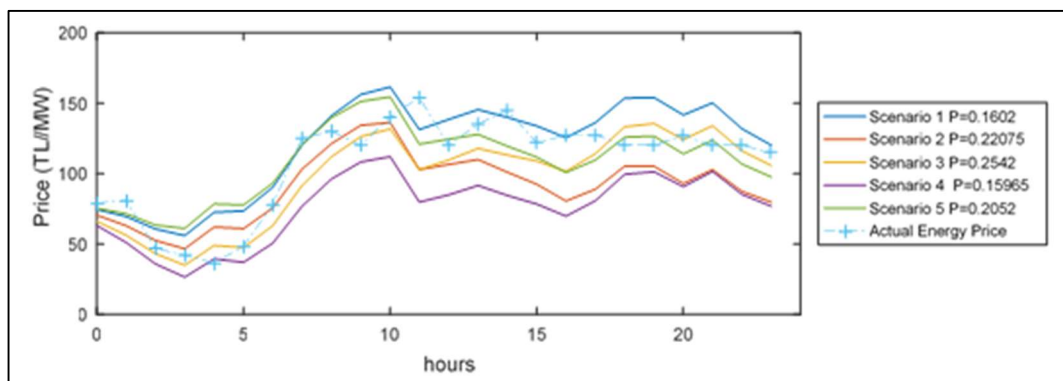
Figure 9.10. Day-ahead price scenarios and actual prices

For a specific day, the parts of the wind and price scenarios falling into operation period $(t = 12\text{:}36)$ are depicted in Figure 9.9 and Figure 9.10 and day-ahead bids calculated for $\beta = 0$ and $\beta = 1$ are shown in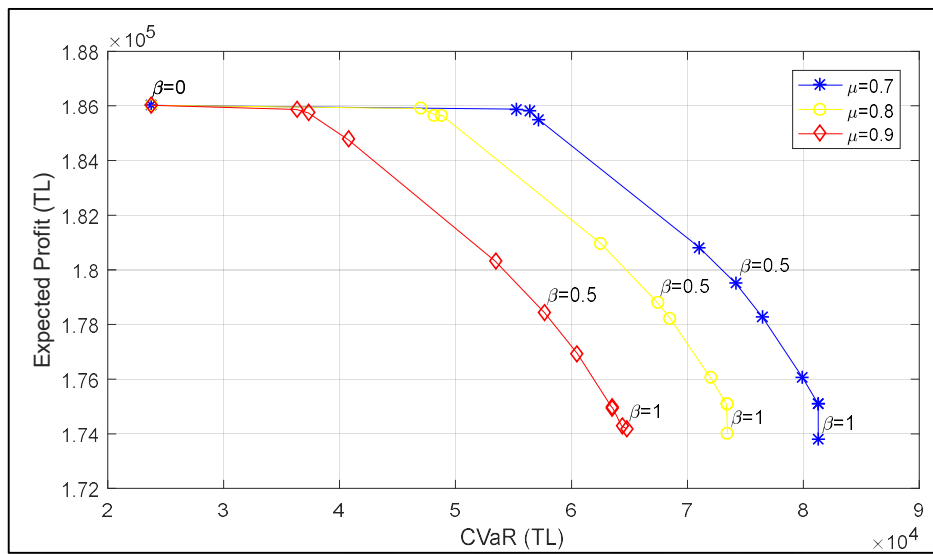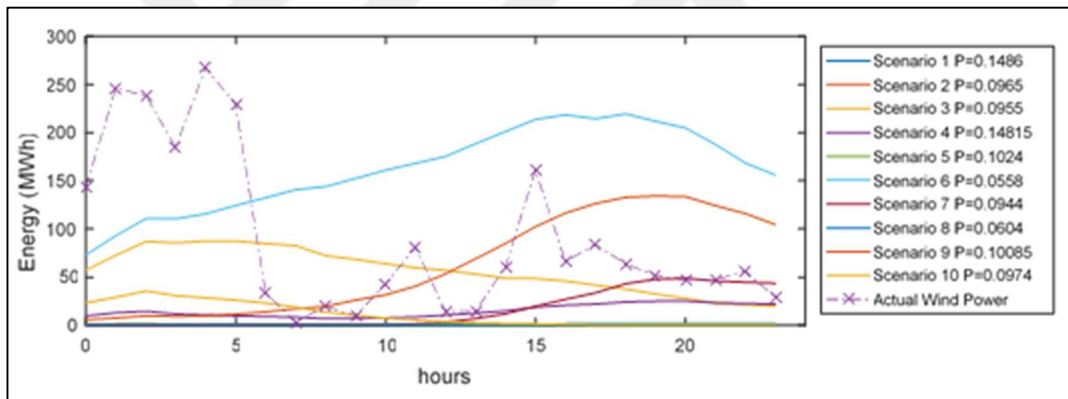 Figure 9.11. When the bidding results are analyzed by ignoring the concept of risk control since both electricity prices and wind energy generation are low between 1h to 5h, in this time interval bids becomes negative to benefit from arbitrage. In the following hours, the energy stored in low price periods is used together with the wind energy at high price times. This explains the intention to sell a relatively large amount of energy between 8h-10h and between 18h-19h.
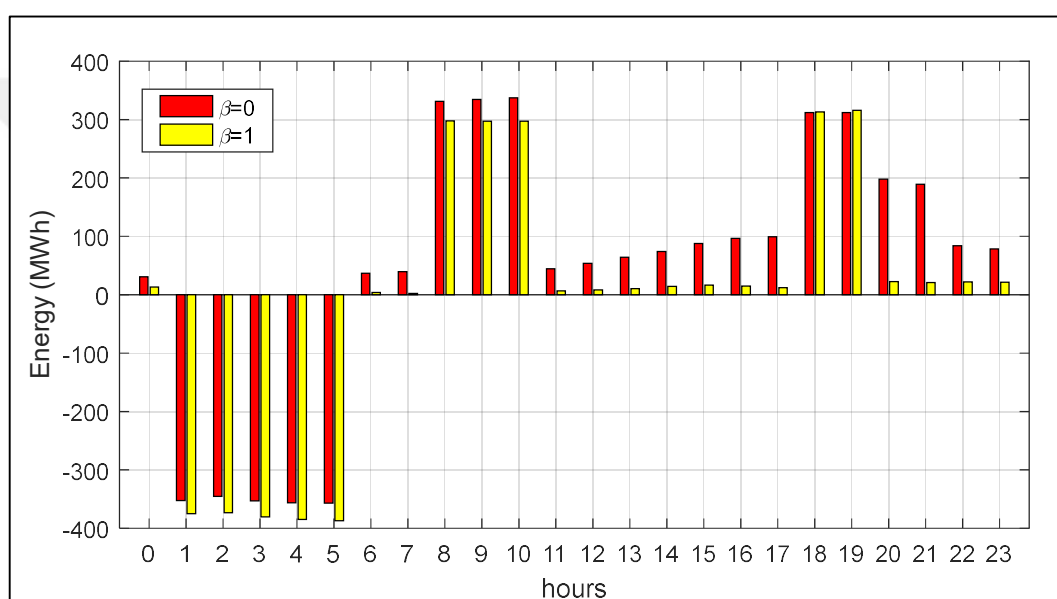
Figure 9.11. Bids for 8 April 2011

Moreover, bids are calculated with two different β like $\beta = 0$ and $\beta = 1$ which are the risk-neutral and risk-averse approach, respectively. As can be clearly seen from the graphs, it becomes more conservative with the implementation of the risk-averse method. Indeed, while more energy was purchased than the grid between 1 h to 5 h, energy sales were significantly reduced when compared to the risk-neutral aspect of the rest of the day. The difference between risk-neutral and risk-averse cases can also be explained with the PHS operation as given in Figure 9.12 and Figure 9.13. As can be seen from these figures, more scenarios operated in generation mode for the risk-neutral case during non-peak price periods. On the other hand, in the risk-averse case, the PHS units were forced to operate in peak price periods to hedge against the worst-case price scenarios.
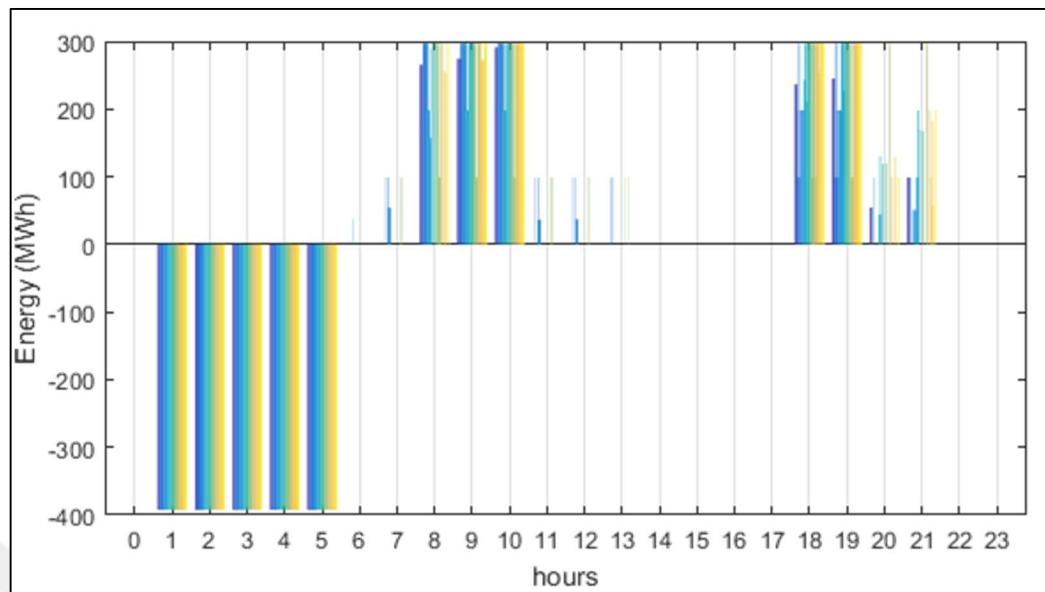
Figure 9.12. Operation of PHS units for all scenarios when β=0
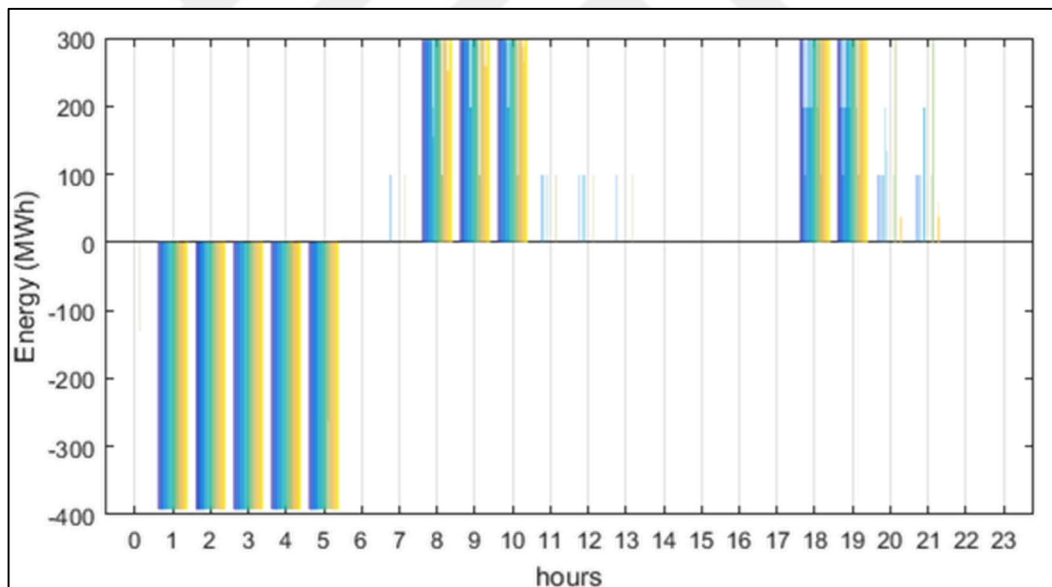
Figure 9.13. Operation of PHS units for all scenarios when β=1

As expected, risk-averse strategy reduces average profits while hedging against worst-case scenarios. The trade-off can be assessed by calculating the expected profit and CVaR for different values of β and visualizing the resulting limit which is shown in Figure 9.8. Not surprisingly, with the increasing values of β, the expected profit decreases while CVaR increases. Nevertheless, the relative reduction in the former is fairly small when compared

with the gain obtained for the latter. To be more specific, when β changes from 0 to 1, the expected profit goes down from 186,021 TL to 174,188 TL, while CVaR goes up from 23,740 TL to 64,751 TL. Thus, by sacrificing the expected profit a little bit, considerable improvements can be achieved on the losses incurred by worst-case scenarios.

The results of the analyzes based on the bidding model are given above, and this is the standard approach used in the literature to evaluate the results of the bidding methods and the effects of risk control. However, it will be shown later that these results do not reflect the actual performance achieved. Actual performance depends on the process used. It calculates interest statistics using the results of the real-time operation to make a more realistic assessment.

9.4. DAILY ANALYSIS OF OPERATION STRATEGIES

For the real-time operation, in addition to the methods in the literature, two versions of SMPC are implemented which differs in the tree structure employed for the wind scenarios. In one of them, denoted as SMPC 4x2, the nodes at $t = t_0 + 1, t_0 + 2$ branches into four nodes without further branchings in the following hours. This leads to the structure appearing in Figure 9.14.a. In the other one, SMPC 2x4, all nodes branches into two nodes for $t = t_0 + 1 : t_0 + 4$ then no branching occurs as shown in Figure 9.14.b. In both trees, the node at $t = t_0$ has a single child to be able to have a single decision as described in Section 3.2.
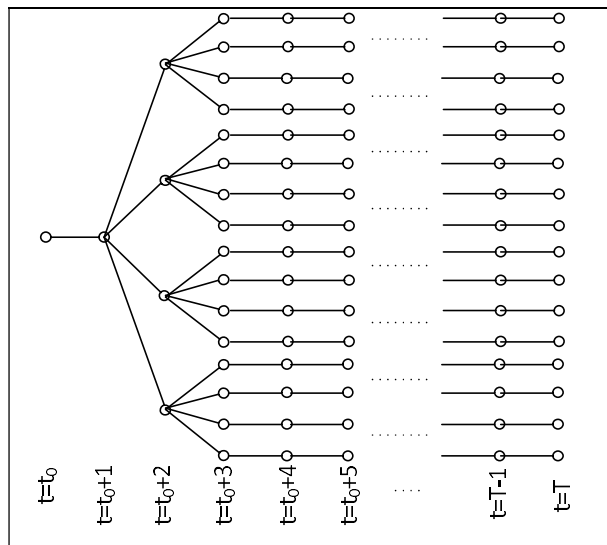
(a)
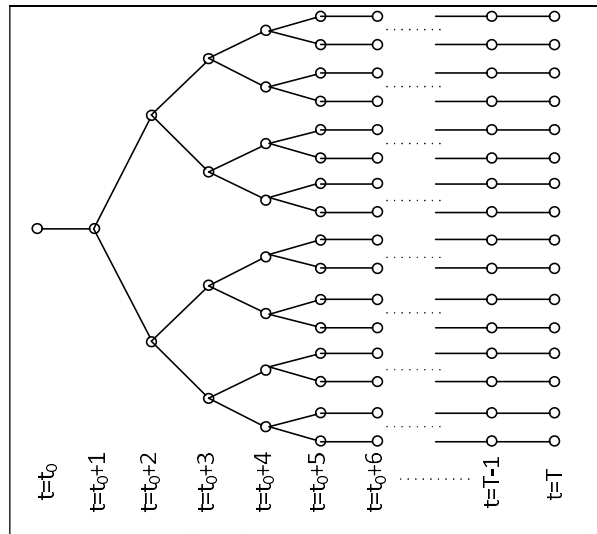
(b)

Figure 9.14. Scenario tree structures used in the real-time operation: (a) SMPC 4x2, (b) SMPC 2x4

In numerical computations of all operations strategies summarized in Section 8.2 and the bids are given in Figure 9.11 are employed. The hourly energy exchange with the grid for each operation method is given in Figure 9.15, Figure 9.16 and Figure 9.17 while the time evolution of the water volume stored in PHS system is depicted in Figure 9.18. Also, the PHS system operation is given in Figure 9.19. Bids, actual wind energy realization, and operation decisions of perfect information case are taken as references with respect to which the behavior and performance of the other methods are evaluated. Hence, their graphics are put into all figures from Figure 9.15 to Figure 9.17.

If the behavior of the perfect information case is investigated in Figure 9.15, it can be seen that the exchange level with the grid stays consistently above the bid. This is because the total energy delivered by the actual wind realization is higher than the expected total energy of wind scenarios used for bidding. The deviation becomes significant, especially in the first seven hours due to excessive wind power observed during this period.

As can be observed from Figure 9.15, the behavior of the bid-following method differs considerably from that of the perfect information solution. This is because the underlying algorithm merely tries to follow day-ahead contracts without considering the future

consequences of its actions. As a result, a certain amount of water remains in the upper reservoir at the end of the day as can be verified from Figure 9.18. The algorithm fails to capture bids for the first seven h due to the abundance of wind power in this period. Even if turbines pump at full capacity, the excess energy cannot be stored completely.

Operation of open-loop and ratio based algorithms are based on the wind power forecast made at the beginning of the day. Therefore, differences between these estimates from their actual values affect the performance of the method considered. Indeed, Figure 9.16 shows that the actions taken by these methods deviate from the ideal decisions of the perfect information algorithm at many time instances, which is a natural consequence of the forecasting error. Nevertheless, unlike the bid following heuristic, both algorithms utilize all the stored energy for attaining a higher income, and they follow ideal solutions more closely.

When the behaviors of MPC based methods are investigated, it can be seen from Figure 9.17 their decisions are the same as the perfect information case except for five hours for DMPC and three hours for SMPC algorithms. Even if their operations do not follow the ideal case perfectly, they perform significantly better when compared with the other algorithms analyzed above. This superior performance can be attributed to the accuracy of the wind energy and energy storage level resulting from the latest measurements available. Because the SMPC method uses scenarios instead of point estimates, it almost matches solution decisions based on the perfect forecast.

In addition, the methods can be compared with Figure 9.19 which shows the pumping and generation decisions of the PHS system. As can be observed from this figure, the bid following algorithm makes the most different decisions with respect to the perfect information solution. On the other hand, the proposed method exhibits the closest performance to the reference solution for that day.

Lastly, it is also important to verify that the optimization performed at each time step for finding control decisions is carried out fast enough to satisfy the timing limitations of the real-time operation. When all simulations given above are considered, the maximum computation time is found to be 82.9 seconds. This is much shorter than the available time limit of one hour and justifies the applicability of the method in practice.
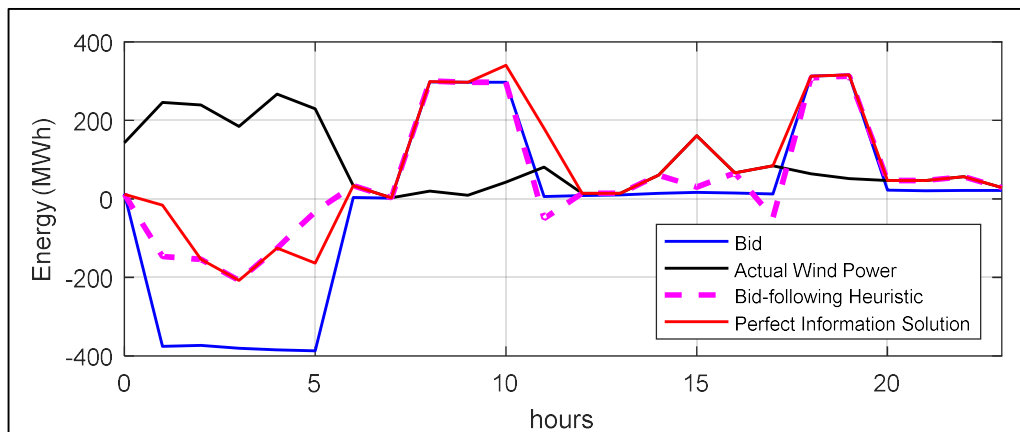
Figure 9.15. Energy exchange with the grid for perfect information and bid following heuristic methods
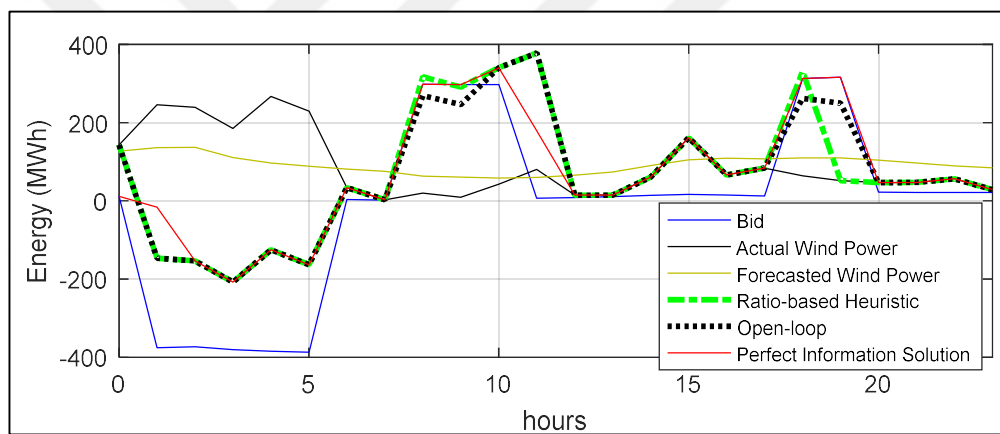
Figure 9.16. Energy exchange with the grid for perfect information, open-loop and ratio based heuristic methods
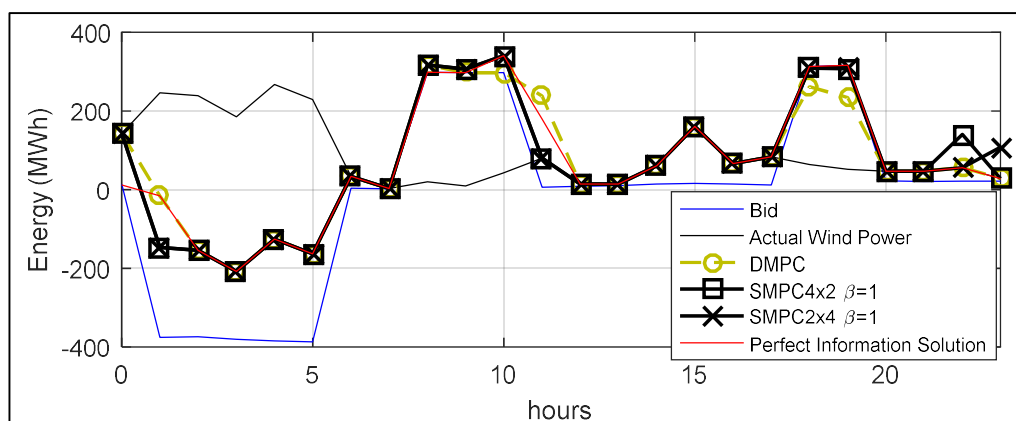
Figure 9.17. Energy exchange with the grid for DMPC and SMPC methods
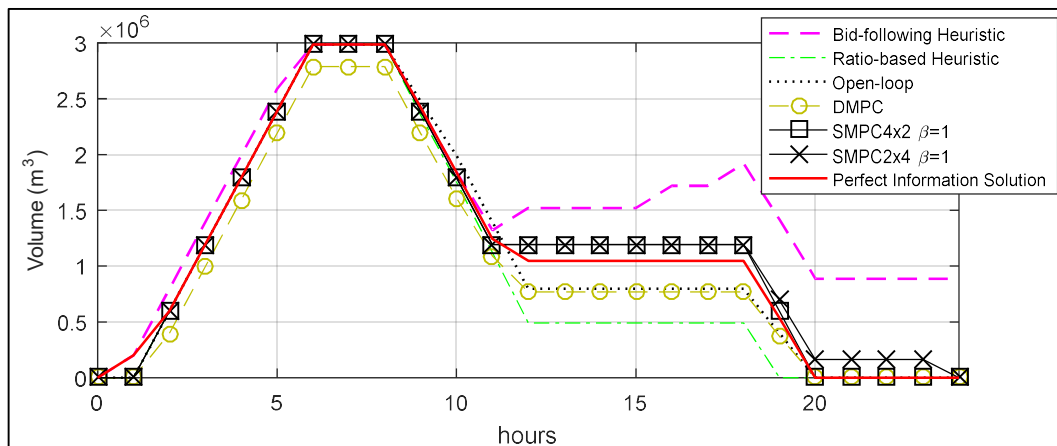
Figure 9.18. Evaluation of water volume in the upper reservoir of PHS for all methods
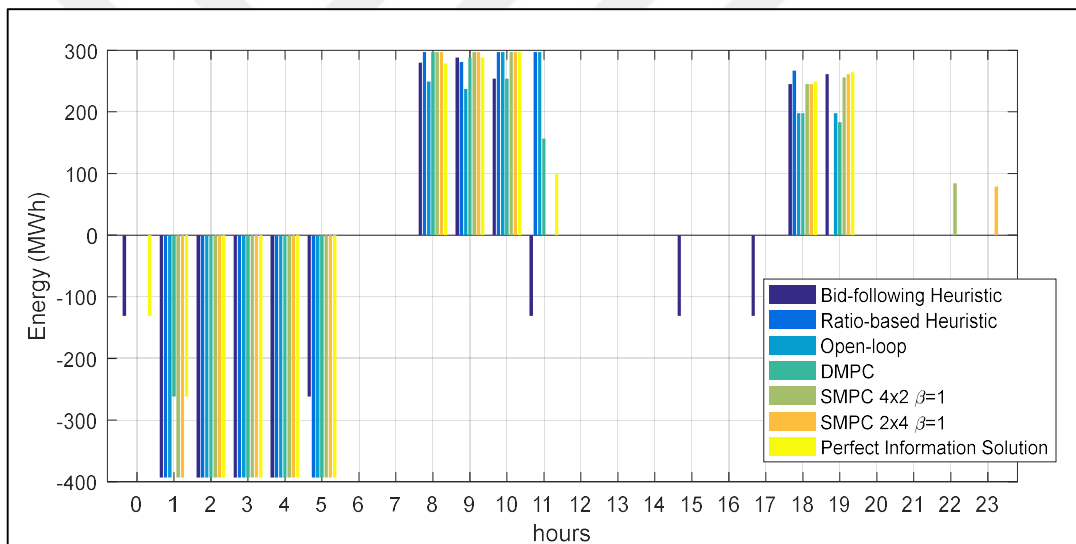
Figure 9.19. Operation of the PHS system for all methods

9.5. MONTE CARLO SIMULATION AND PARETO ANALYSIS

The observations made above for a single simulation run should be justified by statistical analysis. To this end, Monte Carlo simulations were performed for the same day. Simulations were carried out for a range of values of β from 0 to 1 and 100 runs were taken for each operation method. The expected profits and CVaR values calculated are depicted in Figure 9.20 together with the frontier previously obtained for the bidding problem. Plots show the tradeoff between the expected profit and the risk measure. Apart from a few points,

the former goes down as the latter goes up with the increasing values of β in all graphs. It can be seen that the curves do not intersect implying that moving from one method to another one can improve both the expected profit and CVaR for all values of β or vice versa. Therefore, a ranking can be established among the algorithms independent of the weighting factor. Since the perfect information case has the best achievable performance, it gives the Pareto-optimal solution. This is followed by SMPC, DMPC, open-loop, ratio-based heuristic and bid-following methods in that order. In order to compare the performance of the different methods quantitatively, the averages of expected profit and CVaR values were computed for each method and are presented in Table 9.5.

9.5.1. Comparison of Real-time Operation Methods

As can be seen from Figure 9.21, the performances of SMPC methods are very close to the perfect information case and they are followed by the DMPC method. The difference between the expected profits of SMPC and DMPC algorithms is a consequence of using uncertainty information. The resulting Value of Stochastic Solution (VSS), which is the relative improvement achieved by the stochastic solution over the deterministic one, is about 0.8 percent for the expected profit. On the other hand, the relative improvement in CVaR is around 1.5 percent, which comes from the risk control capability of the proposed SMPC approach.

The gap between the MPC based algorithms and the open-loop method is more significant as can be verified from Figure 9.20 and Table 9.5. This is due to the certainty gain arising from the periodic measurements. Relative to the open-loop method, expected profit and CVaR values of the DMPC method are 1.25 percent and 19.6 percent higher, respectively. This shows the importance of using the most recent information while making operation decisions.

The ratio-based heuristic algorithm performs worse than the open-loop algorithm, although it uses the new information to adapt its initial plan. Indeed, the corresponding frontier is considerably below that of the open-loop method. This is in agreement with the numerical values provided in Table 9.5. The averages of the expected profit and CVaR for the open-loop method are 5.8 percent and 20 percent higher, respectively, when compared with the

ratio-based heuristic method. This shows that the online adaptation of a precomputed schedule did not work as expected.

The worse performance is achieved by the bid-following algorithm whose frontier is well below the others pointing to a significant loss in the expected profit. This loss is about 41 percent relative to the ratio-based heuristic algorithm. Surprisingly, there is an improvement in the average CVaR value given in Table 9.5, which seems to contradict with Figure 9.20 and Figure 9.21. The reason is that the points are accumulated toward the right of the curve of the bid-following method.

9.5.2. An Analysis of Bidding Results

Another important conclusion is about the results provided by the solution of the bidding problem. The performance calculated turns out to be very low relative to all real-time operation methods, as can be seen from Figure 9.20, Figure 9.21 and Table 9.5. This happens as a result of the certainty loss arising from the considerable lead time between bidding the computations and the operation period. Therefore, one should be careful about using bidding outcomes for evaluating the performance, which is a common practice employed in the literature. The results presented above show that it can be misleading in general.

Table 9.5. Average expected profit and CVaR values for operation methods

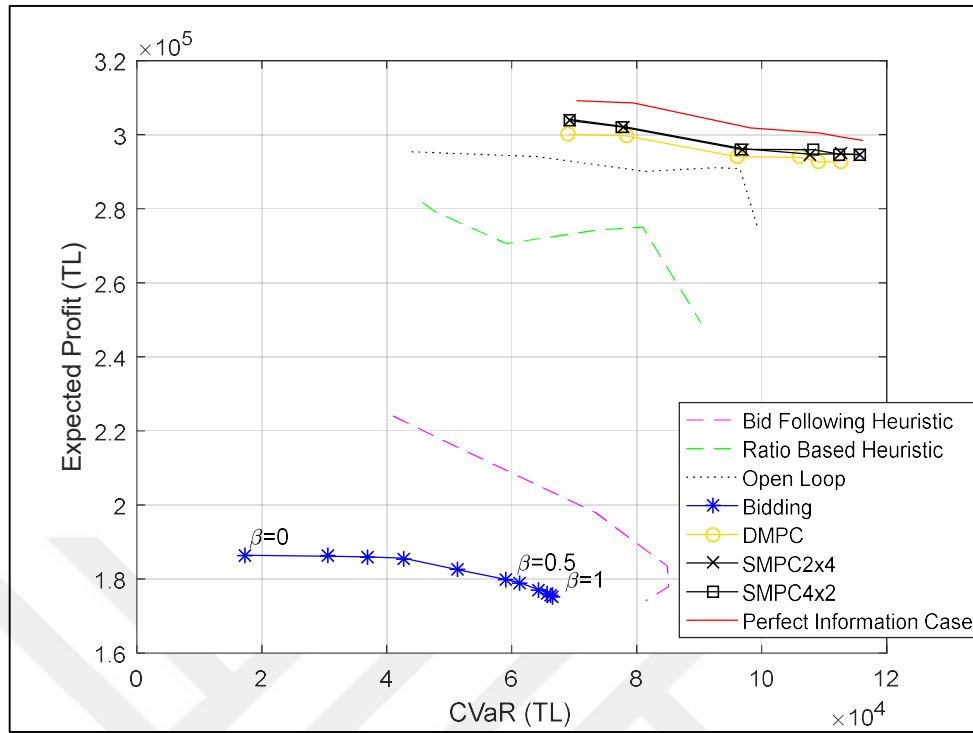|	Expected profit (TL)	CVaR (TL)
Bidding model	180,895	51,073
Bid-following heuristic	195,872	69,086
Ratio-based heuristic	275,968	66,255
Open Loop	291,887	79,603
DMPC	295,523	95,216
SMPC 4x2	297,788	96,692
SMPC 2x4	297,875	96,656
Perfect information case	302,959	97,727

Figure 9.20. CVaR-expected profit frontiers for all methods and the bidding model
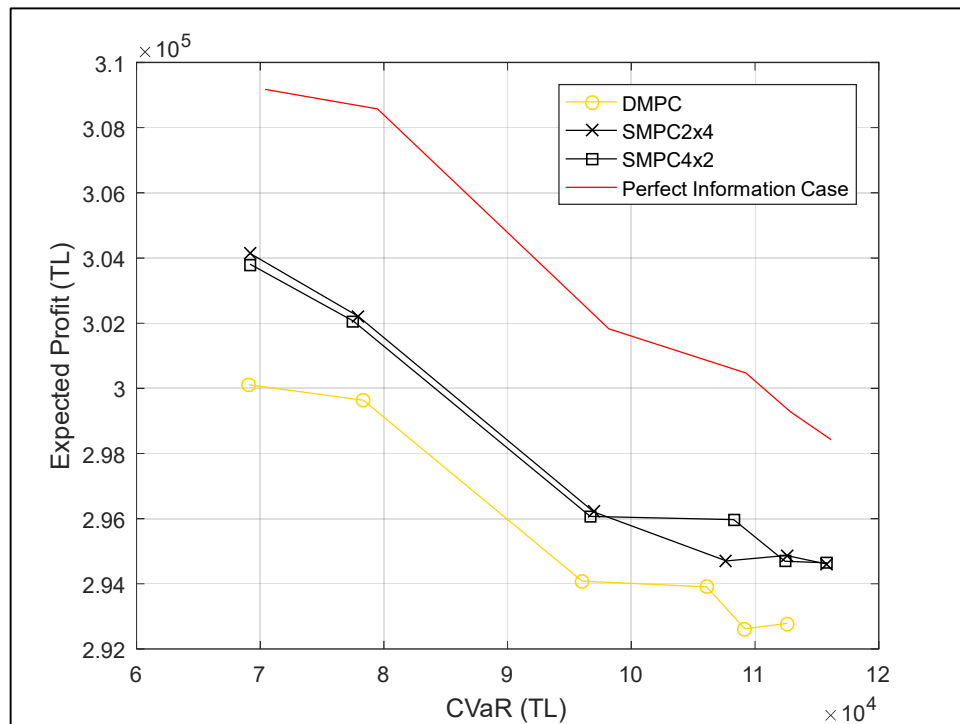
Figure 9.21. CVaR-expected profit frontiers. DMPC, SMPC, and perfect information case

9.6. LONG-TERM RESULTS AND SENSITIVITY ANALYSIS

The results of the previous section are based on the simulations of one day. In order to have a fair assessment of economic performance, it is also necessary to carry out out-of-sample analysis [130] for several days. Moreover, the performance of real-time operation methods highly depends on the balancing market conditions. Therefore, it would be informative to investigate how the operation methods compare as the imbalance price ratios vary. Motivated by these facts, long-term Monte Carlo simulations were performed. In the computations, the positive and negative imbalance ratios were taken equally, $r^+ = r^- = r$, and the operation methods were analyzed for different values on r in the presence/absence of risk control.

The time interval of simulations is taken between 1 April 2011 and 30 April 2011. At the beginning of each day, bids are calculated, and all algorithms make operation decisions based on the same bids. The daily profits of the operation methods are accumulated to obtain total profit over the time interval of interest. These computations are repeated for different values of r and for $\beta = 1$ and $\beta = 0$. Risk-aversion weight of SMPC method is taken the same as that of bidding. That is, risk-aversion is present during the operation when it is in bidding and vice versa. Under these conditions, the graphs given in Figure 9.22 are attained which show the percentage profit loss of each operation method relative to the perfect information case. Recall that the perfect information solution gives the upper bound of the best performance that can be achieved.

9.6.1. Comparison of Real-time Operation Methods

As can be seen from Figure 9.22, for all values of r and β, the SMPC based algorithm exhibits the best performance, and it is followed by DMPC, open-loop, ratio-based heuristic and bid-following heuristic methods in that order. These rankings are in agreement with the results of the previous section and similarly show the importance of incorporating uncertainty information, risk-control and repeated measurements into the real-time operation. The use of these features becomes more crucial with the increasing values of the penalty factor since the gaps between the expected profits of the algorithms increase with r as evident from Figure 9.22. Similar to the observations of the previous section, ratio-based

heuristic and especially bid-following heuristic performs very poorly while the differences between the other methods are less severe.
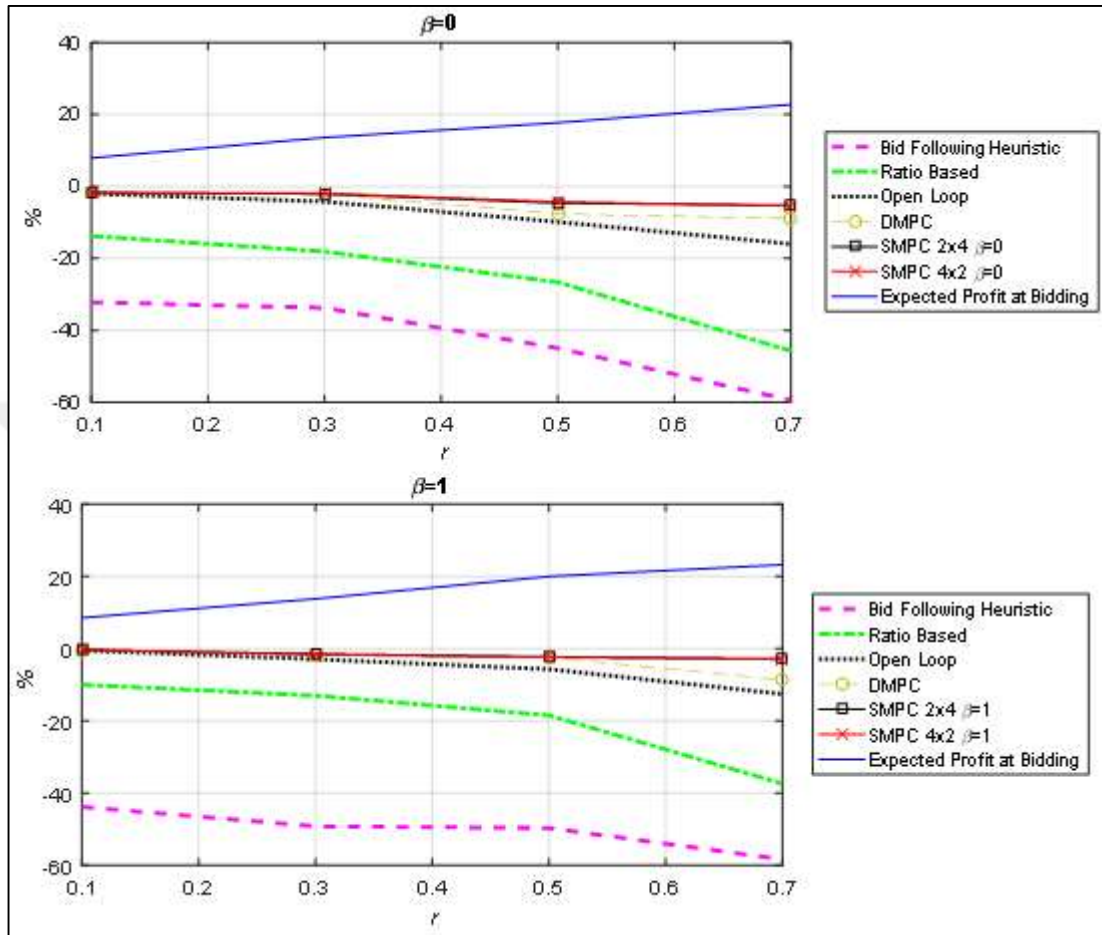
Figure 9.22. Profit losses of the algorithms relative to the perfect information solution for changing imbalance price ratio values

9.6.2. An Analysis of Bidding Results

In order to evaluate the reliability of bidding based computations, expected profits estimated by them are also depicted in Figure 9.22. The plots show that these values differ significantly from the best performance that can be achieved. This is again due to the certainty loss arising from the large lead time between the bidding and operation phases. However, different than the results found earlier, the values are overestimates instead of underestimates. This should not be surprising. In general, the expected profits given by any operation method must be lower than that of the perfect information case. On the other hand, there is no such guarantee

for an optimal solution obtained from the bidding optimization. This is because the optimization model is based on estimations of the future and these estimations may turn out to be different from the actual realizations.

10. CONCLUSION

In this thesis, a novel SMPC algorithm having risk control capability is proposed for the real-time operation of a wind energy generation system equipped with a PHS unit. The real-time operation is integrated with a bidding phase formulated as a risk-averse two-stage stochastic program. Optimization problems of SMPC algorithm and bidding are modeled as MILPs and CVaR is used as the risk measure. When the literature is investigated, the risk-control was only considered in the bidding phase in most of the studies. Also, there was only one study that considers risk control in the real-time operation which uses linear decision rules. Thus, this is the first study which incorporates risk-control into SMPC method for real-time operation.

In this thesis, imbalance market modeling, start-up and shut-down cost, transmission efficiency, stochastic bidding, forecasting and scenario generation and detailed model for PHS system were all taken into account to obtain more realistic results, which was not done in the previous works on the real-time operation.

Although there are different real-time operation methods proposed in the literature, only a few of them were compared in previous studies. In this thesis, an extensive comparison of available real-time operations was carried out by simulations. One set of simulations was conducted for a specific day. In these simulations, daily schedules of all operation methods were obtained and compared. In addition, a Monte Carlo analysis was conducted to investigate the Pareto optimality to confirm observations of daily schedules statistically. The second set of simulation was performed for long term analysis. From all simulations, it is observed that among the methods investigated, bid-following algorithm exhibited the worst performance because this algorithm only tries to follow day-ahead bids without considering the future consequences of its actions. The ratio-based heuristic method achieved a better performance than the bid-following but its performance was very poor with respect to the perfect information solution. Because the open-loop method optimizes the decisions by using future uncertainties, it calculated better operational decisions for PHS than the heuristic algorithms. On the other hand, there was still significant deviations from the perfect information case because the wind forecast errors were considerably high. The behavior of the DMPC was much closer to the ideal solution than the algorithms analyzed above because

of the certainty gain arising from the latest available measurements of wind power. Lastly, the proposed SMPC method exhibited the best performance in all simulations. This comes from its ability to exploit the most recent information and underlying scenario tree-based stochastic optimization approach. Advantages of risk-averse operation capability of SMPC strategy are analyzed. As expected, introducing risk control into real-time decisions leads to further improvements in the profits of the worst-case scenarios while yielding to a relatively small loss on the expected profit. This justifies the use of risk-averse operation.

In addition, by the long term simulations, the performance of the operation methods was investigated under changing imbalance market conditions. As expected, as the imbalance prices get higher, using MPC based methods becomes more advantageous for both risk-neutral and risk-averse cases, again SMPC yielding to the best performance. The effect of the scenario structure on the performance of the SMPC method was also investigated. It was observed that the choice of scenario tree structure did not have a significant effect on the results.

Another contribution is the comparison of risk-profit analyses made for real-time operation and bidding, the latter is the standard approach followed in the literature. Results of Monte Carlo simulations showed that the expected profit and CVaR values computed from the real-time operation and bidding simulations differ considerably. It is deduced that the difference can be attributed to two facts. One is the certainty gain due to the availability of the new information with the start of the real-time operation. As a result, profits obtained becomes higher. Second, naturally, the actual performance realized depends on the outcomes of the real-time operation. Thus, real-time operation should be used to asses the economic performance of the system.

In addition, the approach proposed in this thesis is not limited to the case study considered. In a similar manner, it can be adopted to the systems composed of other storage and renewable generation technologies as well. This amounts to changing the associated equations employed in the bidding and operation models. As long as the optimization problem is tractable, the algorithm will exhibit similar behavior and perform better relative to the alternative strategies investigated owing to its abilities to utilize new information, exploit the probability distribution of uncertainties and incorporate risk-control.

In the application considered, although the transmission losses were taken into account, transmission capacity constraints were neglected. It was done partly because the storage unit and the energy sources are closely located. Apart from this, in general, one may expect that the need for energy storage will be higher during off-peak periods since energy prices will be lower and wind speeds will likely be higher (nighttime). This reduces the chances of experiencing congestion. Nevertheless, in general, there may be a long distance between the energy source and the PHS unit and one may want to work with a more realistic model by incorporating transmission constraints. In that case, the profits may become lower since the storage utilization would decrease. However, the real-time operation algorithms are expected to behave relatively similar although gaps between their performances may get smaller.

Lastly, the case study considered in this study has a relatively small size in terms of generation and storage capacity when compared with the systems currently operational in the regions having large-scale wind generation and hydro storage facilities including USA, Canada, Australia and Northern Europe. The application of the advanced operation methods as the one proposed in this thesis will have a more profound impact on such large-scale systems as far as financial gains concerned.

REFERENCES

1. Zhao H, Wu Q, Hu S, et al. Review of energy storage system for wind power integration support. *Applied Energy*. 2015; 137: 545–553.

2. Rehman S, Al-Hadhrami LM, Alam MMM, et al. Pumped hydro energy storage system: A technological review. *Renewable and Sustainable Energy Reviews*. 2015; 44: 586–598.

3. Global Wind Report: Annual market update 2017, [cited 2019 10 January]. Available from: https://www.researchgate.net/publication/324966225_GLOBAL_WIND REPORT - Annual_Market_Update_2017.

4. Dincer SK, Kaymil K. Potential and utilization of wind and solar energy in Turkey. *Journal of Engineering Research and Applied Science*. 2017; 6: 599–604.

5. Türkiye Rüzgar Enerjisi İstatistik Raporu Ocak 2018, [cited 2019 15 January]. Available from: https://www.tureb.com.tr/files/tureb_sayfa/duyurular/2018/03/ turkiye ruzgar_enerjisi_istatistik_raporu_ocak_2018.pdf.

6. Kumar Y, Ringenberg J, Depuru SS, et al. Wind energy: Trends and enabling technologies. *Renewable and Sustainable Energy Reviews*. 2016; 53: 209–224.

7. Nurbay N, Çınar A. Rüzgar türbinlerinin çeşitleri ve birbirleriyle karşılaştırılması. *III. Yenilenebilir Enerji. Kaynakları Sempozyumu, Mersin*. 2005: 164–168.

8. Betz A. *Introduction to the theory of flow machines*. Oxford: Pergamon Press; 1966.

9. Mukund RP. *Wind and solar power systems*. Florida: CRC Press; 1999.

10. Rüzgar Türbini, [cited 2018 19 December]. Available from: http:/ www. enerjiatlasi.com/ruzgar-turbini/.

11. Enercon product overview, [cited 2019 13 January]. Available from: https://www.enercon.de/fileadmin/Redakteur/Medien-Portal/broschueren/pdf/en/ ENERCON_Produkt_en_06_2015.pdf.

12. Sohoni V, Gupta SC, Nema RK. A critical review on wind turbine power curve

modelling techniques and their applications in wind based energy systems. *Journal of Energy*. 2016; 2016: 1–18.

13. Kusiak A, Song Z. Design of wind farm layout for maximum wind energy capture. *Renewable Energy*. 2010; 35: 685–694.

14. Diaf S, Belhamel M, Haddadi M, et al. Technical and economic assessment of hybrid photovoltaic/wind system with battery storage in Corsica island. *Energy Policy*. 2008; 36: 743–754.

15. Diaf S, Notton G, Belhamel M, et al. Design and techno-economical optimization for hybrid PV/wind system under various meteorological conditions. *Applied Energy*. 2008; 85: 968–987.

16. Deshmukh MK, Deshmukh SS. Modeling of hybrid renewable energy systems. *Renewable and Sustainable Energy Reviews*. 2008; 12: 235–249.

17. Katsigiannis YA, Georgilakis PS, Karapidakis ES. Hybrid simulated annealing–tabu search method for optimal sizing of autonomous power systems with renewables. *IEEE Transactions on Sustainable Energy*. 2012; 3: 330–338.

18. Ai B, Yang H, Shen H, et al. Computer-aided design of PV/wind hybrid system. *Renewable Energy*. 2003; 28: 1491–1512.

19. Li L, Liang W, Lian H, et al. Compressed air energy storage: characteristics, basic principles, and geological considerations. *Advances in Geo-Energy Research*. 2018; 2: 135–147.

20. Aneke M, Wang M. Energy storage technologies and real life applications--A state of the art review. *Applied Energy*. 2016; 179: 350–377.

21. Zakeri B, Syri S. Electrical energy storage systems: A comparative life cycle cost analysis. *Renewable and Sustainable Energy Reviews*. 2015; 42: 569–596.

22. Skyllas-Kazacos M, Chakrabarti MH, Hajimolana SA, et al. Progress in flow battery research and development. *Journal of The Electrochemical Society*. 2011; 158: R55–R79.

23. Luo X, Wang J, Dooner M, et al. Overview of current development in electrical energy storage technologies and the application potential in power system operation. *Applied Energy*. 2015; 137: 511–536.

24. Ralon P, Taylor M, Ilas A, et al. Electricity storage and renewables: costs and markets to 2030, [cited 2019 3 February]. Available from: https://www.irena.org/-/media/Files/IRENA/Agency/Publication/2017/Oct/IRENA_Electricity_Storage_Costs_2017.pdf.

25. Hydropower Status Report: Sector trends and insights 2018, [cited 2019 1 February]. Available from: https://www.hydropower.org/sites/default/files/publications-docs/2018_hydropower_status_report_0.pdf.

26. Gimeno-Gutiérrez M, Lacal-Arántegui R. Assessment of the European potential for pumped hydropower energy storage based on two existing reservoirs. *Renewable Energy*. 2015; 75: 856–868.

27. Çetinkaya S. *Capacity Determination of Pumped Storage Projects Using Market Electricity Prices*. PhD thesis, Middle East Technical University; 2014.

28. Karagöl ET, Kavaz İ. Dünyada ve Türkiye'de yenilenebilir enerji. *Analiz Seta*. 2017; 197: 18–28.

29. Elektrik İsleri Etüt İdaresi Genel Müdürlüğü. 2008 Yılı Faaliyet Raporu, [cited 2018 5 January]. Available from: http://www.eie.gov.tr/document/2008_Faaliyet_Raporu.doc.

30. The study on optimal power generation for peak demand in Turkey, [cited 2017 25 December]. Available from: http://open_jicareport.jica.go.jp/pdf/12019790.pdf.

31. Karaçay P. *Pompaj Depolamalı Hidroelektrik Santraller Ve Türkiye'deki Durum*. Master's thesis, İstanbul Technical University; 2010.

32. Kucukali S. Finding the most suitable existing hydropower reservoirs for the development of pumped-storage schemes: An integrated approach. *Renewable and Sustainable Energy Reviews*. 2014; 37: 502–508.

33. Deane JP, Gallachóir BPÓ, McKeogh EJ. Techno-economic review of existing and

new pumped hydro energy storage plant. *Renewable and Sustainable Energy Reviews*. 2010; 14: 1293–1302.

34. Perez-Diaz JI, Chazarra M, García-González J, et al. Trends and challenges in the operation of pumped-storage hydropower plants. *Renewable and Sustainable Energy Reviews*. 2015; 44: 767–784.

35. Norang I. Pump Storage Hydropower for delivering balancing power and ancillary services-A case study of Illvatn pump storage power plant, [cited 2019 13 March]. Available from: https://ntnuopen.ntnu.no/ntnu-xmlui/bitstream/handle/11250/ 2350526/13093_FULLTEXT.pdf?sequence=1.

36. Chazarra M, Pérez-Díaz JI, García-González J. Optimal energy and reserve scheduling of pumped-storage power plants considering hydraulic short-circuit operation. *IEEE Transactions on Power Systems*. 2017; 32: 344–353.

37. Alvarez GE, Marcovecchio MG, Aguirre PA. Security-Constrained unit commitment problem including thermal and pumped storage units: An MILP formulation by the application of linear approximations techniques. *Electric Power Systems Research*. 2018; 154: 67–74.

38. Diaz FJ, Contreras J, Munoz JI, et al. Optimal scheduling of a price-taker cascaded reservoir system in a pool-based electricity market. *IEEE Transactions on Power Systems*. 2011; 26: 604–615.

39. Katsaprakakis DA, Christakis DG. Seawater pumped storage systems and offshore wind parks in islands with low onshore wind potential. A fundamental case study. *Energy*. 2014; 66: 470–486.

40. Manfrida G, Secchi R. Seawater pumping as an electricity storage solution for photovoltaic energy systems. *Energy*. 2014; 69: 470–484.

41. Vespucci MT, Maggioni F, Bertocchi MI, et al. A stochastic model for the daily coordination of pumped storage hydro plants and wind power plants. *Annals of Operations Research*. 2012; 193: 91–105.

42. Garcia-Gonzalez J, de la Muela RMR, Santos LM, et al. Stochastic joint optimization

of wind generation and pumped-storage units in an electricity market. *IEEE Transactions on Power Systems*. 2008; 23: 460–468.

43. Kazempour SJ, Hosseinpour M, Moghaddam MP. Self-scheduling of a joint hydro and pumped-storage plants in energy, spinning reserve and regulation markets. *2009 IEEE Power & Energy Society General Meeting*. IEEE; 2009: 1–8.

44. Kanakasabapathy P, Swarup KS. Bidding strategy for pumped-storage plant in pool-based electricity market. *Energy Conversion and Management*. 2010; 51: 572–579.

45. Borghetti A, Member S, Ambrosio CD, et al. An MILP approach for short-term hydro scheduling and unit commitment with head-dependent reservoir. *IEEE Transactions on Power Systems*. 2008; 23: 1115–1124.

46. Abhyankar AR, Khaparde S. Introduction to deregulation in power industry, [cited 2017 10 March]. Available from: https://nptel.ac.in/courses/108101040/ Module 7/L01-Introduction to Deregulation-1.pdf.

47. Kirschen DS, Strbac G. *Fundamentals of power system economics*. New York: John Wiley & Sons; 2004.

48. SMF Hesaplanması, [cited 2018 16 July]. Available from: https://www.epias.com.tr/ dengeleme-guc-piyasasi/smf-hesaplanmasi.

49. Di Domenica N, Lucas C, Mitra G, et al. Scenario generation for stochastic programming and simulation: A modelling perspective. *IMA Journal of Management Mathematics*. 2009; 20: 1–38.

50. Dantzig GB. Linear programming under uncertainty. *Management Science*. 1955; 1: 197–206.

51. Van Slyke RM, Wets R. L-shaped linear programs with applications to optimal control and stochastic programming. *SIAM Journal on Applied Mathematics*. 1969; 17: 638–663.

52. Benders JF. Partitioning procedures for solving mixed-variables programming problems. *Numerische Mathematik*. 1962; 4: 238–252.

53. Dantzig GB, Wolfe P. Decomposition principle for linear programs. *Operations Research*. 1960; 8: 101–111.

54. Birge JR, Louveaux F. *Introduction to stochastic programming*. New York: Springer-Verlag; 1997.

55. Shapiro A, Dentcheva D, Ruszczyński A. *Lectures on stochastic programming: modeling and theory*. Philadelphia: SIAM; 2009.

56. Rockafellar RT, Uryasev S. Optimization of conditional value-at-risk. *Journal of Risk*. 2000; 2: 21–42.

57. Charnes A, Cooper WW, Symonds GH. Cost horizons and certainty equivalents: an approach to stochastic programming of heating oil. *Management Science*. 1958; 4: 235–263.

58. Van W, Zorgati R, Henrion R, et al. Chance constrained programming and its applications to energy management. *Stochastic Optimization - Seeing the Optimal for the Uncertain*. 2011: 291–320.

59. Pagnoncelli BK, Ahmed S, Shapiro A. Sample average approximation method for chance constrained programming: theory and applications. *Journal of Optimization Theory and Applications*. 2009; 142: 399–416.

60. Gabrel V, Murat C, Thiele A. Recent advances in robust optimization: An overview. *European Journal of Operational Research*. 2014; 235: 471–483.

61. Soyster AL. Convex programming with set-inclusive constraints and applications to inexact linear programming. *Operations Research*. 1973; 21: 1154–1157.

62. Mulvey JM, Vanderbei RJ, Zenios SA. Robust optimization of large-scale systems. *Operations Research*. 1995; 43: 264–281.

63. Goh J, Sim M. Robust optimization made easy with ROME. *Operations Research*. 2011; 59: 973–985.

64. Ben-Tal A, Goryashko A, Guslitzer E, et al. Adjustable robust solutions of uncertain linear programs. *Mathematical Programming*. 2004; 99: 351–376.

65. Ben-Tal A, Nemirovski A. Robust convex optimization. *Mathematics of Operations Research*. 1998; 23: 769–805.

66. Bertsimas D, Sim M. The price of robustness. *Operations Research*. 2004; 52: 35–53.

67. Soman SS, Zareipour H, Malik O, et al. A review of wind power and wind speed forecasting methods with different time horizons. *North American Power Symposium 2010*. 2010: 1–8.

68. Weron R. Electricity price forecasting: A review of the state-of-the-art with a look into the future. *International Journal of Forecasting*. 2014; 30: 1030–1081.

69. Ventosa M, Baillo A, Ramos A, et al. Electricity market modeling trends. *Energy Policy*. 2005; 33: 897–913.

70. Benth FE, Benth JŠ, Koekebakker S. *Stochastic modeling of electricity and related markets*. Singapore: World Scientific; 2008.

71. Weron R, Misiorek A. Forecasting spot electricity prices: A comparison of parametric and semiparametric time series models. *International Journal of Forecasting*. 2008; 24: 744–763.

72. Misiorek A, Trueck S, Weron R. Point and interval forecasting of spot electricity prices: Linear vs. non-linear time series models. *Studies in Nonlinear Dynamics & Econometrics*. 2006; 10: Article 2.

73. Lin WM, Gow HJ, Tsai MT. An enhanced radial basis function network for short-term electricity price forecasting. *Applied Energy*. 2010; 87: 3226–3234.

74. Chen X, Dong ZY, Meng K, et al. Electricity price forecasting with extreme learning machine and bootstrapping. *IEEE Transactions on Power Systems*. 2012; 27: 2055–2062.

75. García-Ascanio C, Maté C. Electric power demand forecasting using interval time series: A comparison between VAR and iMLP. *Energy Policy*. 2010; 38: 715–725.

76. Sharma V, Srinivasan D. A hybrid intelligent model based on recurrent neural networks and excitable dynamics for price prediction in deregulated electricity

market. *Engineering Applications of Artificial Intelligence*. 2013; 26: 1562–1574.

77. Niu D, Liu D, Wu DD. A soft computing system for day-ahead electricity price forecasting. *Applied Soft Computing*. 2010; 10: 868–875.

78. Wang X, Sideratos G, Hatziargyriou N, et al. Wind speed forecasting for power system operational planning. *Probabilistic Methods Applied to Power Systems, 2004 International Conference on*. 2004: 470–474.

79. More A, Deo MC. Forecasting wind with neural networks. *Marine Structures*. 2003; 16: 35–49.

80. Barbounis TG, Theocharis JB. Locally recurrent neural networks for wind speed prediction using spatial correlation. *Information Sciences*. 2007; 177: 5775–5797.

81. Kariniotakis GN, Stavrakakis GS, Nogaret EF. Wind power forecasting using advanced neural networks models. *IEEE Transactions on Energy Conversion*. 1996; 11: 762–767.

82. Kariniotakis G. Forecasting of wind parks production by dynamic fuzzy models with optimal generalisation capacity. *12th Intelligent Systems Application to Power Systems Conference (ISAP 2003)*. 2003.

83. Vahidinasab V, Jadid S, Kazemi A. Day-ahead price forecasting in restructured power systems using artificial neural networks. *Electric Power Systems Research*. 2008; 78: 1332–1342.

84. Taylor JW. Triple seasonal methods for short-term electricity demand forecasting. *European Journal of Operational Research*. 2010; 204: 139–152.

85. Jonsson T, Pinson P, Nielsen HA, et al. Forecasting electricity spot prices accounting for wind power predictions. *IEEE Transactions on Sustainable Energy*. 2013; 4: 210–218.

86. Cadenas E, Jaramillo OA, Rivera W. Analysis and forecasting of wind velocity in chetumal, quintana roo, using the single exponential smoothing method. *Renewable Energy*. 2010; 35: 925–930.

87. Van der Walt CM, Botha N. A comparison of regression algorithms for wind speed forecasting at Alexander Bay. *2016 Pattern Recognition Association of South Africa and Robotics and Mechatronics International Conference (PRASA-RobMech)*. 2016: 1–5.

88. Schmutz A, Elkuch P. Electricity price forecasting: Application and experience in the European power markets. *Proceedings of the 6th IAEE European Conference, Zürich*. 2004: 1–13.

89. Cuaresma JC, Hlouskova J, Kossmeier S, et al. Forecasting electricity spot-prices using linear univariate time-series models. *Applied Energy*. 2004; 77: 87–106.

90. Torres JL, García A, Blas M De, et al. Forecast of hourly average wind speed with ARMA models in Navarre (Spain). *Solar Energy*. 2005; 79: 65–77.

91. Conejo AJ, Plazas MA, Espinola R, et al. Day-ahead electricity price forecasting using the wavelet transform and ARIMA models. *IEEE Transactions on Power Systems*. 2005; 20: 1035–1042.

92. Palomares-Salas JC, de la Rosa JJG, Ramiro JG, et al. ARIMA vs. Neural networks for wind speed forecasting. *2009 IEEE International Conference on Computational Intelligence for Measurement Systems and Applications*. 2009: 129–133.

93. Cadenas E, Rivera W. Wind speed forecasting in the south coast of Oaxaca, México. *Renewable Energy*. 2007; 32: 2116–2128.

94. Bivona S, Bonanno G, Burlon R, et al. Stochastic models for wind speed forecasting. *Energy Conversion and Management*. 2011; 52: 1157–1165.

95. Muche T. Optimal operation and forecasting policy for pump storage plants in day-ahead markets. *Applied Energy*. 2014; 113: 1089–1099.

96. Contreras J, Espinola R, Nogales FJ, et al. ARIMA models to predict next-day electricity prices. *IEEE Transactions on Power Systems*. 2003; 18: 1014–1020.

97. Jakaša T, Androček I, Sprčić P. Electricity price forecasting — ARIMA model approach. *2011 8th International Conference on the European Energy Market (EEM)*. 2011: 222–225.

98.   Olsson M, Soder L. Modeling real-time balancing power market prices using combined SARIMA and markov processes. *IEEE Transactions on Power Systems*. 2008; 23: 443–450.

99.   Haldrup N, Nielsen MØ. A regime switching long memory model for electricity prices. *Journal of Econometrics*. 2006; 135: 349–376.

100. Ambach D, Schmid W. A new high-dimensional time series approach for wind speed, wind direction and air pressure forecasting. *Energy*. 2017; 135: 833–850.

101. Lucheroni C. A hybrid SETARX model for spikes in tight electricity markets. *Operations Research and Decisions*. 2012; 22: 13–49.

102. Bollerslev T. Generalized autoregressive conditional heteroskedasticity. *Journal of Econometrics*. 1986; 31: 307–327.

103. Jiang R, Wang J, Guan Y. Robust unit commitment with wind power and pumped storage hydro. *IEEE Transactions on Power Systems*. 2012; 27: 800–810.

104. Garcia RC, Contreras J, Van Akkeren M, et al. A GARCH forecasting model to predict day-ahead electricity prices. *IEEE Transactions on Power Systems*. 2005; 20: 867–874.

105. Di Domenica N, Mitra G, Valente P, et al. Stochastic programming and scenario generation within a simulation framework: An information systems perspective. *Decision Support Systems*. 2007; 42: 2197–2218.

106. Jobst NJ, Zenios SA. Tracking bond indices in an integrated market and credit risk environment. *Quantitative Finance*. 2003; 3: 117–135.

107. Efron B. Bootstrap methods: another look at the jackknife. *The Annals of Statistics*. 1979; 7: 1–26.

108. Jerrum M, Sinclair A. The Markov chain Monte Carlo method: an approach to approximate counting and integration. *Approximation algorithms for NP-hard problems*. 1996; 482–520.

109. Frauendorfer K. Barycentric scenario trees in convex multistage stochastic

programming. *Mathematical Programming*. 1996; 75: 277–293.

110. Dupacova J, Consigli G, Wallace SW. Scenarios for multistage stochastic programs. *Annals of Operations Research*. 2000; 100: 25–53.

111. Šutiene K, Makackas D, Pranevičius H, et al. Multistage k-means clustering for scenario tree construction. *Informatica*. 2010; 21: 123–138.

112. Dupacová J, Gröwe-Kuska N, Römisch W. Scenario reduction in stochastic programming. *Mathematical Programming*. 2003; 95: 493–511.

113. Heitsch H, Römisch W. Scenario tree modeling for multistage stochastic programs. *Mathematical Programming*. 2009; 118: 371–406.

114. Šutiene K, Makackas D, Pranevičius H. Multistage k-means clustering for scenario tree construction. *Informatica*. 2010; 21: 123–138.

115. Díaz-González F, Sumper A, Gomis-Bellmunt O, et al. A review of energy storage technologies for wind power applications. *Renewable and Sustainable Energy Reviews*. 2012; 16: 2154–2171.

116. Kiviluoma J, Meibom P, Tuohy A, et al. Short-term energy balancing with increasing levels of wind energy. *IEEE Transactions on Sustainable Energy*. 2012; 3: 769–776.

117. Vilim M, Botterud A. Wind power bidding in electricity markets with high wind penetration. *Applied Energy*. 2014; 118: 141–155.

118. Foley AM, Leahy PG, Marvuglia A, et al. Current methods and advances in forecasting of wind power generation. *Renewable Energy*. 2012; 37: 1–8.

119. Tascikaraoglu A, Uzunoglu M. A review of combined approaches for prediction of short-term wind speed and power. *Renewable and Sustainable Energy Reviews*. 2014; 34: 243–254.

120. Exizidis L, Kazempour SJ, Pinson P, et al. Sharing wind power forecasts in electricity markets: A numerical analysis. *Applied Energy*. 2016; 176: 65–73.

121. Wang Q, Wu H, Florita AR, et al. The value of improved wind power forecasting: Grid flexibility quantification, ramp capability analysis, and impacts of electricity

market operation timescales. *Applied Energy*. 2016; 184: 696–713.

122. Zhang Y, Wang J, Wang X. Review on probabilistic forecasting of wind power generation. *Renewable and Sustainable Energy Reviews*. 2014; 32: 255–270.

123. Reddy SS, Panigrahi BK, Kundu R, et al. Energy and spinning reserve scheduling for a wind-thermal power system using CMA-ES with mean learning technique. *International Journal of Electrical Power & Energy Systems*. 2013; 53: 113–122.

124. Pinson P, Chevallier C, Kariniotakis GN. Trading wind generation from short-term probabilistic forecasts of wind power. *IEEE Transactions on Power Systems*. 2007; 22: 1148–1156.

125. Bitar EY, Rajagopal R, Khargonekar PP, et al. Bringing wind energy to market. *IEEE Transactions on Power Systems*. 2012; 27: 1225–1235.

126. Zugno M, Jónsson T, Pinson P. Trading wind energy on the basis of probabilistic forecasts both of wind generation and of market quantities. *Wind Energy*. 2013; 16: 909–926.

127. Wallace SW, Fleten S-E. Stochastic programming models in energy. *Stochastic Programming*. 2003; 10: 637–677.

128. Matevosyan J, Soder L. Minimization of imbalance cost trading wind power on the short-term power market. *IEEE Transactions on Power Systems*. 2006; 21: 1396–1404.

129. Morales JM, Conejo AJ, Pérez-Ruiz J. Short-term trading for a wind power producer. *IEEE Transactions on Power Systems*. 2010; 25: 554–564.

130. Rahimiyan M, Morales JM, Conejo AJ. Evaluating alternative offering strategies for wind producers in a pool. *Applied Energy*. 2011; 88: 4918–4926.

131. Pousinho HMI, Mendes VMF, Catalão JPS. A stochastic programming approach for the development of offering strategies for a wind power producer. *Electric Power Systems Research*. 2012; 89: 45–53.

132. Varkani AK, Daraeepour A, Monsef H. A new self-scheduling strategy for integrated

operation of wind and pumped-storage power plants in power markets. *Applied Energy*. 2011; 88: 5002–5012.

133. Matevosyan J, Olsson M, Sader L. Hydropower planning coordinated with wind power in areas with congestion problems for trading on the spot and the regulating market. *Electric Power Systems Research*. 2009; 79: 39–48.

134. Zima-Bočkarjova M, Matevosyan J, Zima M, et al. Sharing of profit from coordinated operation planning and bidding of hydro and wind power. *IEEE Transactions on Power Systems*. 2010; 25: 1663–1673.

135. Moghaddam IG, Nick M, Fallahi F, et al. Risk-averse profit-based optimal operation strategy of a combined wind farm-cascade hydro system in an electricity market. *Renewable Energy*. 2013; 55: 252–259.

136. Akhavan-Hejazi H, Mohsenian-Rad H. Optimal operation of independent storage systems in energy and reserve markets with high wind penetration. *IEEE Transactions on Smart Grid*. 2014; 5: 1088–1097.

137. Tajeddini MA, Rahimi-Kian A, Soroudi A. Risk averse optimal operation of a virtual power plant using two stage stochastic programming. *Energy*. 2014; 73: 958–967.

138. Dabbagh SR, Sheikh-El-Eslami MK. Risk assessment of virtual power plants offering in energy and reserve markets. *IEEE Transactions on Power Systems*. 2016; 31: 3572–3582.

139. Bertsekas DP, Bertsekas DP, Bertsekas DP, et al. *Dynamic programming and optimal control*. Massachusetts: Athena Scientific; 1995.

140. Ding H, Hu Z, Song Y. Stochastic optimization of the daily operation of wind farm and pumped-hydro-storage plant. *Renewable Energy*. 2012; 48: 571–578.

141. Castronuovo ED, Lopes JAP. On the optimization of the daily operation of a wind-hydro power plant. *IEEE Transactions on Power Systems*. 2004; 19: 1599–1606.

142. Krishnamurthy D, Uckun C, Zhou Z, et al. Energy storage arbitrage under day-ahead and real-time price uncertainty. *IEEE Transactions on Power Systems*. 2018; 33: 84–93.

143. Bayon L, Grau JM, Ruiz MM, et al. Mathematical modelling of the combined optimization of a pumped-storage hydro-plant and a wind park. *Mathematical and Computer Modelling*. 2013; 57: 2024–2028.

144. Castronuovo ED, Usaola J, Bessa R, et al. An integrated approach for optimal coordination of wind power and hydro pumping storage. *Wind Energy*. 2014; 17: 829–852.

145. Ding H, Pinson P, Hu Z, et al. Integrated bidding and operating strategies for wind-storage systems. *IEEE Transactions on Sustainable Energy*. 2016; 7: 163–172.

146. Wu X, Wang X, Wang J, et al. Schedule and operate combined system of wind farm and battery energy storage system considering the cycling limits. *International Transactions on Electrical Energy Systems*. 2015; 25: 3017–3031.

147. Vasallo MJ, Bravo JM. A MPC approach for optimal generation scheduling in CSP plants. *Applied Energy*. 2016; 165: 357–370.

148. Riveros JZ, Bruninx K, Poncelet K, et al. Bidding strategies for virtual power plants considering CHPs and intermittent renewables. *Energy Conversion and Management*. 2015; 103: 408–418.

149. Zapata J, Vandewalle J, D'haeseleer W. A comparative study of imbalance reduction strategies for virtual power plant operation. *Applied Thermal Engineering*. 2014; 71: 847–857.

150. Luo F, Dong ZY, Meng K, et al. Short-term operational planning framework for virtual power plants with high renewable penetrations. *IET Renewable Power Generation*. 2016; 10: 623–633.

151. Abdeltawab HH, Mohamed YA-RI. Market-oriented energy management of a hybrid wind-battery energy storage system via model predictive control with constraint optimizer. *IEEE Transactions on Industrial Electronics*. 2015; 62: 6658–6670.

152. Perez E, Beltran H, Aparicio N, et al. Predictive power control for PV plants with energy storage. *IEEE Transactions on Sustainable Energy*. 2013; 4: 482–490.

153. Bourry F, Costa LM, Kariniotakis G. Risk-based strategies for wind/pumped-hydro

coordination under electricity markets. *PowerTech, 2009 IEEE Bucharest*. 2009: 1–8.

154. Karagiannopoulos S, Vrettos E, Andersson G, et al. Scheduling and real-time control of flexible loads and storage in electricity markets under uncertainty. *11th International Conference on the European Energy Market (EEM14)*. 2014: 1–5.

155. Ding H, Pinson P, Hu Z, et al. Optimal offering and operating strategies for wind-storage systems with linear decision rules. *IEEE Transactions on Power Systems*. 2016; 31: 4755–4764.

156. Karagiannopoulos S, Vrettos E, Andersson G, et al. Scheduling and real-time control of flexible loads and storage in electricity markets under uncertainty. *11th International Conference on the European Energy Market (EEM14)*. 2014: 1–5.

157. Shapiro A, Dentcheva D, et al. *Lectures on stochastic programming: modeling and theory*. Philadelphia: MPS-SIAM; 2009.